

CIGRE TECHNICAL BROCHURE

ON

MODELING NEW FORMS OF GENERATION AND STORAGE

TF 38.01.10

Contributions by

N. Hatziargyriou (GR) (Convener)

M. Donnelly (USA)

S. Papathanassiou (GR)

J.A. Pecas Lopes (PT)

M. Takasaki (JP)

H. Chao (USA)

J. Usaola (SP)

R. Lasseter (USA)

A. Efthymiadis (UK)

K. Karoui (BE)

S. Arabi (CA)

Contents

Abstract

Chapter 1. Introduction

1.1 Definitions

1.2 Impacts

1.3 Scope and contents of brochure

Chapter 2. Description of Technologies. State of the Art.

2.1 Wind Energy Conversion Systems

2.2 Small Hydro Turbines

2.3 Micro Turbines

2.4 Fuel Cells

2.5 Biomass Systems

2.6 Photovoltaic Systems

2.7 Solar Thermal

2.8 Geothermal

2.9 Superconducting Magnetic Energy Storage Systems

2.10 Battery Energy Storage Systems

2.11 Flywheels

Chapter 3. Stability Modeling

3.1 Types of Stability

3.2 Stability Problems related to new forms of Generation and Storage

3.3 Generic Model

3.4 Electrical Generator models

3.5 Electronic Interface models

Chapter 4. Models for New Generation and Storage Devices

4.1 Wind Energy Conversion Systems

4.2 Small Hydro Turbines

4.3 Power Electronics based Micro-Sources (Micro-turbines and Fuel Cells)

4.4 Photovoltaic Systems

4.5 Superconducting Magnetic Energy Storage Systems

4.6 Battery Energy Storage Systems

4.7 Flywheels

Chapter 5. Software Tools

5.1 Introduction

5.2 Interactive Power System Analysis Package

Chapter 6. Conclusions and Further Work

REFERENCES

Abstract

Several new generation and storage technologies have the potential to significantly impact power system performance. Some of these new technologies are well suited for distributed generation and storage applications.

The purpose of this brochure is to define the characteristics of various new forms of generation and storage salient to studies of power system dynamics in the transient stability range and slower. This type of characterization is the first step in developing models and simulation methods appropriate for studying power system dynamics and the effects of introducing new forms of generation.

Wind energy conversion systems, small hydro turbines, micro-turbines, fuel cells, photovoltaic systems, superconducting magnetic energy storage systems, battery energy storage systems and flywheels are mainly addressed in this brochure.

Chapter 1. Introduction

1.1 Definitions

Several new generation and storage technologies have the potential to significantly impact power system performance. Most of these new technologies are well suited for distributed generation and storage applications and are connected at the MV distribution level. This form of generation is termed Dispersed Generation (DG) or Embedded Generation. On-site Generation is another term frequently used in the USA. It should be noted however, that new generation technologies are also found in larger installations of some 100 MWs, e.g. recent developments of off-shore Wind Energy Conversion Systems (WECS).

New generation and storage technologies include a variety of energy sources, as listed below.

- Wind Energy Conversion Systems (WEC)
- Small Hydro Turbines (HP)
- Diesel Generators (DG)
- Low Inertia Gas Turbines (GT)
- Fuel Cells (FC)
- Biomass Systems (BMS)
- Photovoltaic Systems (PV)
- Solar Thermal (STH)
- Geothermal (GTH)
- Superconducting Magnetic Energy Storage (SMES)
- Battery Energy Storage (BES)
- Compressed Air Energy Storage (CAES)
- Flywheels (FWH)

Deployment of these generation units on distribution networks could potentially increase their reliability and lower the cost of power delivery by placing energy sources nearer to the demand sources. By providing a way to by-pass conventional power delivery systems, distributed generation and storage could also offer additional supply flexibility.

CIGRE WG37-23 [1] and CIRED WG04 [2] have recently published reports dealing with the level and impacts of new generation connected at the distribution level. CIRED's report is based on replies from a questionnaire of 22 questions from 16 countries. On the question of definition of dispersed generation a great diversity among the answers is noted, i.e. definitions were based on voltage levels, type of prime mover, e.g. renewable or co-generation (CHP), maximum power rating or its availability for dispatch. According to CIGRE WG 37-23 Dispersed Generation is not centrally planned, today not centrally dispatched, usually connected to the distribution network, smaller than 50-100 MW. There is a general agreement among the replies however that penetration of dispersed generation is increasing. Currently 35% of total US industrial electric power

demand is met by on-site generation. For industry with stable demand is usually cheaper to generate on-site to avoid charges for transmission, distribution or billing. The potential for smaller users, such as housing developments and office buildings to switch to on-site power is also high. A recent EPRI study indicates as much as 25% of new generation by 2010 will be distributed. The Natural Gas Foundation concluded that this figure could be as high as 30%.

This trend is likely to accelerate in the future. CIGRE WG 37-23 report quotes twelve reasons why dispersed generation is increasing. These can be grouped in two main policy drivers:

- Government support to new renewable energy sources for environmental reasons.
- Competition on generation imposed by electricity market liberalization.

In the following Tables the potential for exploitation of the different renewable energy sources is presented within the framework of the European Commission's Strategy and Action Plan [4]. The contribution that the various renewable energy sectors could make by 2010 towards achieving the indicative objective of 12% share of renewables is estimated.

Type of Energy	Share in the EU in 1995	Projected Share by 2010
1. Wind	2.5 GW	40 GW
2. Hydro	92 GW	105 GW
2.1 Large	(82.5 GW)	(91 GW)
2.2 Small	(9.5 GW)	(14 GW)
3. Photovoltaics	0.03 GWp	3 GWp
4. Biomass	44.8 Mtoe	135 Mtoe
5. Geothermal		
5.1 Electric	0.5 GW	1 GW
5.2 Heat (incl. Heat pumps)	1.3 GWth	5 GWth
6. Solar Thermal Collectors	6.5 Million m ²	100 Million m ²
7. Passive Solar		35 Mtoe
8. Others		1 GW

Table 1. Estimated Contributions in the EU in the 2010 Scenario

Type of Energy	Actual in 1995		Projected for 2010	
	TWh	% of total	TWh	% of total
Total	2,366		2,870 (pre-Kyoto)	
1. Wind	4	0.2	80	2.8
2. Hydro	307	13	355	12.4
2.1 Large	(270)		(300)	

2.2 Small	(37)		(55)	
3. Photovoltaics	0.03		3	0.1
4. Biomass	22.5	0.95	230	8.0
5. Geothermal	3.5	0.15	7	0.2
Total Renewable Energies	337	14.3	675	23.5

Table 2. Current and projected electricity production in EU by Renewable Energy Sources (TWh) for 2010.

New Forms of generation have nowadays mature technology that is readily available and modular in a capacity range from 100 kW to 150 MW. The following Table 3 gives an overview of the costs for the different kinds of DG, as reported in CIGRE WG 37-23 [1]. The values concern EU countries, Australia and Canada. The authors underline that the costs are roughly estimated and in real applications these may be different depending on the individual conditions. Table 4 [5] provides US experience for smaller units.

Technology	Size (kW)	Capital costs (Euro/kW)	Total costs Euro/kWh
WEC (onshore)	15 MW	900-1300	0.04-0.09
WEC (offshore)	100 MW	1500-2000	0.05-0.12
HP (lowhead)	5 MW	900-1000	0.02-0.03
CG (turbine)	5 MW	800-850	0.053-0.057
CG (reciprocating engine)	5 MW	500-750	0.03-0.0453
PV	5 MW	6000-10000	0.75-1
Fuel Cells	5 MW	1100-1600	0.08-0.1
Micro Gen. (reciprocating engine)	50 kW	600-1500	0.07-0.15
Micro Gen. (turbine)	50 kW	~ 300	0.03-0.05
Micro Gen. (fuel cell)	50 kW	~ 900	0.09-0.15

Table 3. Sizes and Costs for different kinds of New Forms of Generation

CG denotes “conventional generators”, a term used to describe small fossil-fuelled plants producing electricity only. The two main kinds of conventional generators that are currently preferred for DG are combustion turbines and reciprocating engines.

Type	Size (kW)	Efficiency	Cost (\$)
Microturbine	25-100 kW	25-30%	~\$350/kW
Fuel Cell	20-2000 kW	30-45%	~\$2000/kW
Automotive Fuel Cell	30-200 kW	30-45%	~\$200/kW
Microturbine/ Fuel Cell	100-200 kW	60-70%	

Battery	10-500 kWh	70-80%	~\$500 kWh
Flywheel	2-100 kWh	70-80%	

Table 4. Size, Efficiency and Costs for different kinds of DG

1.2 Impacts

For utilities the two prime uses for dispersed, small generation are for peak shaving at the distribution level and to deter or avoid the cost of increasing the distribution infrastructure. Dispersed generation enables distribution to shave peaks through generation rather than demand side management (DSM) techniques. In addition to shaving peaks they also provide capacity for emergencies.

Local generation not only increases overall system efficiency but also reduces investments in traditional generation, bulk transmission and distribution facilities. The utility can also serve incremental load growth in areas where there is a shortage of substation and/or distribution feeder capacity. For this to happen however, methods for control and dispatch of 10s to 100s of units are needed.

For major commercial and industrial users of electrical power on-site generation can be used to reduce demand charges. In addition to saving in demand charges the turbines could be connected to the more critical loads to provide emergency power. Since most new generation sources have a power electronics interface, they can provide the quality of power provided by “Custom Power Devices”, such as active filtering and voltage support during single and three phase disturbances.

In a 1994 EPRI study [3], the impacts of DG are grouped according to their main characteristics, as follows:

DS Attribute	Spinning Reserve	Uncertainty or availability	Smallest controllable increment	Control of dispersed systems	Economic Dispatch
Fully Dispatchable (e.g. Fuel cell, Solar-Thermal, CHP, Small HP)	Possible usage	Availability known using standard outage rate information	Cannot realize this category	Typically high degree of control with possible exception of hydro	High penetration base load dispatch or incrementally for peaking
Limited dispatch (storage) (e.g. BES, CAES, SMES, Hydrogen)	A primary application of storage devices	Some long term uncertainty associated with multiple	Typically high degree of control operating within energy	Typically high degree of control operating within energy	Load levelling and peak shaving applications – dispatch comparable

		applications – spinning reserve credit lost when operated for peak shaving	capacity limits	capacity limits	to peaking plants – also includes distribution facilities optimization
Intermittent sources (e.g. PV, WECS)	Cannot be utilized	Most uncertain – prediction possible but not likely to be relied upon	Output reducible to lower levels	Low degree of control – limited to reducing output	Zero fuel cost dispatch scheme – viewed as negative load
Load Following (e.g. Fuel cell, Cogen, Solar-Thermal, BES, SMES)	N/A		Typically high degree of control	Typically high degree of control	Comparable to peaking plant economic dispatch

1.3 Scope and Contents of the Brochure

Scope:

To identify the characteristics of the new forms of generation systems and to investigate the requirements for their modeling and simulation.

To investigate existing tools and techniques for assessing the impact of the new forms of generation systems on power system dynamic performance.

Objectives:

- 1.) To identify new generation technologies and their characteristics salient to assessing the impact on power system dynamic performance. Characteristics will include those associated with mechanical dynamics, electrical behavior, and control system performance.
- 2.) To identify available analytical models and tools and assess their adequacy in capturing device characteristics, specify deficiencies, and additional modeling requirements.
- 3.) Propose models for those devices which models are inadequate or non-existent.
- 4.) To investigate past and current efforts aimed at evaluating the impact of the new forms of generation sources on system dynamic performance.

- 5.) Develop guidelines for planners in selecting models for the new forms of generation systems and propose techniques for assessing their impact on power system dynamic performance.

Chapter 2 provides an overview of the new forms of generation and storage – state of the art.

Chapter 3 provides stability terms and definitions, generic models, common features of all systems.

Chapter 4 provides models.

Chapter 5 should include models developed in commercial software packages.

Chapter 6 concludes.

Chapter 2

Description of Technologies. State of the Art.

2.1 Wind Energy Conversion Systems

Wind Energy Conversion Systems (WECS) transform the energy present in the blowing wind into electrical energy. Wind is a highly variable resource that cannot be stored and Wind Energy Conversion Systems must be operated accordingly.

Windmills have been used since the Xth century A.D. and they were widely spread throughout Europe in the XVIII century. Generation of electricity from windmills begun in the 40s in Germany, United States and Denmark. Since that time, mass production of wind plants has begun and highly reliable and cost-effective units are presently being built. Now there are machines in the 500 - 1500 kW range that are remarkable for their high availability and good return-on-investment potential.

General description of WECS

A general scheme of a WECS is shown in Figure 2.1. In this figure the main parts of a WECS are presented. Parts marked with dotted lines are not always present.

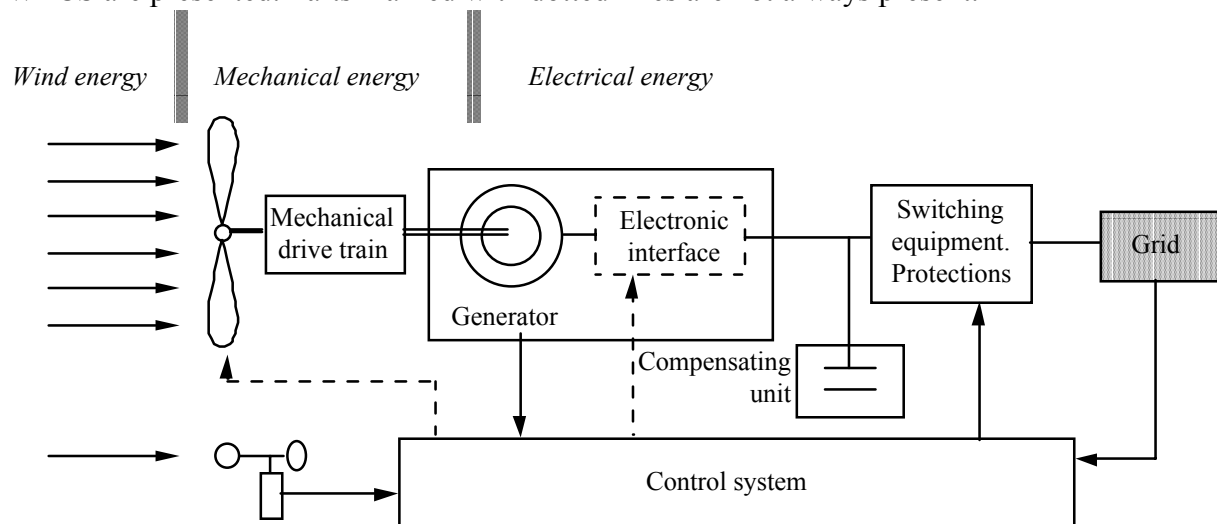


Figure 2.1. General scheme of a WECS.

A short overview of the system is given next. Wind energy is transformed into mechanical energy by means of a wind turbine that has one or several blades (three is the most usual number). The turbine coupled to the generator by means of a mechanical drive train. It usually includes a gearbox that matches the turbine low speed to the higher speed of the generator. New wind turbine designs use multi-pole, low speed generators, usually synchronous with field winding or permanent magnet excitation, in order to eliminate the gearbox. Some turbines include a blade pitch angle control for controlling the amount of power to be transformed. Stall-controlled turbines do not allow such control. Wind speed is measured by means of an anemometer.

The electrical generator transforms mechanical into electrical energy. The generator can be synchronous or asynchronous. In the first case, an excitation system is included or permanent magnets are used. Variable speed systems require the presence of a power electronic interface, that can adopt very different configurations.

The compensating unit may include power factor correction devices (active or passive) and filters. The last ones may be necessary when there are electronic devices connected to the grid.

The switching equipment should be designed to perform a smooth connection, a requirement usual in standards. Standards also specify some protections that, at least, must be present in the generating unit.

Finally, the control system may have different degrees of complexity. Detailed description will be given later on.

The power obtained by the turbine is a function of wind speed. This function may have a shape such as shown in Figure 2.2. For variable speed WECS the upper part of the curve between v_r and v_{c-o} can be kept linear, equal to the reference power P_r .

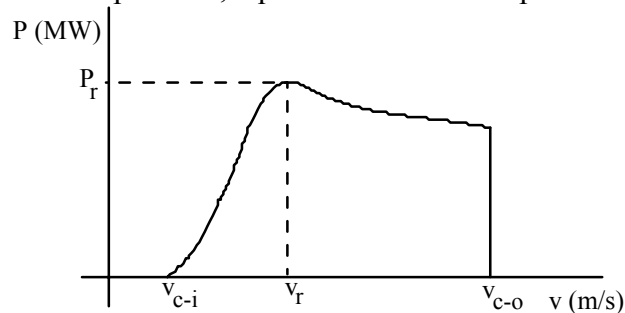


Figure 2.2 Typical power curve for a stall-regulated turbine

The following notation is used:

- P_r : reference power, maximum power that the turbine can attain.
- v_r : reference power wind speed, wind speed for which reference power is achieved.
- v_{c-i} : cut-in wind speed, wind speed at which the turbine starts to produce power.
- v_{c-o} : cut-out wind speed, upper limit of the wind speed at which the turbine can operate.

Energy converter systems

Regarding rotational speed, the wind turbines can be split into two types –variable and fixed rotational speed units. In fixed speed machines, the generator is directly connected to the mains supply grid. The frequency of the grid determines the rotational speed of the generator and thus of the rotor. The low rotational speed of the turbine rotor is translated into the generator rotational speed by a gearbox with a transmission ratio. The generator speed depends of the number of pole pairs and the frequency of the grid.

In variable speed machines, the generator is connected to the grid through an electronic inverter system, or the generator excitation windings are fed by an external frequency from an inverter. The rotational speed of the generator and thus of the rotor is decoupled from the frequency of the grid, the rotor can operate with variable speed adjusted to the actual wind speed situation.

All devices may be pitch or stall regulated. The pitch regulation systems rotate the blade about their long axes through a pitch regulation mechanism. With this mechanism, the mechanical power can be reduced, according to the turbine characteristics. Stall regulated turbines do not have such a mechanism, but when the wind exceeds rated levels, they are prevented from taking excessive power from the wind by an aerodynamical effect.

Most of the existing systems can be classified in the following way:

- I. Wind turbines with fixed rotational speed directly connected to the grid
 - A. Wind turbines with asynchronous generator
 - B. Wind turbines with synchronous generator.
- II. Wind turbines with variable and partly variable rotational speed
 - A. Synchronous or asynchronous generator with converter in the main power circuit.
 - B. Asynchronous generator with variable slip control
 - C. Asynchronous generator with over- or sub-synchronous converter cascade.

All systems can be pitch or stall regulated, as shown schematically in Figure 2.3.

The advantages of fixed speed systems are simplicity and low cost. Asynchronous generators must be provided with reactive power control equipment. Variable speed systems provide more energy production, less mechanical stress on the mechanical parts and a more smooth power production (less dependant on wind variations and system oscillations). In some of these systems, the gearbox can be omitted. Some of these devices may require harmonic compensation, due to the presence of electronic converters.

Direct grid connection of asynchronous generators is the most widely used scheme in a large number of turbines. Power ranges from 50 kW to 1500 kW. The biggest are usually pitch-controlled or they tend to have some kind of control.

Direct grid connection of synchronous generator is only used for a small number of small wind turbines, mainly in stand alone systems.

Variable speed systems are a widely used concept with increasing applications with growing size of wind turbines. The main objective of the variable speed operation of the WTs is to optimize their efficiency, i.e. to maximize the available wind energy capture.

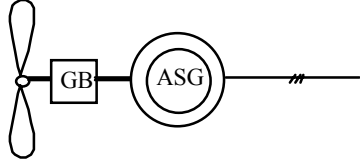
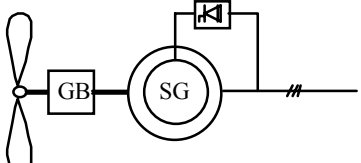
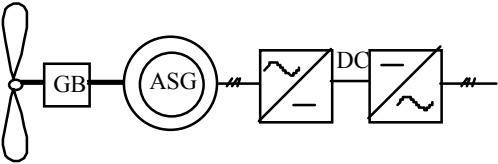
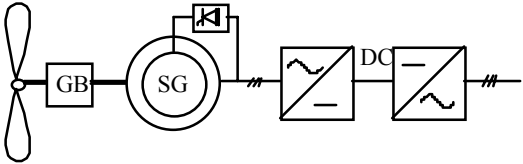
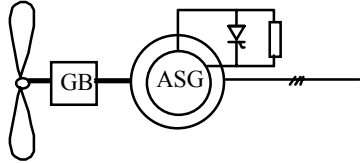
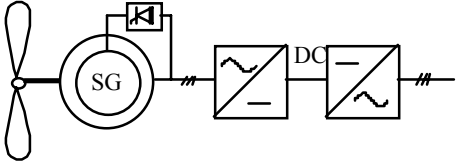
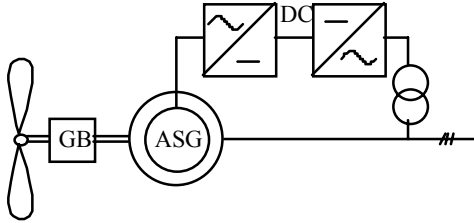
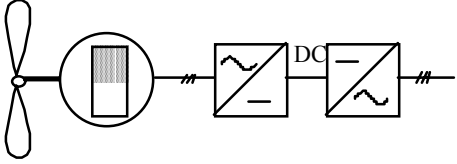
ASYNCHRONOUS GENERATORS	SYNCHRONOUS GENERATORS
<ul style="list-style-type: none"> direct grid connection  <p>$n = (1-s) f/p$ $s = 0 \dots 0.08$ inductive reactive power consumer</p>	<ul style="list-style-type: none"> direct grid connection  <p>$n = f/p$ controllable reactive power output</p>
<ul style="list-style-type: none"> grid connection via DC link  <p>$n = 0.8 \dots 1.2 f/p$ controllable reactive power output with suitable converter</p>	<ul style="list-style-type: none"> grid connection via DC link  <p>$n = 0.5 \dots 1.2 f/p$ controllable reactive power output with suitable converter</p>
<ul style="list-style-type: none"> dynamic slip control  <p>$n = (1-s) f/p$ $s = 0 \dots 0.1 \dots 0.3$ inductive reactive power consumer</p>	<ul style="list-style-type: none"> grid connection via DC link, gear-less  <p>$n = 0.5 \dots 1.2 f/p$ controllable reactive power output with suitable converter</p>
<ul style="list-style-type: none"> doubly-fed asynchronous generator 	<ul style="list-style-type: none"> PMSG connected via DC link  <p>$n = 0.6 \dots 1.2 f/p$ controllable reactive power output with suitable converter</p>

Figure 2.3. Different kind of WECS

The technology of the variable speed wind turbines (VSWTs) comes directly from the field of the adjustable speed electrical drives. Hence, variable speed operation can be achieved using any suitable combination of electrical generator and power electronic converters, such as squirrel cage or wound rotor induction generators and stator or rotor converter cascades, or synchronous generator with field or permanent magnet excitation and stator AC/DC/AC converter interface to the grid. Obviously, each converter-

generator combination presents advantages and disadvantages regarding its cost, complexity, operating and control characteristics, dynamic performance, harmonics, output power factor regulation etc. At present, however, no scheme is clearly favored against the others and various configurations of the electrical part are being tested and evaluated.

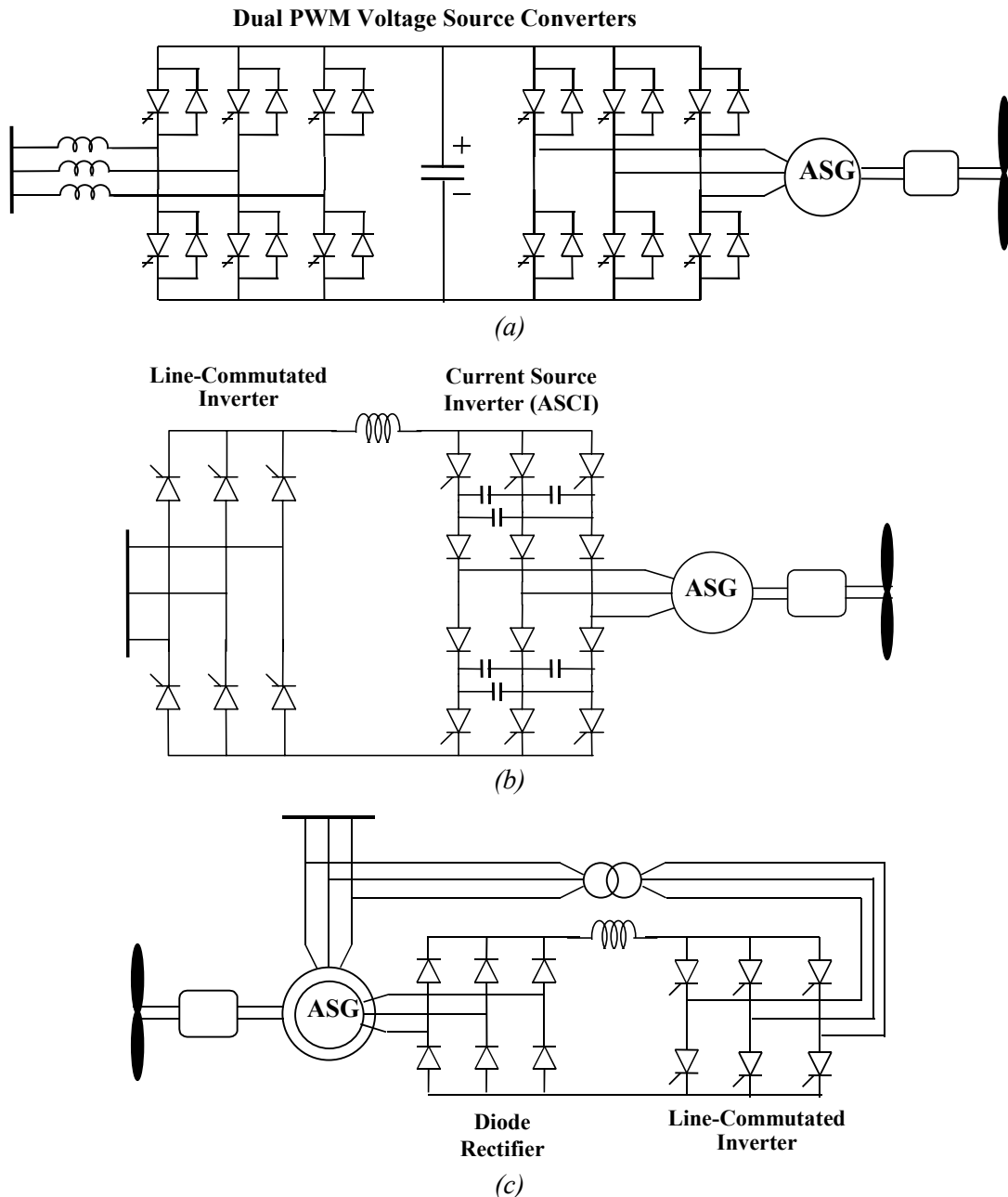


Figure 2.4. VS WT electrical schemes using induction generator. (a) Squirrel cage induction generator and dual PWM voltage source converters. (b) Squirrel cage induction generator and current source converter cascade. (c) Double output induction generator.

For illustration purposes, three possible VS WT schemes using induction generator are shown, in more detail, in Figure 2.4:

- a) Squirrel cage induction generator connected to the grid via a dual PWM voltage-source converter cascade, as shown in figure 2.4(a). The switching elements shown in the figure are GTOs, although for power levels up exceeding 1 MW today IGBTs are also available, permitting significantly higher switching frequencies.
- b) Squirrel cage induction generator and current source inverter cascade, as illustrated in figure 2.4(b). The machine-side converter is of the Auto-Sequential Commutated Inverter (ASCI) type, whereas at the grid-side a conventional phase-controlled thyristor inverter is used.
- c) The double output induction generator, known also as the static Kramer drive, shown in figure 2.4(c). This configuration employs a wound-rotor induction machine and a rotor converter cascade consisting of a diode rectifier and a line-commutated thyristor inverter.

A variable speed synchronous generator is shown in Figure 2.5. The generator is a multipole permanent magnet synchronous machine, permitting the elimination of the gear box in the drive train. The generator output is rectified and subsequently inverted to AC via an IGBT PWM voltage source inverter.

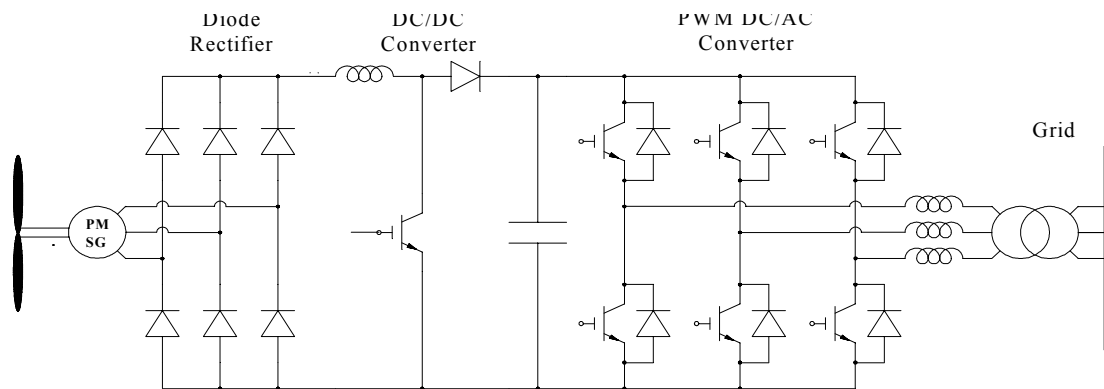


Figure 2.5 Gear-less VS WT using a permanent magnet synchronous generator.

Another alternative is shown in Figure 2.6. It utilizes a wound rotor induction generator, with an electronically controlled external resistance connected to its rotor circuits. This scheme is preferred by certain manufacturers, mainly due to its simplicity. However, it presents a limited range of speed variability (up to 10%), achieving thus the torque smoothing objective (via the increased rotor speed compliance), but not the energy output maximization.

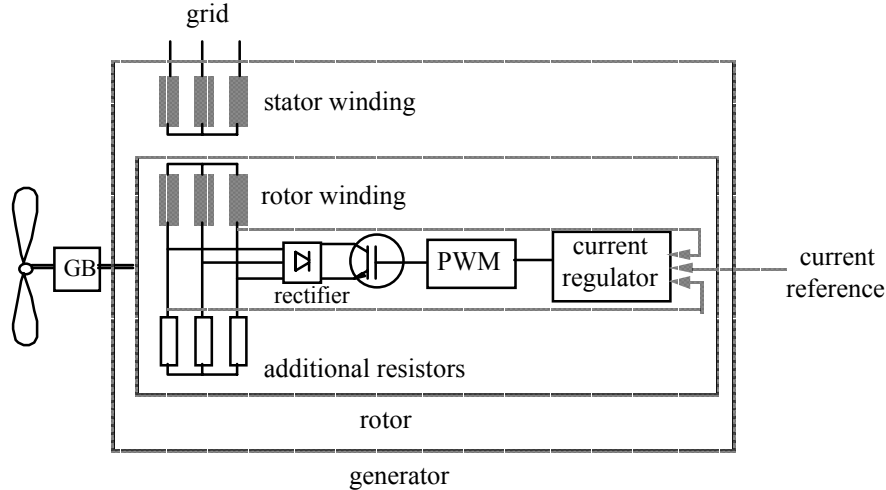


Figure 2.6 Asynchronous generator with variable slip control.

As in the case of the electrical drives, no general model can be introduced, which would represent with sufficient accuracy the dynamic behavior of all VS WT schemes. In fact, each configuration requires the elaboration of an individual model, depending on the type of generator, converters and controls used, as well as on the modeling requirements, i.e. on the time scale and nature of the phenomena to be reproduced.

The following table shows main data of some wind turbines with advanced controls for performance and mechanical load optimization.

Type	Power (kW)	Concept	Regulation	Revolutions (r.p.m.)
Enercon-40 (Germany)	500	Synchronous generator with frequency converter, gear-less.	pitch	18 – 38
Lagerway 45 (Netherlands)	750	Synchronous generator with frequency converter, gear-less.	pitch	20 – 35
Enercon-66 (Germany)	1500	Synchronous generator with frequency converter, gear-less.	pitch	10 – 20.3
Genesys 600 (Germany)	600	Permanent excited synchronous generator with frequency converter, gear-less.	pitch	22 – 32
Wind World W-4500/750 (Denmark)	750	Asynchronous generator with frequency converter.	stall	16 – 30
Windtec 646 (Austria)	600	Doubly fed asynchronous generator.	pitch	15 – 33
Südwind N4660 (Germany)	600	Doubly fed asynchronous generator.	pitch	10 – 35
Zond Z-46 (USA)	750	Doubly fed asynchronous generator.	pitch	16 – 30
Tacke 1.5 (Germany)	1500	Doubly fed asynchronous generator.	pitch	14 – 20

Windtec 1566 (Austria)	1500	Doubly fed asynchronous generator.	pitch	12 – 23.5
Vestas-42 (Denmark)	600	Asynchronous generator with dynamic slip regulation.	pitch	30 – 33
Vestas-63 (Denmark)	1500	Asynchronous generator with dynamic slip regulation.	pitch	21 – 23

Table 2.1 Data of some existing regulated wind turbines

Connection to the grid. Wind farms

Wind turbines can be connected individually to the grid or clustered in wind parks. The electrical components of wind turbines are designed for low voltages up to 1000 V for cost reasons. Therefore, transformers are necessary most of the times. Only when individually connected, or when the rated power of the wind farms is less than 100 kW, they are connected to the low voltage grid. When their power is between 100 kW and 1 MW, they supply to the medium-high voltage grid connection (10-66 kV). Large wind farms (e.g. 50 MW) are connected to the high voltage grid (110 - 132 kV).

In some countries, a usual connection criterion requirement for wind farms is the ratio of the short circuit power of the connection point to the rated power of the wind farm. However, this is difficult to achieve when these farms are located in regions with low power transmission capacity. Wind farms can be configured in several ways. Some common arrangements are shown in Figure 2.7.

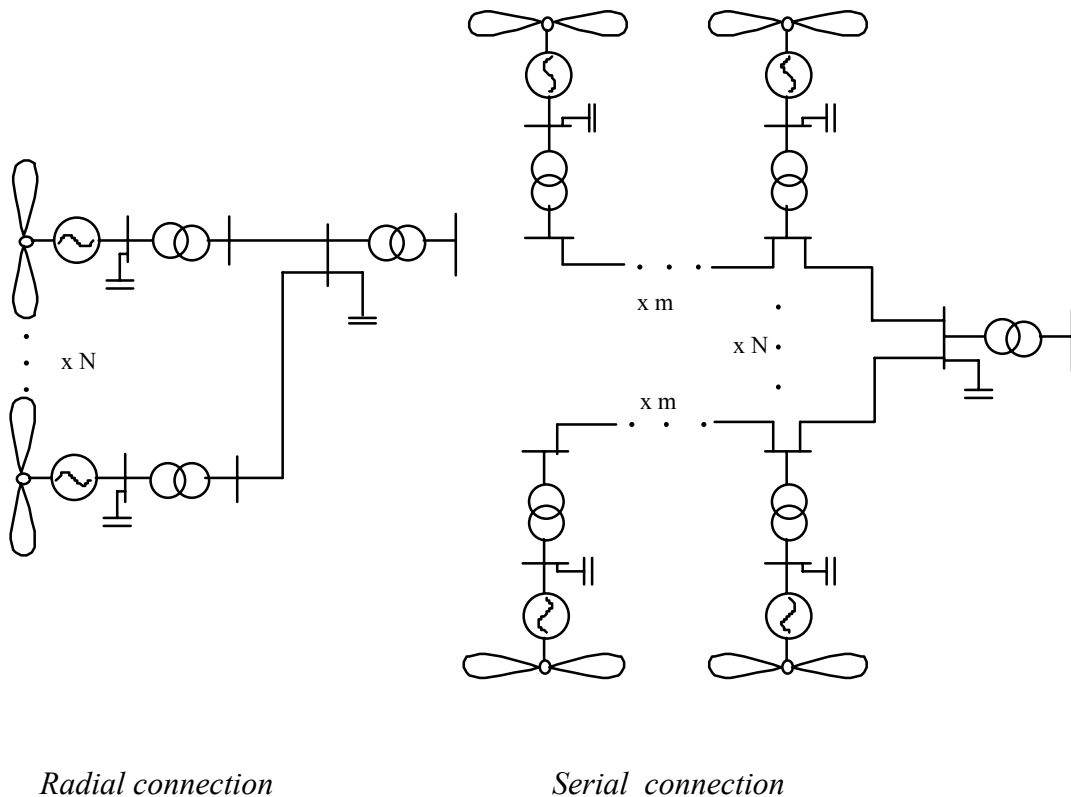


Figure 2.7 Common ways of connecting turbines inside a wind farm

2.2 Small Hydro Turbines

The terms “micro hydro” and “mini hydro” define installations for the production of hydroelectricity at low power levels. In practice, the power from such installations can be in the range of 5 kW to 100 kW for “micro hydroelectric” power stations and between 500 kW and 10 MW for small or mini hydro power stations. The heads of such plants can be in the range of 1,5 to 400 m with flows ranging from several hundreds of liters per second to several tens of cubic meters per second.

In a small hydro power station the technical electro-mechanical solutions to be adopted should be robust and as simple as possible to reduce costs and decrease maintenance, assuring profitability of the investments. Therefore, the various turbine manufacturers have developed standardized units for small hydroelectric systems. Their designs are based on the following principles: a) the optimum use of the latest research into turbine-machinery; b) the supply of the electromechanical equipment in a compact ready-to-install and ready-to-operate form; c) simple hydraulic design, using standard components to reduce costs and delivery times. This approach is applicable to powers between 100 and 2000 kW. Below 100 kW, capital cost become too high and the installation is therefore uneconomic. For powers over 2000 kW, individual design of the hydroelectric units can again be considered. Some small turbines, such as Banki [6], which are particularly suitable for use in the developing countries without interconnected electricity grids, do allow the power to fall below 100 kW.

The standard types of turbine for such a relatively wide range of capacities and heads are a) propeller (or Kaplan) turbines for low heads; b) Francis turbines for medium heads; c) Pelton turbines for high heads and Banki-Mitchel turbines for fairly wide range heads. Some manufacturers have concentrated mainly on low heads so as to develop run-of-the river equipment.

The solution most generally adopted for reasons of mechanical simplicity has been to develop adjustable blades in a range of standard diameters. These are mounted in siphon units or in classical axial flow units. In large rivers in Africa or in South America slow speed hydraulic wheel turbines with horizontal axes have been developed to be installed in the border of the river producing electricity to feed non power quality demanding appliances.

From the electrical point of view the generators can either be synchronous or asynchronous machines. When synchronous machines are used automatic voltage regulators (AVR) and speed regulators are needed, however, for economic reasons, the need for these equipment can be relaxed somewhat depending if the generators are connected in isolated or interconnected networks. Usually AVRs are always used, assuring that voltage will be kept stable within a range of +/- 5% with a power factor larger than 0,8. Due to the low mechanical inertias that characterize micro generation

units, electrical governors using a combined frequency measurement and energy absorption system are preferred to ensure good intrinsic stability. However, in some small hydros connected to networks where frequency is regulated by large conventional units, and assuming that the small production plants are not allowed to operate in isolated grids, speed regulator can be avoided for the sake of simplicity and economy. In this case only the output power is regulated according to water level and flow.

When induction machines are used, the hydro plant is simpler, as no AVR governor or synchronisation device are needed. However the magnetic circuit must receive magnetization energy in the order to produce the flux. This energy needs to be supplied from an external source and it is related to a reactive power consumed by the machine. This reactive power can either be delivered by the grid or by capacitor banks connected in parallel with the induction machine which provide at least part of the required reactive consumption. The use of capacitor banks in parallel with the generator demands that special care should be taken to avoid self-excitation that would damage the machine. To tackle with this issue, the connection and disconnection of the generator, relatively to the grid, usually follows a sequence of the type:

1. Connection:

- Run the induction generator with no load up to a range of 90% to 95% or the synchronous speed;
- Connect the machine to the grid;
- Connect the capacitor banks.

2. Disconnection:

- Disconnect the capacitors first;
- Disconnect the generator from the grid (a simultaneous disconnection of the generator and capacitors can also be performed).

Such a sequence of operations related with the connection and disconnection of the induction machine from the grid provokes electrical impacts in the nearby buses, namely transient voltage fluctuations that need to be properly addressed when power quality issues are a matter of concern. Static switches, as the ones used in wind asynchronous generators, can be used during the connection to grid to avoid namely voltage dips in the nearby buses. In any case simulations studies (dynamic and steady state behaviour) should be performed to evaluate the system operating conditions.

2.3 Micro Turbines

Small gas fired micro-turbines in the 25-100 kW range can be mass-produced at low cost. They are designed to combine the reliability of on board commercial aircraft generators with the low cost of automotive turbochargers. These systems are high speed turbines (50,000-90,000 rpm) with air foil bearings. They are small and use power electronics to interface with the load. Examples include AlliedSignal's 75 kW Turbogenerator, Allison Engine Co's. 50 kW generator and Capstone's 35 kW system.

2.4 Fuel Cells (FCs)

A fuel cell (FC) is an electrochemical energy conversion system, where chemical energy is converted directly into electrical energy and heat. Resulting advantages of this technology are high efficiency almost at partial load, low emissions, noiselessness (due to non existence of moving parts), and free adjustable ratio (50 kW to 3 MW) of electric and heat generation.

The operation of a FC is closely alike to that of a battery system, except that it consumes fuel. The energy savings results from the high conversion efficiency, typically 40% or higher, depending on the type of fuel cell. When utilised in a cogeneration application by recovering the available thermal energy output, overall energy utilisation efficiencies can be in the order of 85% or more.

Physically a FC plant consists of three parts, as shown in Figure 2.5:

- I - A *fuel processor* that removes fuel impurities and may increase concentration of hydrogen in the fuel;
- II - A *Power section* (fuel cell itself) which consists of a set of stacks containing catalytic electrodes, generating the electricity;
- III - A *Power conditioner* that converts the direct current produced in the power section into alternating current (DC to AC converter).

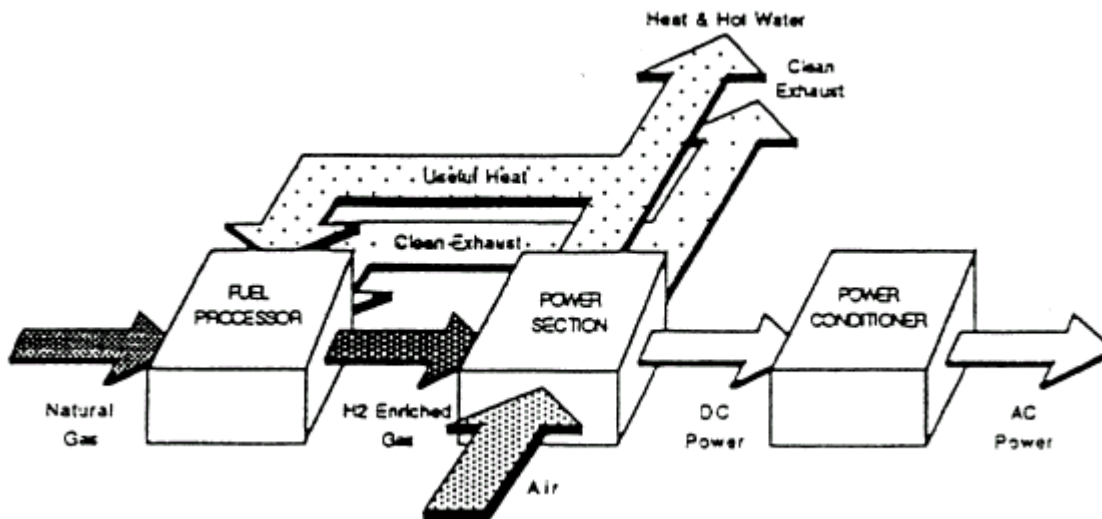


Figure 2.5 - Block diagram of a fuel cell plant

The power section of the fuel cell takes hydrogen (either pure or as part of partially reformulated natural or renewable organic gases) as fuel and oxidizes it, resulting in a release of electrons. The process requires air and catalytic electrodes, which split the hydrogen into positively charged hydrogen ions and electrons. The electrons can be channeled and used as high quality electricity. The hydrogen ions combine with oxygen in the air to produce water and heat. The process is illustrated in Figure 2.6.

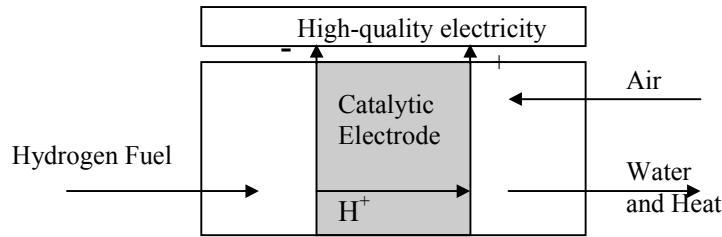


Figure 2.6 - Basic fuel cell operation

While the reaction that drives all FCs involves hydrogen, pure hydrogen is currently too expensive to produce and transport in bulk. The current alternative is to process high-hydrogen-content fuels to free all or most of the hydrogen and removes contaminants that would poison the catalyst. These fuels include fossil fuels as well as other more sustainable types of hydrocarbon-based fuels, such as landfill gas and anaerobic digester gas. Eventually it may be inexpensive to produce hydrogen directly from water, utilising renewable sources of electricity. While this may be considerable as an environmental preferable option, the economics of this process are not yet sustainable.

Currently, FC process fossil and other hydrocarbon-based fuels as part of the FC plant. Each of the different FC technology options has a different level of resistance to non-hydrogen components in the fuel stream. A greater resistance reduces the amount of fuel processing needed by the FC and subsequently.

Development efforts are currently focused on five FC technologies: phosphoric acid (PAFC) proton exchange membrane (PEFC) molten carbonate (MCFC) solid oxide (SOFC) and alkaline. Alkaline fuel cells have only been developed for space use, without application in terrestrial uses. Low temperature systems operating at 80°C, include Polymer Electrolyte FC and Alkaline technologies. Middle temperature systems, like the PAFC, exploit Phosphoric Acid as electrolyte. The operation temperature is about 200°C, being at the moment the most spread technology. Power plants of 200 kW are presently commercially available. Natural gas Fuel Cells that exploit this technology are also presently being used.

Advanced technologies are the high temperature Fuel Cells, including MCFC and especially SOFC. Because of the high operating temperatures, from 650°C (MCFC) up to 1000°C (SOFC), these systems are preferred for co-generation. The main advantage of SOFCs in comparison to MCFC is the higher temperatures, allowing internal reforming of natural gas or other hydrocarbons. Moreover the solid electrolyte of SOFC avoids special protection facilities which are necessary when liquid corrosive electrolytes are used.

Table 2.3 describes some of the main characteristics of this equipment.

Table 2.3

Fuel Cell	PEFC	PAFC	MCFC	SOFC
Electrolyte	Solid Polymer	H ₃ PO ₄	Li ₂ CO ₃ /K ₂ CO ₃	Y doped ZrO ₂

Start-up time	seconds	3-10 h	hours	hours
Power density	400 mW/cm ²	150-300 mW/cm ²	150 mW/cm ²	150 mW/cm ²
Primary fuel	Hydrogen	Hydrogen, Natural gas, methanol, naphtha, lighter oils	Hydrogen, Natural gas, coal gas, methanol, naphtha, petroleum	Hydrogen, Natural gas, coal gas, methanol, naphtha, petroleum
Int. reforming	No	No	Possible	Possible
Gen. Efficiency	40-50%	40-50%	45-60% (75% with gas and steam turbine)	50-60% (75% with gas and steam turbine)

The performance of a fuel cell is represented by the current density vs. voltage curve as shown in Figure 2.7. The open circuit voltage, as determined by the “free energy” property of reactants, is 1.23 volts. In practice, the fuel cell voltage is below the theoretical value. At small current densities (Region 1), the activation energy associated with the chemical reaction accounts for the sharp drop in voltage. At higher current densities (Region 2), the voltage drop is dominated by the losses in the electrode structure and the electrolyte. At even higher current densities (Region 3), the rate at which the reactants can diffuse to or the products to diffuse away from the reaction site determines the losses. Due to the limitation caused by the diffusion process, the current which can be drawn from the fuel cell has a maximum value called the limiting current. Better cells are those with flatter curves and higher limiting currents. Fuel cell performance can be increased by increasing the cell temperature and the reactant pressure. However, at more severe operating conditions, material and hardware problems may be confronted.

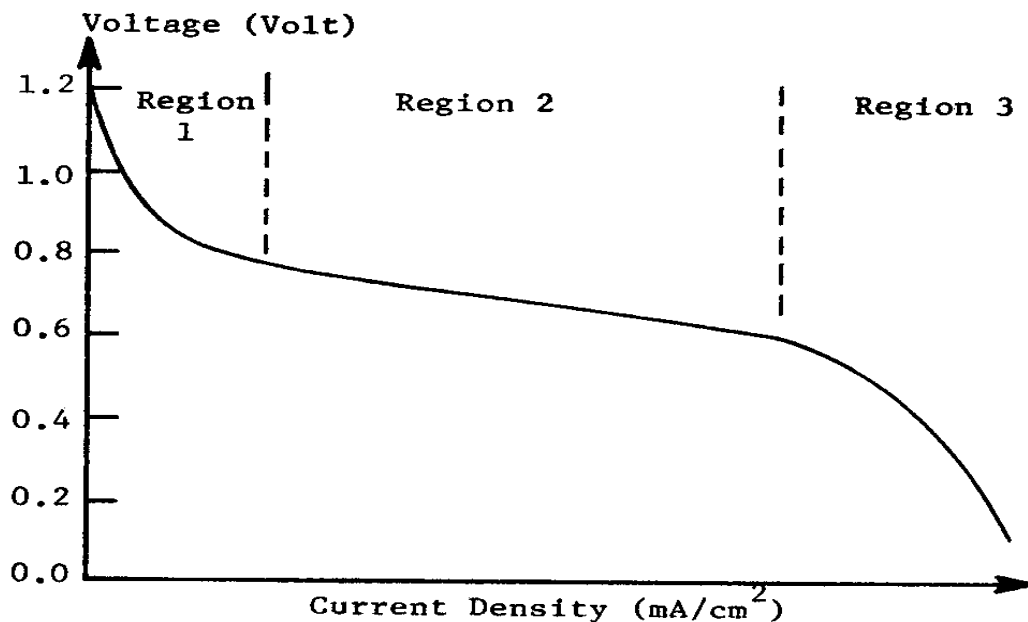


Figure 2.7. Electrical Characteristics of a Fuel Cell

A power station consists of a number of power plants, a station controller and auxiliary sub-systems. Each power plant performs the primary function of generating DC power from fuel and providing DC/AC conversion. Auxiliary subsystems provide fluids and electrical power for effective plant operation.

As the fuel cell energy conversion process is free from thermal and electromechanical conversion, the net efficiency and load response rate are higher than conventional power plants. Some of the distinct features of a fuel cell power plant are listed in the following.

Net efficiencies as high as 80 per cent are theoretically possible for a fuel cell. In its most popular form of implementation, however, the phosphoric acid fuel cell has achieved efficiencies up to 40% at atmospheric pressure and up to 45% for pressurized systems. More importantly, this efficiency level remains essentially constant between 30% to 100% of rated output. In addition, fuel cells have low fuel consumption at idle.

A 40-kW fuel cell power plant designed by the United Technologies Corporation (now IFC) is capable of going from zero power(idling) to full power in approximately 30 milliseconds. The 11 MW prototype fuel cell power plant under development by the same manufacturer can provide a step change in power at the rate of 1 MW per second between 30% and 100% of its full load capacity. The one –megawatt prototype fuel cell power plant being developed under the sponsorship of the New Energy Development Organization in Japan can respond to a change in load from 250 kW to 1000 kW in one minute.

A fuel cell produces approximately 0.6 to 0.75 volts and a current in the range of 1500-3000 Amp/m² of cell area depending on operating temperature and pressure. This is equivalent to 900-1800 W/m² of cell area in the stack. Groups of stacks may be connected in series/parallel combinations to provide the desired output. The power and voltage levels can range from 2 kW to multi-MWs and a few volts to 10,000 volts respectively.

Fuel cells can provide waste heat in an usable form. A 40-kW fuel cell power plant is now providing electricity and hot water to a dormitory building of the Old Dominion University in Norfolk. The heat recovery varies from approximately 18 kW_t at one-half rated power to 44 kW_t at full power. Since heat recovery is approximately equal to electrical output, a fuel cell supplying between half and full electrical load, while all by-product heat is being utilized, will operate at 65-70% overall efficiency. Total fuel utilization as a function of output power is shown in Figure 2.8. The 40-kW fuel cell power plant provides low grade heat up to 80 °C and high grade heat up to 135 °C in the form of hot water and saturated steam.

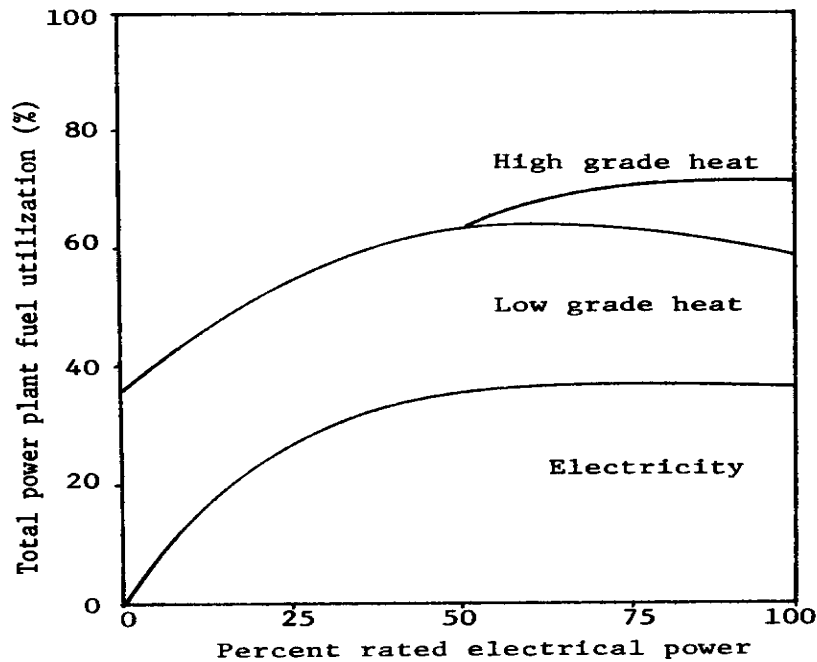


Figure 2.8. Fuel Utilization vs. Power Output

Considering the generalization of the use of natural gas for industrial and domestic purposes and the decrease in the installation costs of the FC conversion equipment, one can foresee that, in the near future, this equipment will start having a large penetration in distribution networks. This penetration will be dispersed, ranging from 50 kW to 3 MW. This means that some of these conversion systems will be connected at the LV network with a large impact in the operation and planning policies. DC to AC converters will become the interface with the AC utility grid and the electrical appliances of each consumer exploiting this technology.

In October 1997 the US Department of Energy and Arthur D. Little unveiled the “first-ever on-board gasoline powered fuel cell for the automobile”. The possibility of using gasoline as fuel for cells has resulted in a major development effort by the automotive companies. This work is focused towards the polymer electrolyte membrane (PEM) fuel cells. By 2002, Ballard Power Systems expects to be selling a 250 kW Fuel Cell based generator at prices competitive with the grid to shopping malls and large commercial buildings. Cinergy Corporation placed a commercial order with Ballard for a 250-kW PEM fuel cell for stationary power [5].

Mixed fuel cell and micro-turbine systems are also available as distributed generation. In a joint DOE Westinghouse project a solid oxide fuel cell has been combined with a gas turbine creating a combined cycle power plant. It has expected electrical efficiency of greater than 70% with low CO₂ and NO_x and virtually zero SO_x. The expected power levels range from 250 kW to 2.5 MW [5].

2.5 Biomass Systems

Biomass is energy derived from any organic or plant matter and, under this term, there is a huge variety of different sources. These include especially the energy stored in trees, grass crops, forestry, vegetal coal, urban wastes, agricultural wastes and forestry wastes.

In terms of resource, biomass is very large, providing about 15 % of the world's primary energy. Biomass has a dominant position for the poor people in the world, who are dependent on wood fuel for cooking and heating. In fact, it plays an important role in developing countries that have large poorest regions. But it is also important in a number of industrialised countries, e.g. the United States, which obtains 4 % of its energy from biomass, and Sweden with 14 %.

The old way of converting biomass to energy, practiced for thousands of years, is simply to burn it to produce heat. This is still the use to which most biomass is put worldwide. The heat can be used directly, for heating, cooking and industrial processes, or indirectly, to produce electricity.

Advances in recent years have shown that there are more efficient ways to use biomass. It can be cooked in a process called gasification (not burning) to produce combustible gases, such as methane, or converted into liquid fuels. These liquid fuels, also called biofuels, include two forms of alcohol: ethanol and methanol.

There are many types of biomass but, in general, we can consider two different ones: biomass residues and dedicated energy crops (fast growing grasses and trees grown specifically for energy production). The former includes wood wastes from industrial wood users, forestry and agricultural residues and also urban wastes.

Wood is currently the largest source of biomass power. The largest users of wood for energy are the pulp and paper manufacturing, lumbermills and other industrial wood users are frequently used for producing biomass electricity. These industries feed wood chips and scraps to their boilers as fuel to produce steam, which is used directly in their manufacturing processes and also piped to a turbine generator for electric power production.

Agricultural wastes are also burned to produce electricity. These power generating wastes include bagasse (sugarcane residue), rice hulls, rice straw, nut shells, crop residues and prunings from orchards and vineyards. Just as in forestry, most crop residues are left in the field.

Besides the biomass resources discussed in the previous paragraphs (plants and trees), another form of biomass is associated more with cities than farms: municipal solid waste (MSW). People generate biomass wastes in many forms, including urban wood waste (like shipping pallets and leftover construction wood), the biomass portion of garbage (paper, food, leather, yardwaste, etc.) and the gas given off by landfills when biomass waste decomposes. Even sewage can be used as energy. Some sewage treatment plants capture the methane given off by sewage and burn it for heat and power.

Other sophisticated technologies of non-combustion methods for converting biomass into electricity are now being commercialised with the purpose to reduce emissions and

improve efficiency. These technologies have one thing in common: they convert raw biomass into a variety of gaseous, liquid or solid fuels before using it. The carbohydrates in biomass, which are compounds of oxygen, carbon and hydrogen, can be broken down into a variety of chemicals.

One example is biomass pyrolysis, which is the liquefaction of biomass with heat. If biomass is heated, but not burned, in the absence of oxygen, it forms a liquid that is a pyrolysis oil. The oil, which is easier to store and transport than solid biomass material, is then burned like petroleum to produce electrical energy.

Perhaps the ultimate use of biomass for power production is biomass gasification. Gasifiers use high temperatures to convert the biomass to a gas (a mixture of hydrogen, carbon monoxide and methane), which is then used to fuel a gas turbine. A gas turbine turns an electric generator to produce electricity. Because the gas turbines operate at very high efficiencies, the combination of a gasifier and a gas turbine will produce electricity more efficiently and more economically than do today's direct-burn plants. Their high efficiency allows these gasification plants to be built in places where the biomass resource is too limited to support one of today's direct-burn plants. This process generates about twice as much electricity as simply burning the raw biomass to produce steam for a steam turbine.

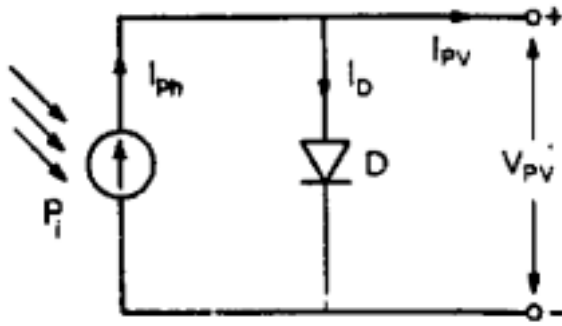
Alternatively, biomass derived methanol or hydrogen can be used in fuel cells, which can be large enough to power businesses or factories.

Municipal waste may also be used in many of the new processes developed: biomass pyrolysis to form gasoline additives or fuel oil substitute and biomass gasification for use with a gas turbine.

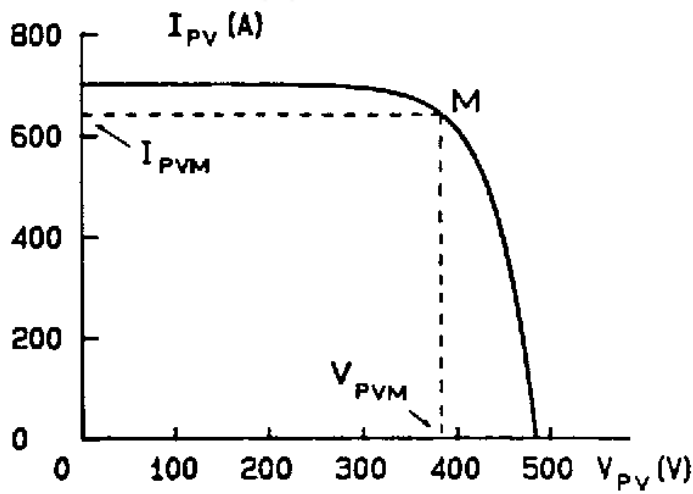
2.6 Photovoltaic Systems (PVs)

The PV technology uses semiconductor cells (wafers), each of which is basically a large area p-n diode with the junction positioned close to the top surface. The PV effect results in the generation of direct voltage and current from the light falling on the cell. Multiple cells are assembled in modules to generate sufficient voltage and current.

The simplified equivalent circuit of Fig.2.9 (a) is adequate for the representation of the PV cell. The output current is a function of solar radiation, temperature, wind speed and coefficients particular to the cell technology [8]. The form of I_{pv} as a function of the array output voltage V_{pv} (V-I characteristic of the array), is given in Fig. 2.9 (b). The maximum power output is obtained when the array operates at point M on the V-I characteristic.



(a)



(b)

Fig. 2.9 (a):PV cell equivalent circuit
(b) : Array V-I characteristic

Because much of the current PV technology utilizes crystalline semiconductor material similar to that used in integrated circuits, the cost of the PV cells has been quite high. Considerable research effort has been devoted during the last two decades in reducing the cost of the cells, without sacrificing excessively their efficiency. The end goal is a substantial reduction of the energy cost per kWh, which is a function of the energy conversion efficiency and the capital cost per Watt capacity.

The continuing development efforts to produce more efficient low cost cells have resulted in various types of PV technologies available in the market today, in terms of conversion efficiency and module cost. Monocrystalline silicon PV modules, widely available in the market, are highly efficient but also expensive, due mainly to their manufacturing process, but also to the fact that extremely pure “electronic-grade” polycrystalline silicon is used for their fabrication. Lower purity, “solar-grade”, silicon is now used, reducing significantly the cost, with only a small reduction in the conversion efficiency. Other,

more radical, approaches to reducing the cost of PV cells and modules have been under development during the past 20 years, such as the fabrication of cells using polycrystalline and semicrystalline materials, the use of amorphous silicon and other thin film materials (Copper Indium Diselenide, Cadmium Telluride etc.), the use of concentrating devices and other innovative approaches.

The advances in the cell manufacturing technologies and the decline in the cost of the other system components have permitted a significant reduction in the capital cost per Watt of installed capacity and thus to the final cost of PV electrical energy. The capital cost has declined during the last two decades from \$20 per Watt to less than \$5 per Watt, while the cost of PV electricity has declined from almost \$1 to less than \$0.20 per kWh and the installed capacity has exceeded 500 MW worldwide, approaching rapidly the 1 GW milestone.

However, the PV energy cost is still far from competing with the conventional sources (e.g. thermal power stations), even if the full “external” costs (environmental and safety issues) of conventional sources are taken into account. For this reason, PV installations are much more attractive in remote and isolated areas, where utility power is not available and the grid connection costs are prohibitive, while the solar radiation levels are high. Yet, grid-connected PVs, along with the other forms of dispersed energy generation, have found a useful role in modern power systems, for peak-shaving purposes, local grid reinforcement and generation of power nearest to the consumption.

Although the majority of the installed PV capacity is still off-grid, the percentage of grid-connected PV installations is rapidly increasing, either in the form of solar power stations or as building-integrated PV systems. Due to the fact that the PV power output matches well with the peak load demand, this tendency is gaining momentum and it is expected to contribute to the decrease of the cost of photovoltaic technologies.

The PV module or array is an unregulated dc power source, which has to be properly conditioned in order to interface it to the grid. For this purpose, a DC/AC inverter has to be used, while a DC/DC converter is also present at the array output for Maximum Power Point Tracking (MPPT) purposes, i.e. for extracting the maximum available power for a given insolation level. This means maintaining the voltage as close as possible to the maximum power point (maximum Power Point Tracking M in Figure 2.9 (b)). The block diagram of a typical grid-connected PV power station is shown in the following figure. It comprises the PV array, a DC/DC converter and the DC/AC inverter at the grid side. Multiple arrays may use the same DC/AC converter, or multiple converters may also be used. A battery storage system may be present at the DC bus, mainly in autonomous and small installations.

The role of the DC/DC converter (chopper) is to regulate the array output voltage (or current) so that the maximum available power is extracted (MPPT). The output stage (inverter) is functionally identical to the units used in other renewable energy converters, such as variable speed wind turbines. In older plants line-commutated units were common, due to their low cost, simplicity and reliability. In modern installations self-

commutated PWM inverters are utilized, basically of the voltage-source type, for their decisive advantages of output power factor control and low harmonic pollution.

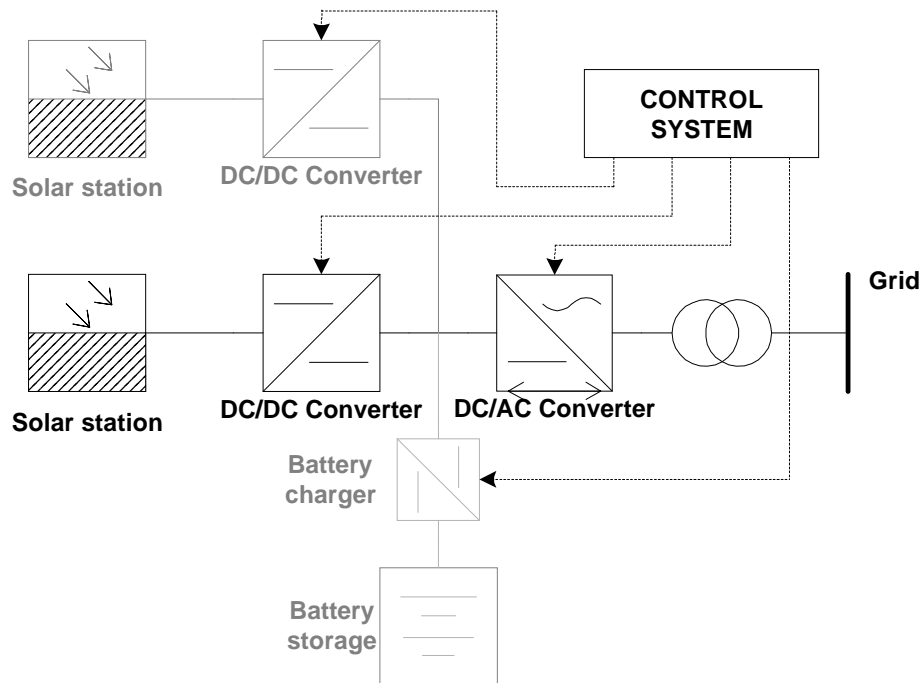


Figure 2.10 Basic PV operation

2.7 Solar Thermal

Solar thermal power plants make use of the thermal energy from the sun to heat a working fluid, which drives an engine or steam-turbine generator [3]. Concentrating mirrors or other reflective materials are used to focus the sunlight on a central vessel containing the working fluid. The three most prevalent types of solar thermal plants are the central receiver, parabolic dish, and parabolic trough systems. Like concentrating PV systems, solar thermal plants track the direct sunlight and are limited in application to arid, sunny climates.

- In a central receiver plant, anywhere from hundreds to thousands of heliostats are focused on a central vessel mounted on a large tower. The heliostats are long focal length glass mirrors or reflective stretched membranes. The receiver vessel absorbs the heat, driving the thermal generator with molten salt flowing through tubes (called salt-in-tube technology), air or fluids.
- The parabolic dish system uses satellite-dish shaped glass mirrors or reflective stretched membranes to concentrate light on a short-distance focal point where fluid is heated for a local heat engine or for contribution to a central system. The collector or engine is mounted directly on the concentrator and tracking apparatus, with power levels around 25 kW per unit.

- In a parabolic trough system, long glass-mirror parabolic troughs concentrate sunlight on a focal line, a tube containing the working fluid, which is then circulated to heat engines. Present parabolic trough systems are hybridized, using fossil fuel in a ranking cycle to supplement the intermittent solar resource.

Central receiver and parabolic trough systems are considered bulk generation due to their size and centralized engine systems. Dish systems with mounted engines are inherently modular.

2.8 Geothermal

Geothermal energy is, after hydro-power and biomass, the third most exploited renewable energy source with more than 6000 MW installed generation capacity in 21 different countries. Geothermal energy abstracts heat from the earth's crust from either pre existing aquifer, or inject water flow in the case of Hot Dry Rock technology. The latter is still in the early stages of development and is not yet commercially exploited.

Energy conversion can be either via mechanical means or the heat can be used directly. Geothermal energy is in one sense only partially renewable, since the reservoir of the heat that is being tapped into is not usually replenished at the rate that energy is extracted. However it does represent a natural energy flow.

Hot aquifers are found in many areas usually associated with the volcanic activity found near tectonic plate boundaries. The mean earth surface value for Geothermal heat emission is only 0,01-0,05 Wm⁻², but there are very great variations in the energy flux, e.g. the Geysers.

Depending on the temperature and pressure of aquifer, the fluid may emerge as either dry steam or hot water under pressure that, in this case, needs to be flashed to steam. For dry steam cases, energy conversion technology involves the following main steps:

- 1 - Steam or hot water under pressure is derived by a borehole from underground aquifers and is after transmitted by pipelines to the power plant;
- 2 - Cyclone separators are used to remove particulate matters, drain pots, along the pipes, are used to remove condensates and moisture separators are also used to "clean" the steam;
- 3 - Steam is then released in a turbine, mechanically coupled to an electrical generator;
- 4 - geothermal fluids can then be released in rivers, but nowadays re-injection is often used.

There are three designs for geothermal power plants, all of which pull hot water and steam from the ground, use it, and then return it as warm water to prolong the life of the heat source. In the simplest design, the steam goes directly through the turbine, then into a condenser where the low-temperature steam is condensed into water. In a second approach, the steam and hot water are separated as they come out of the well; the steam is used to drive the turbine while the water is sent directly back underground.

In the third approach, called a binary system, the hot water and steam mixture is passed through a heat exchanger, where it heats a second liquid (like isobutane) in a closed loop.

The isobutane boils at lower temperatures than water, so as steam it is used to drive the turbine. The three systems are shown in Figure 2.8.

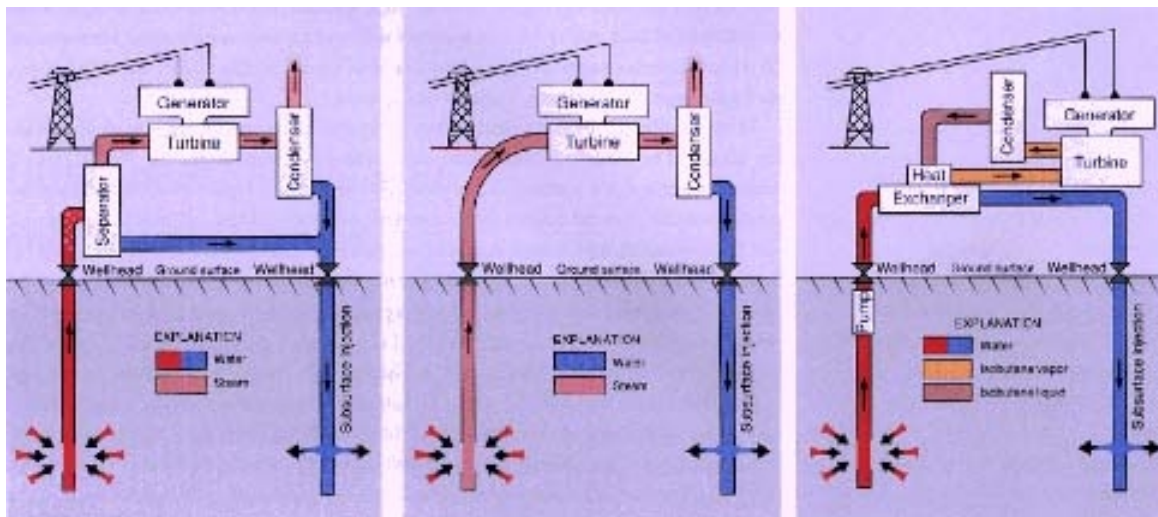


Figure 2.8 - Types of geothermal power plants

The choice of which design to use is determined by the resource. If the water comes out of the well as steam, it can be used directly, as in the first design. If it is hot water, it must go through a heat exchanger. Since there are more hot water resources than pure steam, there is more growth potential in the heat exchanger design.

The largest geothermal system now in operation is a steam-driven plant in an area called The Geysers, north of San Francisco. Despite the name, there are actually no geysers here, and the heat that comes out of the ground is all steam, not hot water. Although the area was known for its hot springs as far back as the mid-1800s, the first well for power production was drilled in 1924. Deeper wells were drilled in the 1950s, but real development didn't occur until the '70s and '80s. By 1990, 26 power plants had been built, for a capacity of over 2,000 megawatts. In 1992, the area produced enough power for a city of 1.3 million.

Because of the rapid development of the area in the '80s, and the technology used, the steam resource has been declining since 1988. In the Geysers, the plants use an evaporative water-cooling process to create a vacuum that pulls the steam through the turbine, producing power more efficiently. But this process loses 60 to 80 percent of the steam to the air, not reinjecting it underground. While the steam pressure may be declining, the rocks underground are still hot. Some efforts are under way to remedy the situation, including reinjecting water pumped in through a 26-mile pipeline, and replacing the water-cooled systems with air-cooled.

Geothermal plants of considerable installed capacities also exist in islands, using synchronous generators. In general, in normal operation they are no source of concern

either from the steady state or dynamic point of view. However, in what regards expansion planning these plants should be treated carefully, as they become a source of uncertainty regarding the amount of power that can be obtained in the future because the power that can be obtained can be reduced with time namely due to problems in the drill pipe sections.

As the investment needed to build an industrial geothermal power plant is, in general, large, these plants have at least an installed capacity of a few tens of MWs.

2.9 Superconducting Magnetic Energy Storage Systems (SMES)

SMESS technology requires two basic components, conversion equipment to convert ac to low voltage, high current dc and back to ac plus a superconducting coil to store high levels of dc current. Designs have been developed using either current source converters or voltage source converters with choppers to convert ac to dc and back to ac. Converter technology with pulse-width modulation is continuing to be developed with lower losses and higher reliability. The converter costs are based on the maximum power exchange with the system and are not significantly affected by the amount of energy stored in the superconducting coils.

The superconducting coils have also been developed and implemented in small applications. Some larger prototypes have been tested, but at the present only small systems around one MVA or less are commercially available. One limitation is the cost of the superconducting coils for large energy storage. Due to these costs, current applications of SMES for power quality improvement generally only provide a few seconds of stored energy.

A SMES system can basically control the real and reactive power exchange with the ac system. The SMES is a fast controllable device which can either absorb or supply real and reactive power. With the energy storage typically limited to a few seconds, the SMES can only provide reactive power control in steady-state and in steady-state simulations can be modeled similar to an SVC or synchronous condenser which control voltage by varying the reactive power between the maximum and minimum limits.

Model Development

For dynamic simulations, a controller must be developed which simulates the control strategy and supplemental controls of the SMES in order to provide the proper real and reactive power exchange with the system for which the SMES is designed. Besides the control of the power exchange, the maximum and minimum power exchange with the system must be kept within limits and the total energy available for exchange with the system must be observed. The maximum power exchange with the system is generally a function of the converter design and capability while the energy stored is the capability of the superconducting coil. For studies on the performance of an interconnected ac system, the details of the converter and superconducting coil are not important beyond developing the proper limits for the power exchange and available energy.

The same considerations will apply to any energy storage model using converters to exchange energy with the ac system.

If SMES were to become widespread on the distribution system, the main impact is to prevent loads from tripping during faults and help support the voltage during and after a disturbance. By providing temporary power and voltage support during a fault, motors at the SMES locations will not slow and then drag down the voltage as they re-accelerate following fault clearing. Following the disturbance, the SMES can also provide reactive power support to boost low voltages on the system. In an aggregate model of the loads, this may mean that it will not be as important to model the dynamic induction motor effects since they will not be affected by the fault.

2.10 Battery Energy Storage Systems (BESS)

The following is a brief list of the main technologies that have been used or proposed for energy storage applications [3,10]:

a) Lead-acid batteries are typically inexpensive and can be produced in the large capacities that are often required for energy storage. They can be designed for short, high rate discharges or for bulk energy storage. Vented lead-acid batteries are the traditional ‘wet’ or ‘flooded’ types. In the last 20 years, valve-regulated lead-acid (VRLA) batteries have come to dominate the stationary battery market, particularly in telecommunications.

b) Nickel-Cadmium (Ni-Cd) batteries provide very long lives in stationary applications and are typically quite resistant to abuse. Their cost is typically rather high and this limits their application to the most demanding duties. For stationary applications, almost all Ni-Cd batteries are flooded types.

c) Nickel-Metal Hybride (NiMH) batteries represent a newer technology that has been used extensively in portable applications. In recent years, large injections of money have been made to support scaling up of the technology for electric vehicle applications. The principal advantage of NiMH over Ni-Cd is a higher energy density.

d) Lithium ion batteries are the newest types and are also very different from the others. They are non-aqueous and their chemistry is simply the passage of lithium ions from one electrode to the other through an organic electrolyte, inserting and deinserting in the microstructure of the electrodes. Development and industrialization is still in process, but Li ion batteries promise very high energy density, good cycling capability and the possibility of long life in stationary applications.

e) Lithium polymer batteries include lithium ion technology and related chemistries using metallic lithium negatives. In all cases, the electrodes are bonded together with a polymer matrix to form a thin laminar construction. Most portable batteries of this type use lithium ion chemistry and have a liquid electrolyte in the polymer matrix. This gives benefits in energy density, by avoiding the use of heavy cell casings.

The battery requirements for energy storage are: high energy density, high power, high charge efficiency, good cycling capability, long life and low initial cost. The bulk of existing utility-scaled battery storage systems are made up of large numbers of lead-acid cells, utilizing technology similar to that found in automobile batteries. A typical battery is composed of one to six 2-volt cells. Large battery plants combine hundreds to thousands of batteries in series and parallel strings and interconnect to the utility via an electronic interface. Today there are dozens of utility-scaled battery plants built for load-leveling and dynamic applications, the largest of which is a 10 MW – 40 MWhr plant operated by Southern California Edison in Chino. In 1997 a 6 MW, 48 MWh sodium/sulfur (NaS) battery was installed at a TEPCO substation in Japan and a second like energy storage plant was fabricated and installed in 1999 at the TEPCO Ohito substation.

Flow batteries, sometimes known as redox batteries, flow cells or regenerative fuel cells are a special kind of electrochemical device, lying between a secondary battery and a fuel cell. In common with a secondary battery they can be charged and discharged. Fuel cells can deliver power for as long as they are supplied with fuel and an oxidising agent. Flow batteries can deliver power as long as they are supplied with charged electrolytes. The polysulphide/bromide technology known as Regenesys has been developed by National Power in UK. Modules of varying sizes (5-100 kW) have been assembled and tested. The Regenesys technology is particularly well suited to large scale applications and construction of a 120 MWh utility scale plant is due to start in 2000. The plant will comprise a number of modules nominally rated at 100 kW and will have a peak output of 14.75 MW. It will be sited on a UK power station and be used for energy management and provision of ancillary services.

2.11 Flywheels

A flywheel is an electromechanical storage system in which energy is stored in the kinetic energy of a rotating mass [3]. Flywheel systems under development include those with steel flywheel rotors and resin/glass or resin/carbon-fiber composite rotors. In both systems the momentum of the rotating rotor stores energy. The rotor contains a motor/generator that converts energy between electrical and mechanical forms. In both types of systems the rotor operates in vacuum and spins on bearings to reduce friction and increase efficiency. Steel-rotor systems rely mostly on the mass of the rotor to store energy while composite flywheels rely mostly on speed. During charging, electric current flows through the motor increasing the speed of the flywheel. During discharge, the generator produces current flow out of the system slowing the wheel down.

Steel flywheel systems are currently being marketed in US and Germany and can be connected in parallel to provide greater power, if required. Sizes range from 40 kW to 1.6 MW for 5-120 seconds. The suppliers of the composite type flywheel systems are currently in the prototype stages of development.

Flywheel energy storage combined with micro-sources provides peak power and ride-through capabilities during disturbances. A flywheel energy storage, when integrated into weak grid-connected and autonomous power systems supplied from wind turbines generators and/or other renewable energy sources can provide an effective short-term storage for filtering wind power fluctuations due to wind turbulence and unpredictable load-leveling. Other power disturbances caused by the turbine tower shadow, wind shear, rotational sampling and drive train resonance can also be reduced when the flywheel system is combined with a fast response power electronic interface. In addition, the storage system can be capable of working as a reactive power source/sink according to power system requirements. The relevant equations are provided in Section 4.12.

Chapter 3

Stability Modeling

3.1 Types of stability

Power system stability is that property of a power systems which enables it to remain in a state of operating equilibrium under normal operating conditions and to regain an acceptable state of equilibrium after being subjected to a disturbance [11].

Rotor angle stability is concerned with the ability of interconnected synchronous machines of a power system to remain in synchronism under normal operating conditions and after being subjected to a disturbance. It depends on the ability to maintain/restore equilibrium between electromagnetic torque and mechanical torque of each synchronous machine in the system. Instability that may result occurs in the form of increasing angular swings of some generators leading to their loss of synchronism with other generators.

- (a) Small signal stability is concerned with the ability of the power system to maintain synchronism under small disturbances. The disturbances are considered to be sufficiently small that linearization of system equations is permissible for purposes of analysis.
- (b) Transient stability is concerned with the ability of the power system to maintain synchronism when subjected to a severe transient disturbance. The resulting system response involves large excursions of generator rotor angles, and is influenced by the non-linear power-angle relationship.

Voltage stability is concerned with the ability of a power system to maintain steady acceptable voltages at all buses in the system under normal operating conditions and after being subjected to a disturbance. Instability may occur in the form of a progressive fall or rise of voltage of some buses. The main factor causing voltage instability may occur in the form of a progressive fall or rise of voltage of some buses. The main factor causing voltage instability is the inability of the power system to maintain a proper balance of reactive power throughout the system.

- (a) Large disturbance voltage stability is concerned with a system's ability to maintain steady voltages following large disturbances.
- (b) Small disturbance voltage stability is concerned with a system's ability to control voltages following small perturbations, such as incremental changes in system load.

Frequency stability is the ability of a power system to maintain the frequency within a nominal range, following a severe system upset which may or may not result in the system being divided into subsystems. It depends on the ability to restore balance between system generation and load with minimum loss of load.

The various types of instability can be classified according to the relevant size of disturbance and time span in the following diagram.

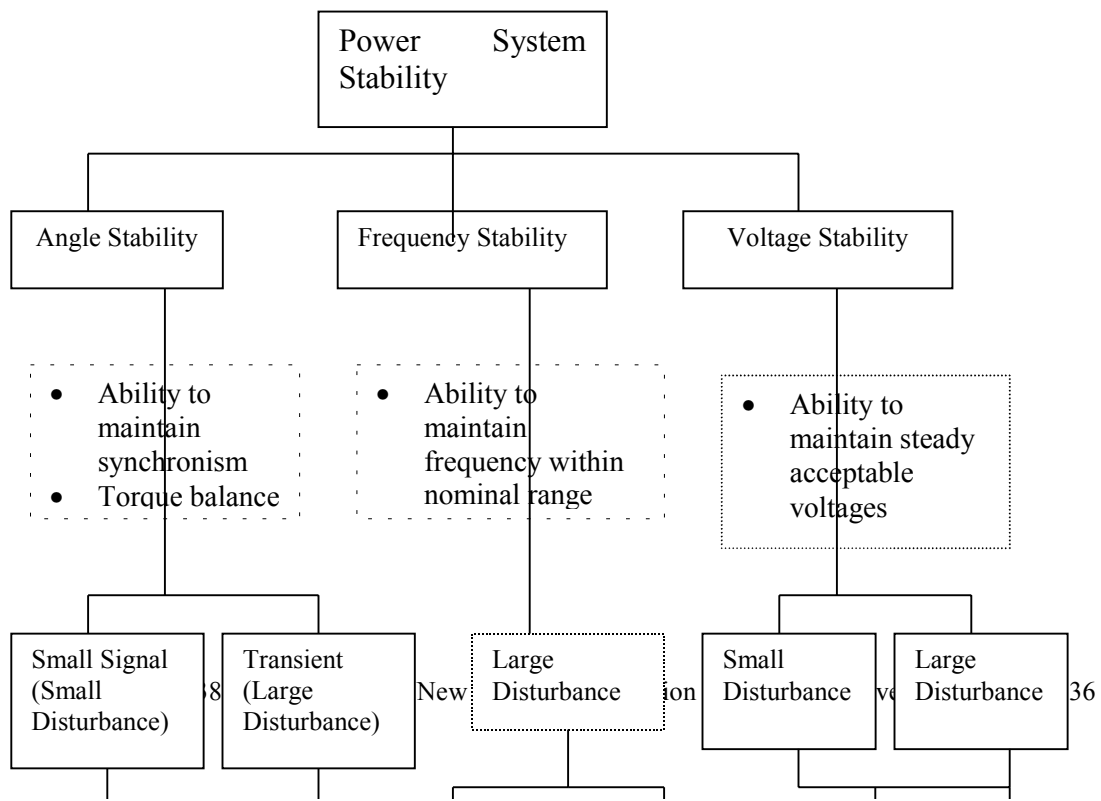


Figure 3.1

3.2 Stability Problems related to New Forms of Generation and Storage

The integration of new forms of Generation and Storage Systems can affect significantly all types of stability, i.e. angle, frequency and voltage stability. As discussed in the introduction, the majority of these power sources are connected at the distribution level.

Modern distribution systems were designed to accept bulk power from the transmission network and to distribute it to customers. Thus the flow of both real power and reactive power was always from the higher to the lower voltage levels. However, with significant penetration of embedded generation the power flows may become reversed and the distribution network is no longer a passive circuit supplying loads but an active system with power flows and voltages determined by the generation as well as the loads. The change in real and reactive power flows caused by embedded generation has important technical and economic implications for the power system [12].

Traditionally, distribution network analysis did not need to consider issues of stability as the network was passive and remained stable under most circumstances provided the transmission network was itself stable. Further, for early embedded generation schemes, whose object was to generate kWh from new renewable energy sources, considerations of generator transient stability tended not to be of great significance. If a fault occurred somewhere on the distribution network to depress the network voltage and the embedded generator tripped then all that was lost was a short period of generation. The embedded generator tended to overspeed and trip on its internal protection. The control scheme of the embedded generator then waited for the network conditions to be restored and then re-start automatically. Of course if the generation scheme is intended mainly as a provider of steam for a critical process then more care is required to try to ensure that the generator does not trip for remote network faults. However, as the inertia of embedded generation plant is often low and the tripping time of distribution protection long it may not be possible to ensure stability for all faults on the distribution network. A particular problem in some countries is nuisance tripping of rocof relays. These are set sensitively to detect islanding but, in the event of a major system disturbance, e.g. loss of a large

central generator, mal-operate and trip large amounts of embedded generation. The effect of this is, of course, to depress the system frequency further.

Synchronous generators will pole-slip during transient instability but when induction generators overspeed they draw very large reactive currents which then depress the network voltage further and lead to voltage instability. The steady-state stability limit of induction generators can also limit their application on very weak distribution networks as a very high source impedance, or low network short circuit level, can reduce their peak torque to such an extent that they cannot operate at rated output.

In most countries at present, stability is hardly considered when assessing embedded renewable generation schemes. However, this is likely to change as the penetration of renewable increases and their contribution to network security becomes greater. The areas which need to be considered include angle and voltage stability. In isolated systems normally operated on islands, frequency stability issues become of major concern. In this case the consequence of a sudden trip of a large amount of embedded generation on the dynamic performance of the system must be carefully studied. Thus, a network failure, a conventional generator trip or other disturbing network conditions may cause a dropout of a large number of Dispersed Generators, which would cause a major lack of generation and temporary drop in frequency. In the case of a large integration of wind power, fast wind changes and very high wind speeds may result in the sudden loss of production causing frequency excursions and dynamically unstable situations. This is due to the fact that frequency oscillations might easily activate the frequency protection relays of the windfarms. Setting of a too high under-frequency protection makes severe situations after a generation dropout even worse, because the frequency relays may disconnect the Dispersed Generators and even increase the lack of generation. This might lead to frequency instability and eventually collapse of the system [13,14].

3.3 Generic Model

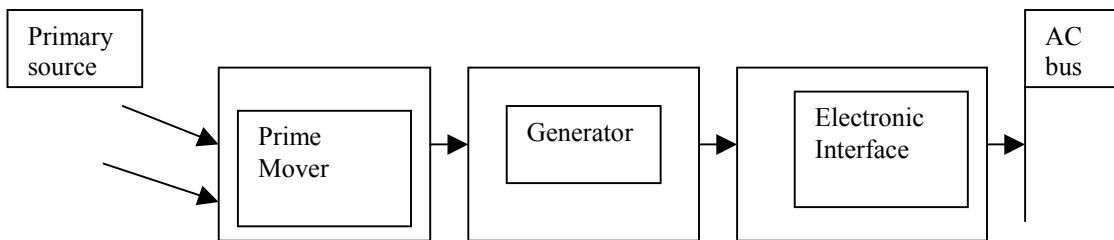


Figure 3.2 Generic Model

Based on the state of the art description of Chapter 2 the following Table 3.1 is provided:

DS Technology	Primary Source	Prime Mover	Electrical Generator	Electronic Interface
---------------	----------------	-------------	----------------------	----------------------

WECS	Wind	Yes	Yes	Yes (optional)
HP	Water	Yes	Yes	No
Micro Turbines	Diesel or gas	Yes	Yes	Yes (optional)
Fuel Cells	Hydrogen	No	Yes (optional)	Yes
Biomass	Biomass	Yes	Yes	No
Photovoltaics	Sun	No	No	Yes
Solar Thermal	Sun	Yes?	Yes	No
Geothermal	Earth Temper.	Yes?	Yes	No
SMES	storage	No?	No?	Yes
BES	storage	No	No	Yes
Flywheels	Storage	Yes	Yes (optional?)	Yes

Table 3.1

The EPRI study [3] provides the following table of impacts according to the type of interface:

DS Type	Voltage Control	T&D line loading	Control of dispersed systems	Harmonics	Voltage surges and dips	Protection
Direct Interface: Solar Thermal, WECS, Small HP, CAES, Thermal Storage	Control at PCC is function of real power output of the plant	Loading reduced to extent (in kW) resource operated during high load periods	Start-up, control and shutdown control of generators well known.	Not considered a problem with most 3 phase rotating generators	Generator windings well-suited to handle voltage excursions	Standards well known and documented
Electronic Interface Fuel Cell, PV BES, SMES WECS	Control at PCC is function of real power output and dispatchable reactive power of the plant	Loading reduced to extent resource operated during high load periods; Reactive power available to optimize total KVA.	Generally, fast response control is inherent in electronic interface based systems. Output variation control of intermittent resource systems is limited	Older technologies require heavy filtering – Advanced technologies cleaner, but higher order harmonics still need consideration. Cancellation of externally	Historically sensitive to excursions – advanced types more flexible – can be designed to provide ride-through capability	Standard relay schemes can be applied to electronic interface – trend is to allow internal software based schemes.

				created harmonics possible.		
--	--	--	--	-----------------------------	--	--

Table 3.2 Impacts by Type of Interface [3]

Taking into account the scope of the Task Force in modelling power system stability effects, there is varying interest in modelling the primary source and mechanical system behavior among the various DG technologies. For example, Geothermal systems provide stable output and their dynamic modeling for stability studies is trivial. From a stability point of view, Biomass systems are basically the same as conventional power plants. In all systems involving electrical generators, the following standard machine models can be used.

3.4 Electrical Generator Models

Geothermal, Biomass, Hydro Power, Micro Turbine and most Wind Energy Conversion, Fuel Cell (optional) and Flywheel (optional) systems employ synchronous or asynchronous generators. Their modeling characteristics depend on the generator type (induction, synchronous, etc.), the governor controls and VAR compensation included (if any). Well known mathematical representations (equivalent circuits) are regularly used in dynamic stability studies [17]. These are reviewed in this Section.

3.4.1 Synchronous Generator

The equations of a synchronous machine in the rotor's qd0 reference frame are the following:

$$\begin{aligned}
 u_q &= r_s i_q + \frac{d\lambda_q}{dt} + \lambda_d \frac{d\theta_r}{dt} \\
 u_d &= r_s i_d + \frac{d\lambda_d}{dt} - \lambda_q \frac{d\theta_r}{dt} \\
 u_0 &= r_s i_0 + \frac{d\lambda_0}{dt} \\
 u'_f &= r'_f i'_f + \frac{d\lambda'_f}{dt} \\
 u'_{kd} &= r'_{kd} i'_{kd} + \frac{d\lambda'_{kd}}{dt} \\
 u'_g &= r'_g i'_g + \frac{d\lambda'_g}{dt}
 \end{aligned} \tag{3.1}$$

$$u'_{kq} = r'_{kq} i'_{kq} + \frac{d\lambda'_{kq}}{dt}$$

Where the flux linkages are given in Wb.turn by

$$\begin{aligned}\lambda'_q &= L_q i'_q + L_{mq} i'_g + L_{mq} i'_{kq} \\ \lambda'_d &= L_d i'_d + L_{md} i'_f + L_{md} i'_{kd} \\ \lambda'_o &= L_{ls} i'_o \\ \lambda'_f &= L_{md} i'_d + L_{md} i'_{kd} + L'_{ff} i'_f \\ \lambda'_{kd} &= L_{md} i'_d + L_{md} i'_f + L'_{kd} i'_{kd} \\ \lambda'_g &= L_{mq} i'_q + L'_{gg} i'_g + L_{mq} i'_{kq} \\ \lambda'_{kq} &= L_{mq} i'_d + L_{mq} i'_g + L'_{kq} i'_{kq}\end{aligned}\quad (3.2)$$

and

$$\begin{aligned}i'_f &= \frac{N_f}{N_s} i_f = \frac{2}{3} \frac{N_f}{N_s} i_f \\ i'_{kd} &= \frac{N_{kd}}{N_s} i_{kd} = \frac{2}{3} \frac{N_{kd}}{N_s} i_{kd} \\ i'_{kq} &= \frac{N_{kq}}{N_s} i_{kq} = \frac{2}{3} \frac{N_{kq}}{N_s} i_{kq}\end{aligned}\quad (3.3)$$

$$u'_f = \frac{N_s}{N_f} u_f \quad u'_{kd} = \frac{N_s}{N_{kd}} u_{kd}$$

$$u'_g = \frac{N_s}{N_g} u_g \quad u'_{kq} = \frac{N_s}{N_{kq}} u_{kq}$$

$$\lambda'_f = \frac{N_s}{N_f} \lambda_f \quad \lambda'_{kd} = \frac{N_s}{N_{kd}} \lambda_{kd}$$

$$\begin{aligned}\lambda'_g &= \frac{N_s}{N_g} \lambda_g & \lambda'_{kq} &= \frac{N_s}{N_{kq}} \lambda_{kq} \\ r'_f &= \frac{3}{2} \left(\frac{N_s}{N_f}\right)^2 r_f & r'_{kd} &= \frac{3}{2} \left(\frac{N_s}{N_{kd}}\right)^2 r_{kd} \\ r'_g &= \frac{3}{2} \left(\frac{N_s}{N_g}\right)^2 r_g & r'_{kq} &= \frac{3}{2} \left(\frac{N_s}{N_{kq}}\right)^2 r_{kq}\end{aligned}$$

The generator electromagnetic torque is given in N.m by:

$$T_{em} = \frac{3P}{22} (\lambda_d i_q - \lambda_q i_d) \quad (3.4)$$

Explanation of notation needed

3.4.2 Induction Generator

The induction generator is simulated by the standard 4th order dq model, the equations of which are the following, expressed in p.u., in the arbitrary reference frame:

$$\begin{aligned}u_{sd} &= -r_s i_{sd} - \omega \lambda_{sq} + p \lambda_{sd} \\ u_{sq} &= -r_s i_{sq} + \omega \lambda_{sd} + p \lambda_{sq} \\ u_{rd} &= 0 = r_r i_{rd} - (\omega - \omega_r) \lambda_{rq} + p \lambda_{rd} \\ u_{rq} &= 0 = r_r i_{rq} + (\omega - \omega_r) \lambda_{rd} + p \lambda_{rq}\end{aligned} \quad (3.5)$$

The flux linkages $\lambda_{sd}, \lambda_{sq}, \lambda_{rd}, \lambda_{rq}$ are given by

$$\begin{aligned}\lambda_{sd} &= -X_s i_{sd} + X_m i_{rd} \\ \lambda_{sq} &= -X_s i_{sq} + X_m i_{rq} \\ \lambda_{rd} &= -X_m i_{sd} + X_r i_{rd} \\ \lambda_{rq} &= -X_m i_{sq} + X_r i_{rq}\end{aligned} \quad (3.6)$$

where $\omega_0 = 2\pi 50 \text{ rad/sec}$ the base electrical angular frequency
 ω the arbitrary dq frame angular frequency (p.u.)
 ω_r the generator speed (p.u.)
 u_{sd}, u_{sq} the stator voltage d and q components (p.u.)
 $i_{sd}, i_{sq}, i_{rd}, i_{rq}$ the stator and rotor d and q windings currents (p.u.)
 r_s, r_r the stator and rotor windings resistance
 X_s, X_r the stator and rotor windings reactance
 X_m the magnetizing reactance
 $p \equiv (1/\omega_0)(d/dt)$

Substituting (4.2) in (4.1) and solving for the derivatives of the currents, the state equations of the machine with the currents as state variables are derived:

$$\frac{d}{dt} \begin{bmatrix} i_{sd} \\ i_{sq} \\ i_{rd} \\ i_{rq} \end{bmatrix} = \frac{\omega_0}{D} \begin{bmatrix} -r_s X_r & (\omega D + \omega_r X_m^2) & -r_r X_m & -\omega_r X_r X_m \\ -(\omega D + \omega_r X_m^2) & -r_s X_r & \omega_r X_r X_m & -r_r X_m \\ -r_s X_m & \omega_r X_s X_m & -r_r X_s & (\omega D - \omega_r X_s X_r) \\ -\omega_r X_s X_m & -r_s X_m & -(\omega D - \omega_r X_s X_r) & -r_r X_s \end{bmatrix} \begin{bmatrix} i_{sd} \\ i_{sq} \\ i_{rd} \\ i_{rq} \end{bmatrix} + \frac{\omega_0}{D} \begin{bmatrix} -X_r & 0 \\ 0 & -X_r \\ -X_m & 0 \\ 0 & -X_m \end{bmatrix} \begin{bmatrix} u_{sd} \\ u_{sq} \end{bmatrix} \quad (3.7)$$

where $D = X_s X_r - X_m^2$.

The generator electromagnetic torque T_e is given by

$$T_e = \Psi_{rd} i_{rq} - \Psi_{rq} i_{rd} = X_m (i_{sq} i_{rd} - i_{sd} i_{rq}) \quad (3.8)$$

where all quantities are expressed in p.u. and generator convention is assumed for T_e .

The 2nd order “transient” model of the induction generator is also used, mainly in stability studies of large systems. Its equations are described in the following.

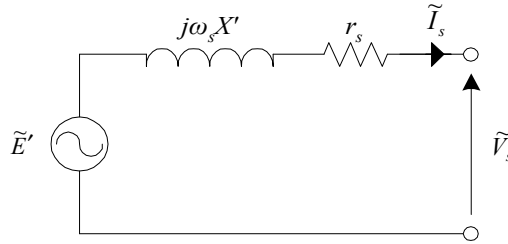


Figure 3.3 Induction generator transient equivalent circuit.

The stator equivalent circuit is shown in Figure 3. Its equations are

$$\begin{aligned} u_{sd} &= -r_s i_{sd} + \omega_s X' i_{sq} + E_d' \\ u_{sq} &= -r_s i_{sq} - \omega_s X' i_{sd} + E_q' \end{aligned} \quad (3.9)$$

where ω_s is the electrical frequency of the stator voltage

X' the transient reactance defined as $X' = X_s - \frac{X_m^2}{X_r}$ and

E_d' , E_q' the transient EMFs, defined by

$$\begin{aligned} E_d' &= -\omega_s \frac{X_m}{X_r} \lambda_{rq} \\ E_q' &= \omega_s \frac{X_m}{X_r} \Psi_{rd} \end{aligned} \quad (3.10)$$

State equations of the model, with the rotor flux linkages as state variables are:

$$\begin{aligned}\frac{d\lambda_{rd}}{dt} &= \omega_0 \left[-r_r \frac{X_m}{X_r} i_{sd} - \frac{r_r}{X_r} \lambda_{rd} + (\omega - \omega_r) \lambda_{rq} \right] \\ \frac{d\lambda_{rq}}{dt} &= \omega_0 \left[-r_r \frac{X_m}{X_r} i_{sq} - \frac{r_r}{X_r} \lambda_{rq} - (\omega - \omega_r) \lambda_{rd} \right]\end{aligned}\quad (3.11)$$

The generator electromagnetic torque T_e is given by (4.4), which can also be written as

$$T_e = \frac{X_m}{X_r} (\lambda_{rd} i_{sq} - \lambda_{rq} i_{sd}) \quad (3.12)$$

An alternative formulation of the model differential equations, frequently used when the change of the system frequency ω_s can be neglected, are the following, expressed in the synchronous reference frame:

$$\frac{dE'_d}{dt} = -\frac{1}{T'} [E'_d - (X_s - X') i_{sq}] + s \omega_s E'_q \quad (3.13)$$

$$\frac{dE'_q}{dt} = -\frac{1}{T'} [E'_q + (X_s - X') i_{sd}] - s \omega_s E'_d$$

where s is the slip, defined as $s = \frac{\omega_s - \omega_r}{\omega_s}$ and

$$T' \text{ the transient time constant, } T' = \frac{L_r}{r_r}$$

In such a case, if the drive train is modelled by a single inertia, the swing equation can be written as:

$$\frac{ds}{dt} = \frac{1}{2H} (T_g - T_m) \quad (3.14)$$

3.5 Electronic Interface Models

3.5.1 Introduction

A typical structure of a power source with a converter interface is shown in Figure 3.4. The energy source may be a DC-power source by itself (e.g. BES, PV etc.) or an AC source, which is rectified into DC (a wind turbine, a micro-turbine etc.). In any case, the source itself may include other power electronics converters (AC/DC and DC/DC), in order to create and/or regulate the DC voltage or current.

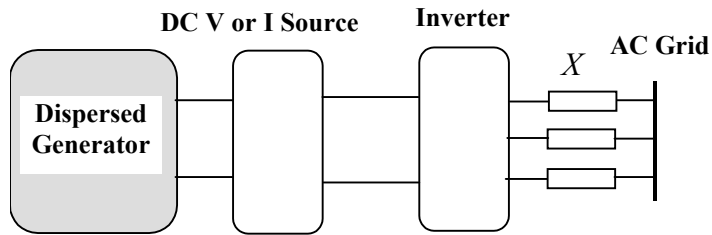


Figure 3.4. *Typical converter interface to grid*

Although it is not possible to derive a general model, which would represent with sufficient accuracy the dynamics of all possible converter interfaces, some general principles and typical examples are presented in the following, concentrating on the schemes most common in practice. In the following section the modelling and control of the grid side converter is addressed. Subsequently, a discussion is made on the control of the power converter at the dispersed generator side for the case of a wind turbine.

3.5.2 Grid-Side Converter

In Figure 3.5 the most commonly used scheme is illustrated, utilizing a voltage source DC/AC converter. Nevertheless, other types of converter interfaces (such as current source inverters or converter cascades used in the rotor circuits of doubly fed induction generators) are also used in practice and require a different modeling approach, not covered in the following.

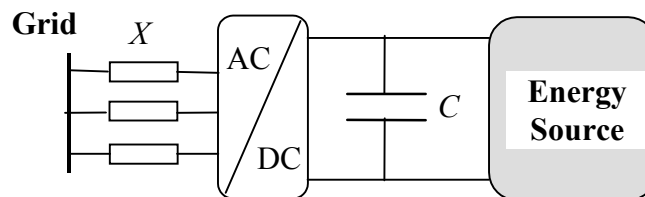


Figure 3.5. *Typical converter interface to grid*

First the operating and control principle of such a device is outlined and average value models are presented (i.e. non-fundamental frequency components are neglected), since they are simpler, more general and often suffice for examining the interaction between the dispersed generation and the power system.

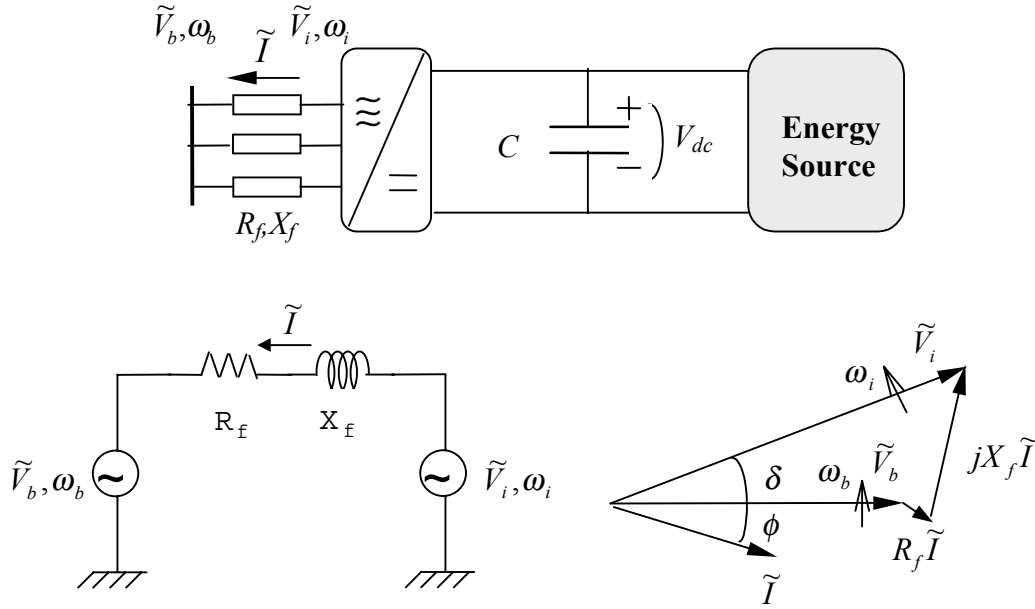


Figure 3.6. Fundamental frequency equivalent circuit and phasor diagram for the output converter.

In Figure 3.6, the fundamental frequency simplified diagrams are shown for the voltage source DC/AC converter. The active and reactive power at the output is given by the following relations:

$$P = \frac{V_i V_b}{X_f} \sin(\delta)$$

$$Q = \frac{V_i^2}{X_f} - \frac{V_i V_b}{X_f} \cos(\delta)$$

The active power P is predominantly dependent on the power angle δ between the inverter and grid voltage phasors, while Q is mainly determined by the inverter voltage magnitude V_i .

The control of the active and reactive power flow to the grid is performed by the DC/AC converter. In the case of a voltage source inverter, the controlled variables are the frequency ω_i and the magnitude V_i of the fundamental component of its AC voltage, which is synthesized by properly switching on and off its valves (usually IGBTs). The relatively decoupled regulation of P and Q permits the implementation of the control principle schematically illustrated in Figure 3.7. The active and reactive power regulation loops are independent, but not fully decoupled.

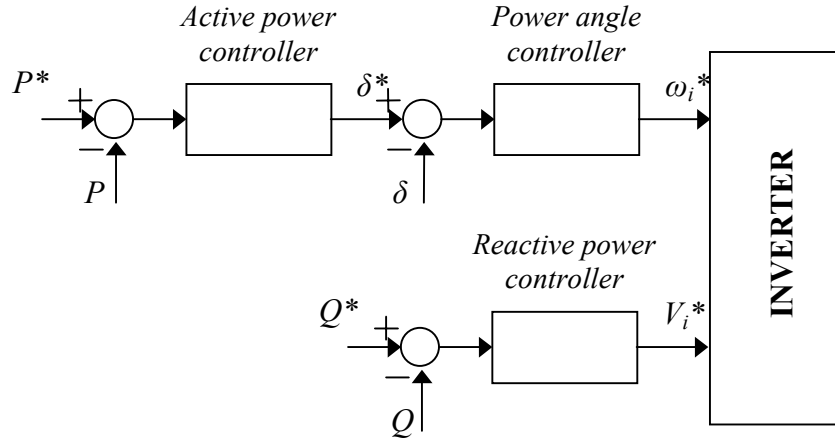


Figure 3.7. Active and reactive output power control principle for the voltage source inverter of Figure 3.6.

P^* and Q^* are the setpoints for the output active and reactive powers, P and Q , whereas the actual P and Q , along with the power angle δ , are calculated from measurements of the phase voltages and currents.

The determination of the P^* and Q^* reference values depends on the specific application and installation considered. A usual practice is to utilize the Q^* input in order to maintain constant output power factor (often unity, hence $Q^*=0$). Alternatively, Q^* may be varied in order to regulate -or simply support- the bus voltage at (or near to) the output of the converter, provided that the current rating of the converter permits it. This is shown in the block diagram of Figure 3.8, where V_b^* is the desired bus voltage level. If the DC voltage source is not stiff, the P^* input can be used for regulating the DC bus voltage, as shown in Figure 3.8, where V_{dc}^* is the DC voltage setpoint. If the converter active output power exceeds the instantaneous supply of the energy source, the DC capacitor is discharged, and vice versa.

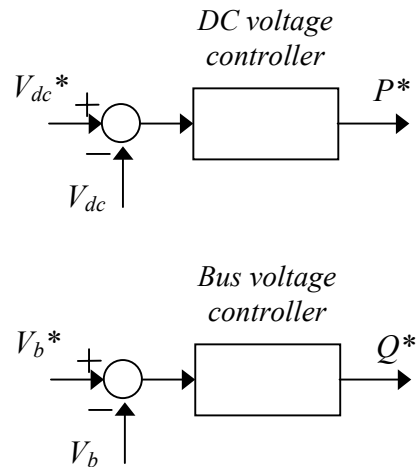


Figure 3.8. DC voltage and power system voltage regulation using inputs P^* and Q^* respectively of the DC/AC converter.

Lately, with the advent of fast switching elements at high power levels, such as IGBTs, the current control principle is increasingly favored, among other things due to its inherent superiority in case of grid disturbances, such as faults, voltage dips etc. If the DC/AC converter is current controlled, then the full decoupling of the active and reactive power regulation loops can be easily achieved, employing the vector control principle, as shown in Figure 3.9.

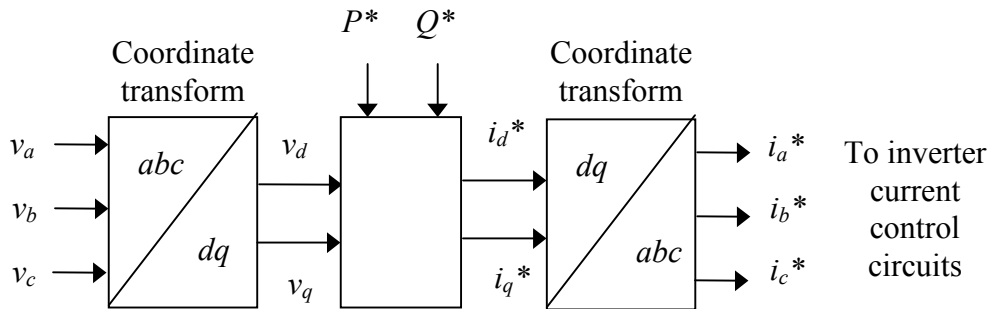


Figure 3.9. Active and reactive power regulation with a current controlled converter.

A more detailed implementation of this principle is illustrated in Figure 3.10(a) and (b). In the block diagram of 3.10(a), the DC voltage error determines the active power command, P^* , through a PI controller. From P^* , Q^* and the measured terminal voltages, the desired phase currents are found, i_a^* , i_b^* and i_c^* , which are the inputs to the hysteresis controllers. Outputs of the controllers are the gating signals to the inverter bridge switches. To overcome the limitations and drawbacks of the hysteresis scheme, such as the varying switching frequency, a triangle comparison PWM current controller may be adopted. Such a scheme is shown in Figure 3.10(b), where the current reference determination part has been omitted, being identical to that of Figure 3.10(a).

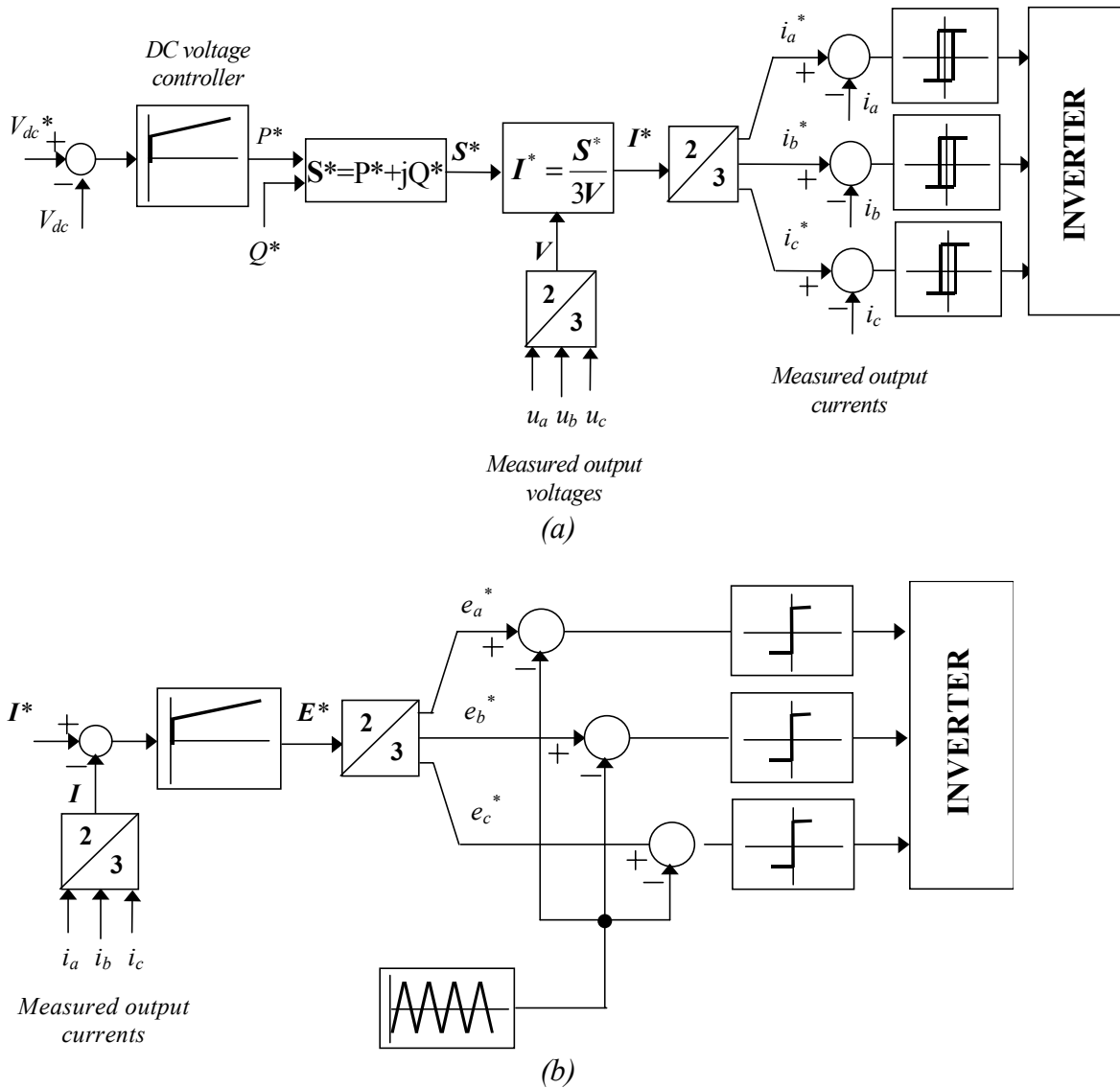


Figure 3.10. Block diagram of inverter current control. (a) Hysteresis scheme, (b) Triangular carrier PWM scheme.

For the fundamental frequency modelling of the converter system shown in Figure 3.6, the differential equations of the DC capacitor and the output inductances are used, along with the power balance equation of the DC/AC converter (input power = output power, if a lossless converter is assumed). In the case of a current controlled converter, the differential equations of the R-L filters are not required.

In the following, a particular case where a stiff DC voltage source is present is analyzed in more detail, as an example. The control logic of the inverter is described and appropriate models are given, both switching and fundamental frequency, along with simulation results.

3.5.2.a Stiff DC Voltage Source

When interfaced to the grid with the auxiliary help of a battery to supply the transient need of power, the details on the distributed source behavior tend to lose importance when looking at the performance of the unit as seen from the grid terminals. Indeed, the inverter will be connected to the terminals of the battery, and will only see a relatively stiff DC voltage. The power source is no longer required to have a dramatically fast transient response, since its task will only be to keep the battery charged.

The fact that we can look at the system as an inverter connected to a battery is the simplification that makes the design and analysis of the power electronic interface less burdensome. The nature of the power source (Fuel Cell or Micro Turbine) is no longer crucial and its details during transient response no longer needed. These details, along with the load sensitivities during island mode provided by the customer, are only needed to size the battery.

The most basic requirements for the inverter operations are the capability of delivering a preset amount of active power to the grid along with the ability to hold the voltage magnitude at the point of connection with the AC system to a desired value. To study the dynamic behavior of the power electronics interface, measurements and control block structure must be defined.

Full Model

Figure 3.11 shows the details of the DC/AC interface. The inverter terminals are connected to the grid through an inductance. It is this reactance that allows the dispatching of the desired amount of active power into the grid.

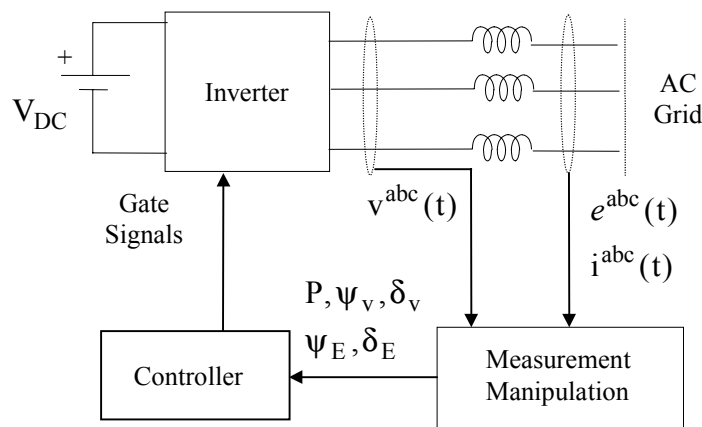


Figure 3.11. General Inverter Scheme

Figure 3.11 allows to follow the flow of information from the measurements, to the control blocks, to the gating signals that command the power electronics in the inverter.

Measurements consist of phase voltage and currents taken at the regulated bus, and the voltage at the inverter terminals. The governor is composed of blocks that are responsible for holding the delivered power and regulated bus voltage to the desired values. The gating signals are generated depending on the type of bridge used. Here, we use a six switches bridge combined with a voltage flux control strategy.

The model starts with the manipulation of the time domain quantities as measured from the sensors. These quantities are converted to the inverter and regulated bus voltage flux magnitudes and angles (respectively Ψ_v, δ_v and Ψ_E, δ_E), and the active power injection at the regulated bus, P.

These quantities are fed into the governor block that generates the gating signals. The overall picture is given in Figure 3.12, where it is possible to follow the flow of information as it is processed, from left to right.

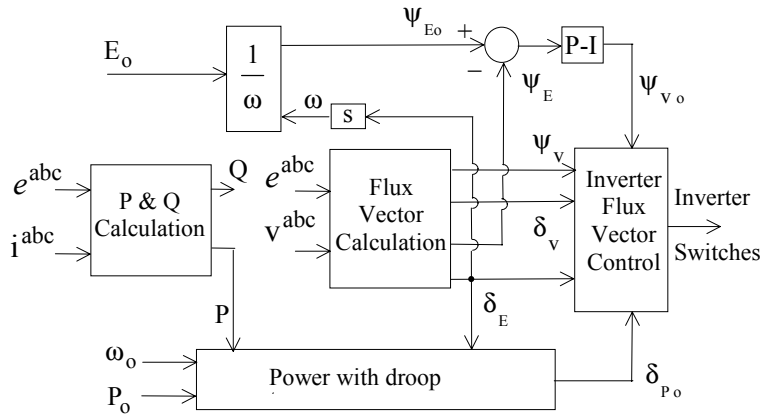


Figure 3.12. Detailed Inverter Control Scheme

More in detail, the following expressions describe how to obtain the voltage flux magnitude and angle for the inverter terminals. The procedure is identically applied to the regulated bus voltage measurements.

$$v_{ds} = \frac{v_c - v_b}{\sqrt{3}}$$

$$v_{qs} = \left(\frac{2}{3}\right) \left(v_a - \frac{1}{2}v_b - \frac{1}{2}v_c\right)$$

$$\Psi_{d,q} = \int_{-\infty}^t v_{ds,qs}(\tau) d\tau$$

$$\Psi_v = \sqrt{\Psi_d^2 + \Psi_q^2}$$

$$\delta_v = -a \tan\left(\frac{\Psi_d}{\Psi_q}\right)$$

In Figure 3.12 it is possible to notice that there are three externally defined setpoints: the requested power injection P_o , the desired regulated bus voltage magnitude E_o , and the nominal grid frequency ω_o . Active power regulation does not track desired requested power when in island mode: a power-frequency droop is applied to ensure proper power sharing between the micro-sources in the isolated network.

The gate pulse generator can be understood by the following diagram of Figure 3.13.

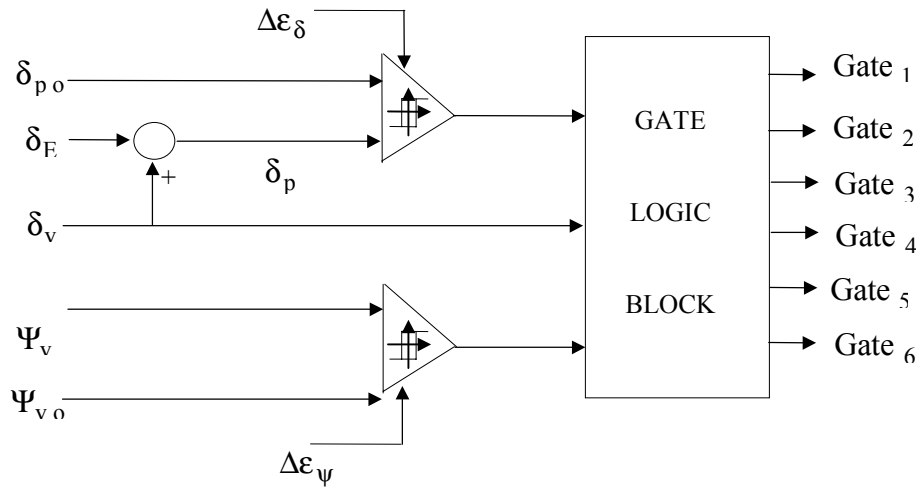


Figure 3.13. Hysteresis Control for Full Model

The errors between actual and desired amounts activate the remainder of the firing scheme only if they exceed a threshold value. If the error is larger than the hysteresis band (whose widths are indicated by $\Delta\epsilon_\delta$ and $\Delta\epsilon_\psi$) then a decision towards a new switching sequence is made. If the errors are within their hysteresis band, the switches will hold their current status.

The new switching position is chosen according to the current angular position of the vector at the inverter terminals defined by δ_v , and depending on the fact that we need to increase/decrease the flux magnitude or its angle. Angle changes have priority on flux magnitude changes. Once the hysteresis threshold is crossed and the direction of the next switching is selected, a lookup table will give the gating sequence for the switches.

More in detail, Figure 3.14 shows the inverter output only possible values, six active and one zero voltages. The inverter terminal voltage can only switch discretely between these values. To reduce δ_p the zero vector is chosen, otherwise one of the six states is chosen based on need to increase or decrease the flux magnitude. A lookup table indexed by sector number and the need to increase/decrease Ψ_v , provides switching logic.

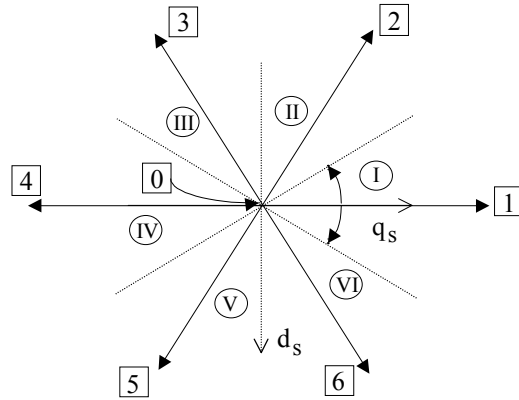


Figure 3.14. Inverter Output Voltages.

Table 3.3 summarizes the choices for the active vectors. Sectors are also shown in Figure 3.14. Sector "I" is centered about voltage vector "1".

	Sector number					
	I	II	III	IV	V	VI
Increase Ψ_v	2	3	4	5	6	1
Decrease Ψ_v	3	4	5	6	1	2

Table 3.3. Choice of Switching Vector

Ideal Model

Along with this full detailed model, it is possible to define a simpler phasor model for the power electronic interface. This model takes the same outputs quantities coming from the controller, and uses them to create a set of ideal voltage sources. The magnitude and phase angle of the ideal sources are created starting from the output signals of the governor as Figure 3.15 indicates:

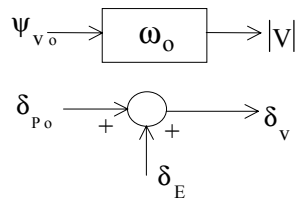


Figure 3.15 Ideal Inverter Model

The value that the sources have is given by:

$$V^a(t) = |V| \cos(\omega t + \delta_v)$$

$$V^b(t) = |V| \cos(\omega t + \delta_v - \frac{2}{3} \pi)$$

$$V^c(t) = |V| \cos(\omega t + \delta_v + \frac{2}{3} \pi)$$

These are line to ground values for the sources, but in reality the sources are connected to delta as Figure 3.16 shows.

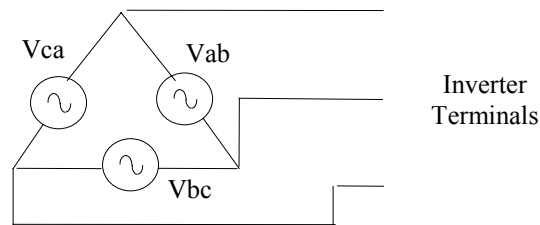


Figure 3.16. Ideal Inverter Model Sources

Then, the values that the actual ideal voltage sources have can be obtained from the line to ground in the following way:

$$V^{ab}(t) = V^a(t) - V^b(t) = \sqrt{3}|V| \cos(\omega t + \delta_v + \frac{\pi}{6})$$

$$V^{bc}(t) = V^b(t) - V^c(t) = \sqrt{3}|V| \cos(\omega t + \delta_v - \frac{\pi}{2})$$

$$V^{ca}(t) = V^c(t) - V^a(t) = \sqrt{3}|V| \cos(\omega t + \delta_v + \frac{5}{6} \pi)$$

To verify the validity of the ideal model, a direct comparison with the full model is carried on. The inverter is connected to a local feeder with a load at the regulated bus, and with a line and transformer connecting with an ideal voltage source. Figure 3.17 gives a diagram of the circuit where the unit is installed.

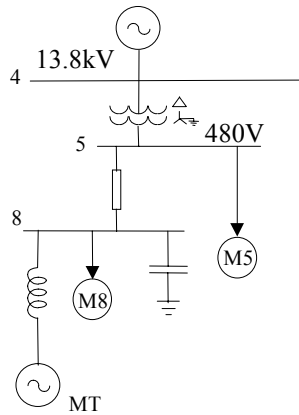


Figure 3.17. Test Circuit for Model Comparison

The unit is turned on, and the voltage and power reach their desired values. Both models are used for the inverter and then compared. Figure 3.18 shows the comparison for the active power injected at the regulated bus, while Figure 3.19 shows the model comparison for the regulated bus voltage magnitude. The match is excellent since responses from either model overlap.

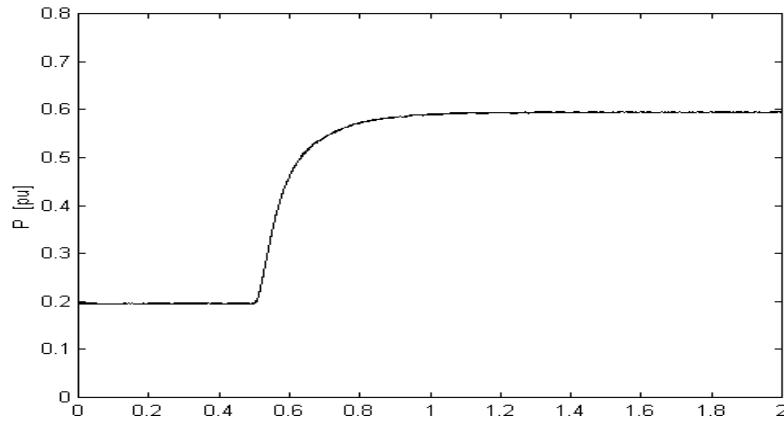


Figure 3.18. Output Power Model Comparison

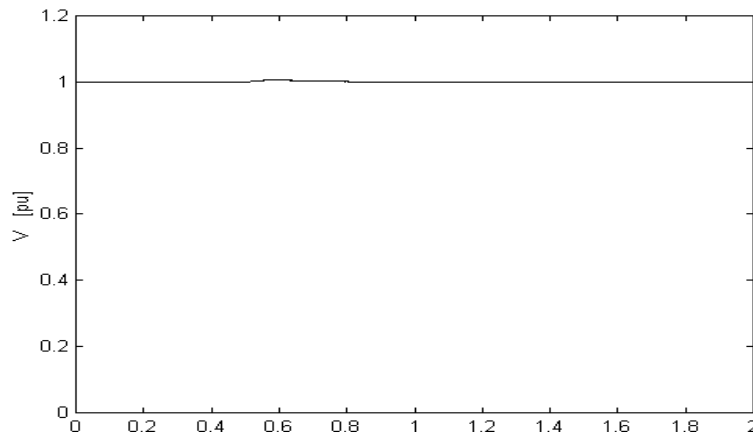


Figure 3.19. Regulated Bus Voltage Comparison

Figure 3.20 shows the inverter line to line voltages. The ideal model has a purely sinusoidal controlled ideal voltage source at the inverter terminals. Figure 3.21 shows the line to ground voltage at the regulated bus. Due to the small width of the hysteresis band, the voltage generated by the full model is nearly sinusoidal when seen at this bus. Figure 3.22 shows the line current injected by the inverter. Due to the switchings, the full model current has a high harmonic content, although it is apparent how the fundamental plays a dominant role. Finally, Figure 3.23 shows few cycles for the current comparison regarding the transient determined by the ramp up command given to the inverter output desired power.

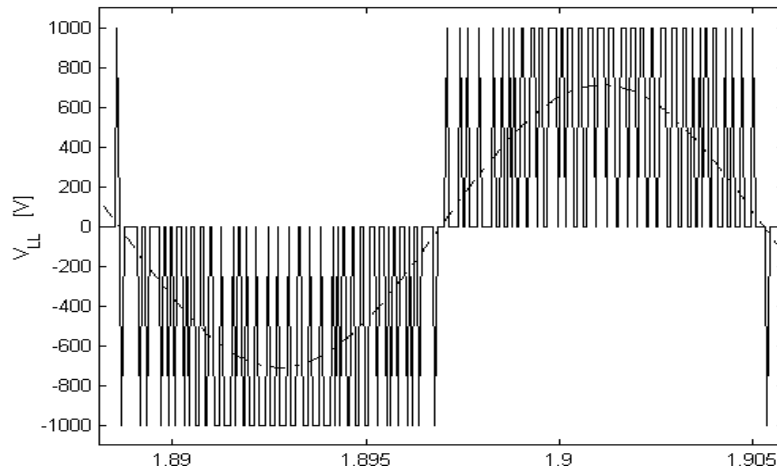


Figure 3.20. Line to Line Inverter Terminal Voltage Comparison

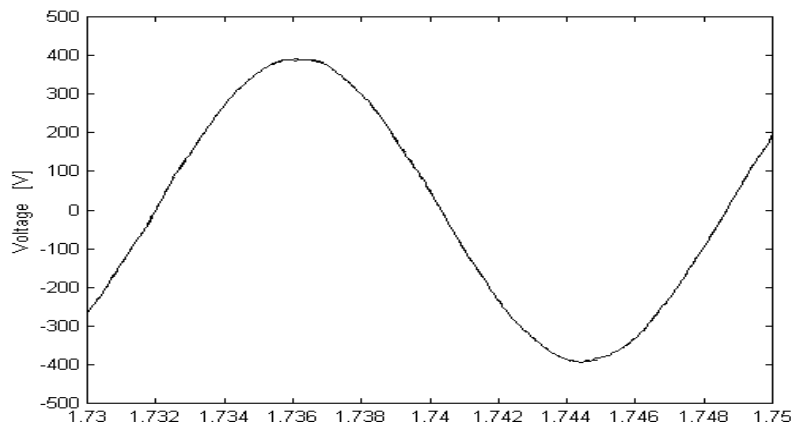


Figure 3.21. Line to Ground Regulated Bus Voltage Comparison

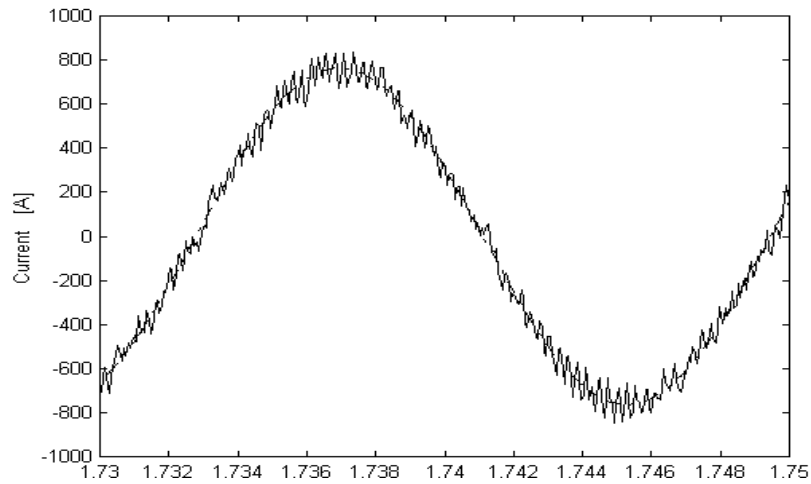


Figure 3.22. Inverter Output Line Current Comparison

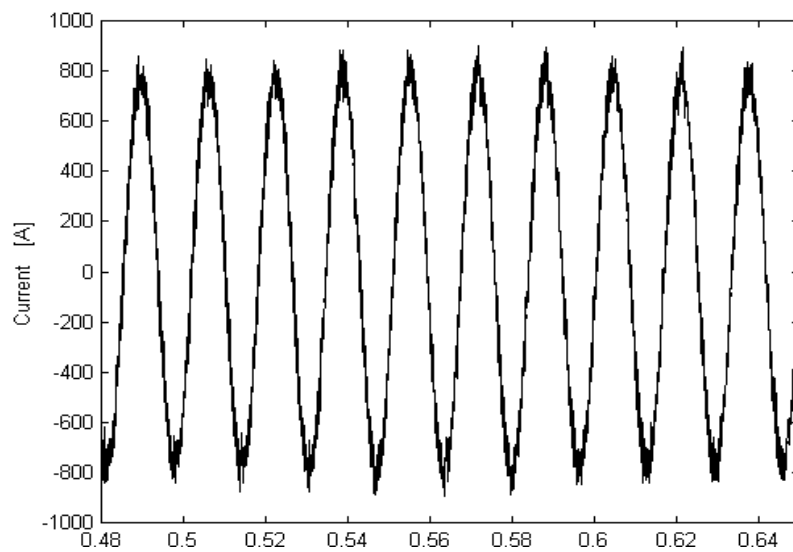


Figure 3.23. Current Comparison after Step Change

3.5.3 Generator Side Converter

As examples, two typical configurations of variable speed wind turbines are presented in this section. The modeling of the energy source is case-specific and depends on the type of source under consideration (wind turbines, photovoltaics, micro-generators etc.). In any case, the developed model is connected and solved together with the model of the output DC/AC converter, to represent the dynamics of the whole system.

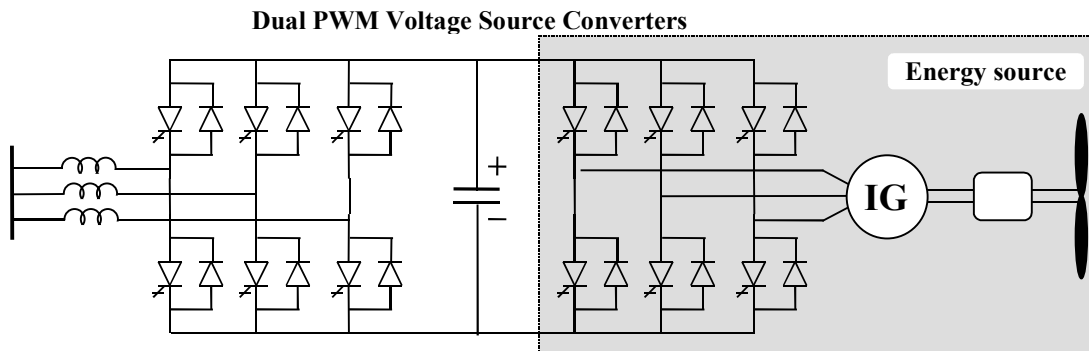


Figure 3.24. Variable speed wind turbine equipped with a squirrel cage induction generator and a dual PWM voltage source converter cascade.

In Figure 3.24 a variable speed wind turbine is shown, equipped with a squirrel cage induction generator. The converter interface to the grid comprises two identical (back-to-back) voltage source converters. The grid-side converter was discussed in the previous section. As in the case of induction motor drives of this type, the generator side converter may be either scalar or vector controlled.

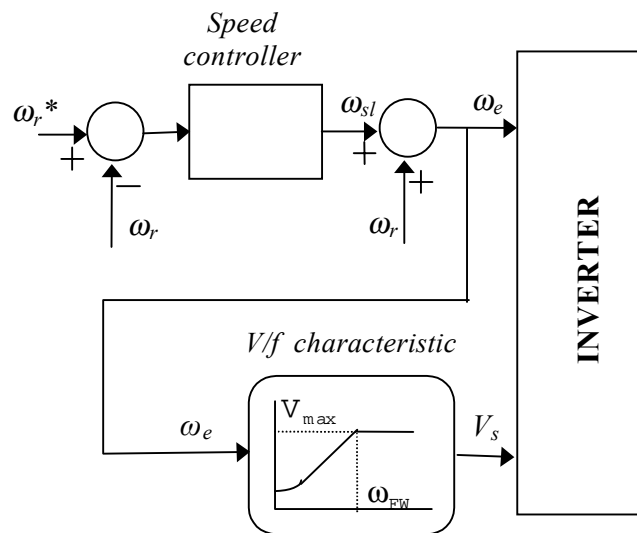


Figure 3.25. Scalar control system of the generator-side converter.

In Figure 3.25 the simplified block-diagram of a typical scalar control system is shown. V_s and ω_e are the stator voltage and frequency, that is the magnitude and frequency of the inverter AC voltage. The frequency control subsystem basically consists of the PI speed

controller. The rotor speed reference, ω_r^* , is externally determined by the optimal control characteristic of the turbine rotor. Output of the speed controller is the slip frequency, ω_{sl} , which is added to the rotor speed, to determine the stator frequency ω_e . For regulating the generator voltage, the constant V/f control principle is employed. It must be noted that practical control systems of this type may comprise several additional blocks (stabilizers, limiters etc.), which have to be included in the dynamic model of the system. For the simulation of the induction generator, the standard 4th order dq model is used.

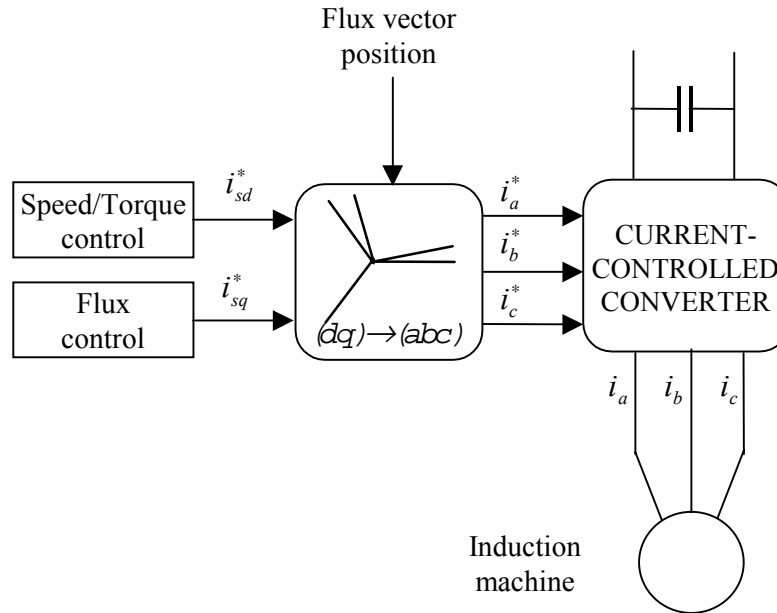


Figure 3.26. *Vector control principle with a current controlled converter.*

The vector control principle, which is now almost exclusively used in practical applications, is schematically illustrated in Figure 3.26, where a current controlled converter has been assumed, although as is usually (but not necessarily) the case. Using the coordinate transformation to the rotating flux reference frame, the decoupled control of the machine torque and flux can be achieved. Several variations of the vector control principle are encountered in the literature and in practice, requiring different modeling approaches. However, due to high bandwidth of the vector controllers, in most cases the machine and controller dynamics can be ignored for the representation of relatively slow phenomena.

In the case of pitch controlled wind turbines, the pitch controller must be also included in the simulation, since it affects significantly the dynamics of the system, particularly in the high wind region.

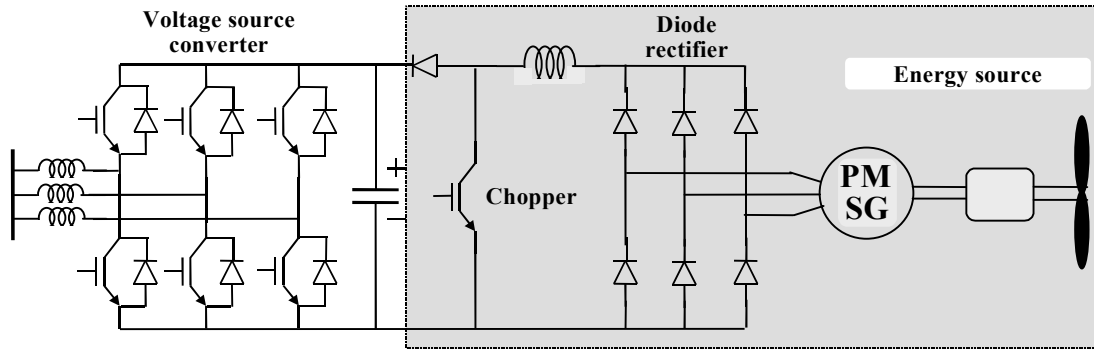
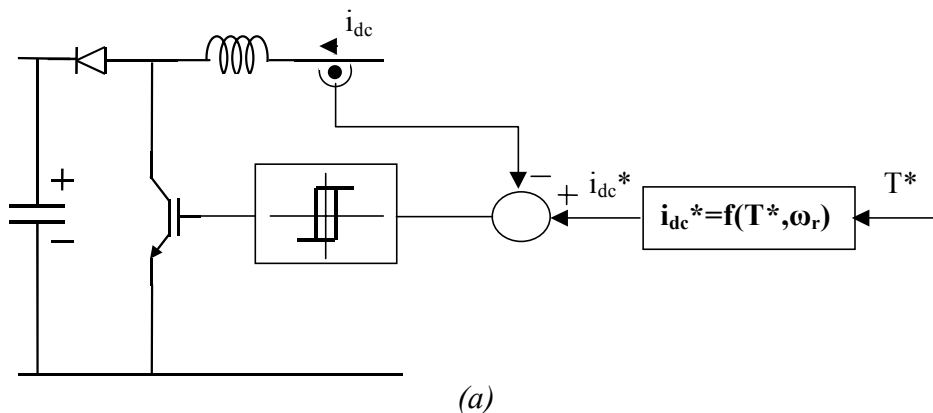
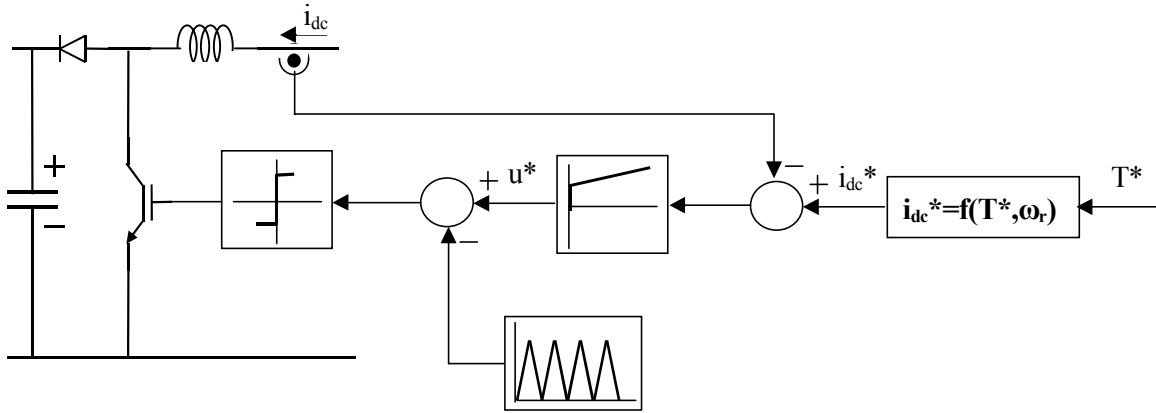


Figure 3.27. Wind turbine equipped with permanent magnet synchronous generator.

In Figure 3.27 a variable speed wind turbine equipped with a permanent magnet synchronous generator is shown. The variable frequency output of the generator is converted to DC by an uncontrolled diode rectifier. A boost DC-DC converter interfaces the rectifier to the DC/AC grid-side converter, which has been described in the previous section.

The generator torque control in this case is performed by the DC chopper, which regulates the rectifier (and hence the generator) current through a simple current control loop, as shown in Figure 3.28. The DC current reference, I_{dc}^* , is determined directly from a torque reference value, assuming that the turbine operates in the torque control mode. The torque may be calculated using a rotor speed measurement and the turbine optimal $T-\omega$ characteristic, as in Figure 3.29, or may be the output of a speed control loop. In diagram (a) of Figure 3.28, a hysteresis controller is used, whereas in diagram (b) a carrier PWM controller is employed. In the scheme of Figure 3.27, the chopper can be also used to control the DC bus voltage. In this case, the generator is loaded using the P^* input of the DC/AC converter, performing thus the speed control function.





(b)

Figure 3.28. Generator torque control scheme for the configuration of Figure 3.27.

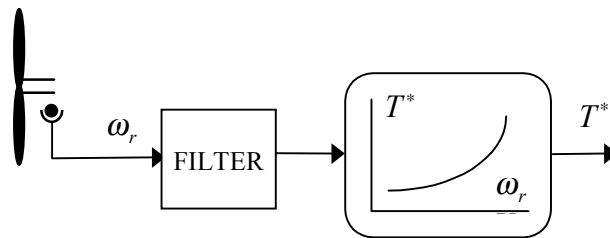


Figure 3.29. Torque reference determination from rotor speed measurement.

For the simulation of the synchronous generator a 4th order dq model can be used (assuming that its rotor circuits are equivalent to two damper windings, each along the d and q axes). However, the stator equations must be properly combined with the DC choke differential equation, since it is physically the same current that flows in the stator winding and the DC side of the rectifier. For this purpose the well-known fundamental frequency relations of the uncontrolled rectifier must be taken into account.

In case of a photovoltaic generator, the rotating parts (rotor, drive train and electrical generator) would be absent, as well as the generator side converter or rectifier. The PV array is usually interfaced to the DC bus via a DC/DC converter, which matches the DC voltages of the array and the converter and performs the maximum power point tracking function (i.e. controls the operating point of the array according to the insolation levels).

Chapter 4

Models for New Generation and Storage Systems

4.1 Wind Energy Conversion Systems (WECS)

4.1.1 The wind. Mechanical torque

The rotor aerodynamic power of a wind turbine, under smooth wind flow conditions, is given by:

$$P = \frac{1}{2} \rho A v^3 C_p(\lambda, \beta) \quad (4.1)$$

where

- ρ density of the air
- A rotor area
- V wind speed
- C_p performance coefficient
- β the pitch angle (see Figure 4.1)
- λ tip speed ratio, defined as

$$\lambda = \frac{\omega R}{v}$$

- R is the radius of the rotor and
- ω the mechanical angular speed of the blades

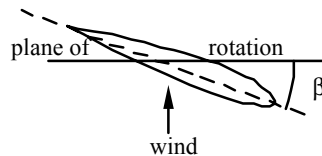


Figure 4.1

The performance coefficient is different for each turbine, and it must be obtained experimentally. However, analytical approximations have been developed. The graph of Figure 4.2 gives the typical shape of $C_p(\lambda, \beta)$ curves.

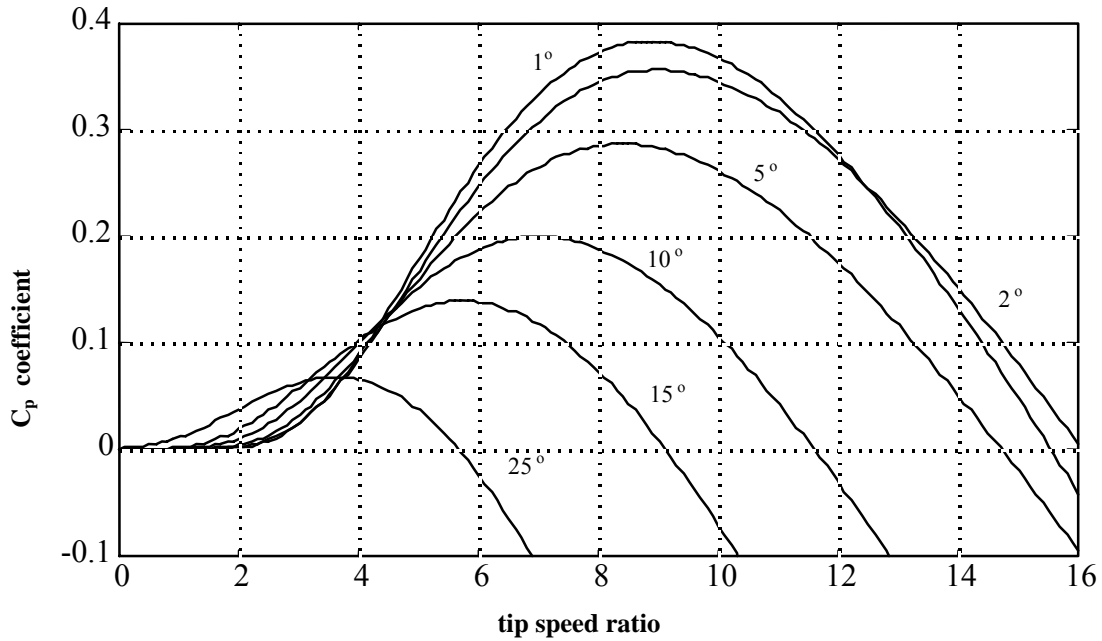


Figure 4.2 Analytical approximation of $C_p - \lambda - \beta$ characteristics

The total aerodynamic torque of the rotor is modeled as a mean torque, to which oscillations are superimposed. The mean torque T_m has the following expression

$$T_m = \frac{1}{2} \pi R^3 \rho v^2 \frac{C_p(\lambda, \beta)}{\lambda} \quad (4.2)$$

The main effects superimposed to the mean torque are the tower shadow, the wind shear and the gravitational loads, due to the weight of each blade. Tower shadow is the reduction of the blade aerodynamic torque, as it passes in front of the tower, due to the disturbance in the wind flow create by the (usually tubular) tower, both upstream and downstream. The torque oscillation in each blade i is:

$$\Delta T_{ts} = 2 \cdot \frac{T_m}{N_b} \cdot W_{ts}(\varphi_i) \quad (4.3)$$

where N_b is the number of blades and W_{ts} a coefficient dependent on the angle φ_i of the blade:

$$W_{ts}(\varphi) = \begin{cases} t_o + t_p \cdot \cos(p(\varphi_i - \varphi^*)) & (\varphi^* - \varphi_T) \leq \varphi \leq (\varphi^* + \varphi_T) \\ 0 & \text{otherwise} \end{cases}$$

$$p = \pi / \varphi_T$$

φ_T is half the angle of the tower shadow

φ_i is the blade angle,

φ^* is the blade azimuth angle and

t_o and t_p are empirical factors.

The wind shear is the increase of wind speed with height. This phenomenon also produces torque oscillations caused by the wind speed gradient along the height of the area swept by the blades. The wind shear effect can be expressed as

$$\Delta T_s = 2 \cdot \frac{T_m}{N_b} \cdot W_s(\varphi_i) \quad (4.4)$$

where

$$W_s(\varphi_i) = m \cdot \frac{0.75 \cdot R}{H} \cdot \sin \varphi_i + \frac{m \cdot (m-1)}{2} \cdot \frac{(0.75R)^2}{H^2} \cdot \cos^2 \varphi_i$$

Another load is produced by the blades' weight. If the blades moved at exactly the same velocity as the hub, i.e. the whole rotor is considered as a single body, then the effect of the blade weights would be cancelled. However, in a more detailed model, where an elastic coupling between each blade and the hub is considered, this effect must be included:

$$\Delta T_w = M_{bi} \cdot r_{cdg} \cdot g \cdot \cos(\varphi_i) \quad (4.5)$$

Therefore, the torque produced by each blade would be

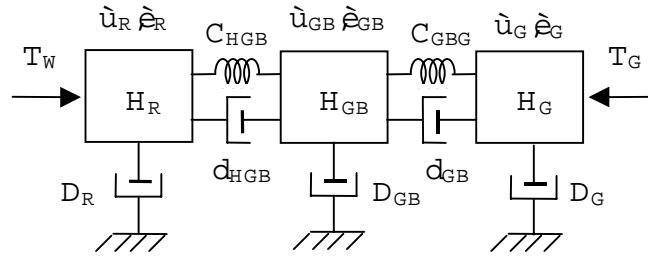
$$T_{bi} = \frac{T_m}{N_b} + \Delta T_{ts} + \Delta T_s + \Delta T_w \quad (4.6)$$

and the total aerodynamic torque of the rotor is the sum of the individual blade torques, calculated independently by the formula above.

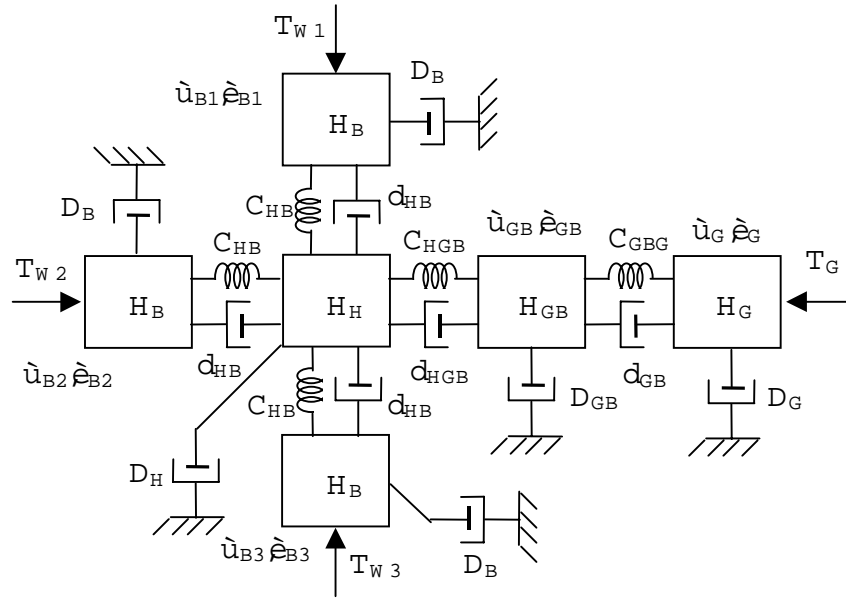
4.1.2 The drive train

Due to the increased compliance of the drive train of almost every wind turbine (usually achieved by “soft” axes or special elastic couplings), suitable multimass equivalents must be employed, in order to represent the low frequency torsional modes, which dominate the dynamic behavior of the WT.

In Figure 4.3, two typical mechanical equivalents are illustrated consisting of rotating masses elastically coupled to each other. In Figure 4.3(a) the three inertias correspond to the turbine rotor, the gearbox and the electrical generator. (The interconnecting axes, disk brakes etc. are incorporated in the lumped inertias of the model). The elasticity and damping elements between adjacent inertias correspond to the low and high-speed shaft elasticities and internal friction, whereas the external damping elements represent the torque losses. In order to reproduce the blade edgewise mode of oscillations, each rotor blade can be modeled by a separate inertia, elastically connected to the hub, as shown in Figure 4.3(b) for a 3-blade rotor. In this case the inertia H_H , adjacent to the gearbox, corresponds only to the hub, and not to the whole turbine rotor, as in Figure 4.3(a).



(a)



(b)

Figure 4.3 (a) 3-mass, (b) 6-mass drive train mechanical equivalents (for a 3-blade rotor)

The state equations for the drive train mechanical equivalent of Figure 4.3 (a) are the following, using the angular positions and velocities as state variables:

$$\frac{d}{dt} \begin{bmatrix} \underline{\theta} \\ \underline{\omega} \end{bmatrix} = \begin{bmatrix} [0]_{3 \times 3} & [I]_{3 \times 3} \\ -[2H]^{-1}[C] & -[2H]^{-1}[D] \end{bmatrix} \begin{bmatrix} \underline{\theta} \\ \underline{\omega} \end{bmatrix} + \begin{bmatrix} [0]_{3 \times 3} \\ [2H]^{-1} \end{bmatrix} \underline{T} \quad (4.7)$$

where

$\underline{\theta}^T = [\theta_R, \theta_{GB}, \theta_G]$ the vector of angular positions of the rotor, gearbox and generator

$\underline{\omega}^T = [\omega_R, \omega_{GB}, \omega_G]$ the vector of angular velocities of the rotor, gearbox and generator

$\underline{T}^T = [T_W, 0, T_G]$ the vector of external torques acting on the turbine rotor side (aerodynamic torque T_W) and on the generator rotor (electromagnetic torque T_G), conventionally accelerating

$[0]_{3 \times 3}$ and $[I]_{3 \times 3}$ the zero and identity 3x3 matrices, respectively

$[2H] = \text{diag}(2H_R, 2H_{GB}, 2H_G)$ the diagonal 3x3 inertia matrix

$[C] = \begin{bmatrix} C_{HGB} & -C_{HGB} & 0 \\ -C_{HGB} & C_{HGB} + C_{GBG} & -C_{GBG} \\ 0 & -C_{GBG} & C_{GBG} \end{bmatrix}$ the 3x3 stiffness matrix, where C_{HGB} and C_{GBG} are the hub to gearbox and gearbox to generator stiffness coefficients

$[D] = \begin{bmatrix} D_R + d_{HGB} & -d_{HGB} & 0 \\ -d_{HGB} & D_{GB} + d_{HGB} + d_{GBG} & -d_{GBG} \\ 0 & -d_{GBG} & D_G + d_{GBG} \end{bmatrix}$ the 3x3 damping matrix, where d_{HGB} and d_{GBG} are the relative dampings of the elastic couplings and D_R, D_{GB}, D_G the external damping coefficients

The state equations of the 6-mass mechanical equivalent of Figure 4.3(b) are the following:

$$\frac{d}{dt} \begin{bmatrix} \underline{\theta} \\ \underline{\omega} \end{bmatrix} = \begin{bmatrix} [0]_{6 \times 6} & [I]_{6 \times 6} \\ -[2H]^{-1}[C] & -[2H]^{-1}[D] \end{bmatrix} \begin{bmatrix} \underline{\theta} \\ \underline{\omega} \end{bmatrix} + \begin{bmatrix} [0]_{6 \times 6} \\ [2H]^{-1} \end{bmatrix} \underline{T} \quad (4.8)$$

where

$\underline{\theta}^T = [\theta_{B1}, \theta_{B2}, \theta_{B3}, \theta_H, \theta_{GB}, \theta_G]$ the vector of angular positions of the blades, hub, gearbox and generator

$\underline{\omega}^T = [\omega_{B1}, \omega_{B2}, \omega_{B3}, \omega_H, \omega_{GB}, \omega_G]$ the vector of angular velocities of the blades, hub, gearbox and generator

$\underline{T}^T = [T_{W1}, T_{W2}, T_{W3}, 0, 0, T_G]$ the vector of external torques, acting on the turbine blades (aerodynamic torques $T_{W,i}$, $i=1,2,3$) and on the generator rotor (electromagnetic torque T_G), conventionally accelerating

$[0]_{6 \times 6}$ and $[I]_{6 \times 6}$ the zero and identity 6x6 matrices, respectively

$[2H] = \text{diag}(2H_B, 2H_B, 2H_B, 2H_H, 2H_{GB}, 2H_G)$ the diagonal 6x6 inertia matrix

$[C] = \begin{bmatrix} C_{HB} & 0 & 0 & -C_{HB} & 0 & 0 \\ 0 & C_{HB} & 0 & -C_{HB} & 0 & 0 \\ 0 & 0 & C_{HB} & -C_{HB} & 0 & 0 \\ -C_{HB} & -C_{HB} & -C_{HB} & C_{HGB} + 3C_{HB} & -C_{HGB} & 0 \\ 0 & 0 & 0 & -C_{HGB} & C_{HGB} + C_{GBG} & -C_{GBG} \\ 0 & 0 & 0 & 0 & -C_{GBG} & C_{GBG} \end{bmatrix}$ the 6x6 stiffness matrix, where C_{HB}, C_{HGB} and C_{GBG} respectively are the blade to hub, hub to gearbox and gearbox to generator stiffness coefficients

$$[D] = \begin{bmatrix} D_B + d_{HB} & 0 & 0 & -d_{HB} & 0 & 0 \\ 0 & D_B + d_{HB} & 0 & -d_{HB} & 0 & 0 \\ 0 & 0 & D_B + d_{HB} & -d_{HB} & 0 & 0 \\ -d_{HB} & -d_{HB} & -d_{HB} & D_H + d_{HGB} + 3d_{HB} & -d_{HBG} & 0 \\ 0 & 0 & 0 & -d_{HGB} & D_{GB} + d_{HGB} + d_{GBG} & -d_{GBG} \\ 0 & 0 & 0 & 0 & -d_{GBG} & D_G + d_{GBG} \end{bmatrix}$$

the 6x6 damping matrix, where d_{HB} , d_{HGB} and d_{GBG} are the relative dampings of the elastic couplings and D_B , D_H , D_{GB} , D_G the external damping coefficients

4.1.3 Generator

For the generator, standard models, such as those given in Section 3.5, are usually employed. In case of variable speed wind turbines, where power electronics converters are connected to the stator terminals, the full models (e.g. 4th order for induction and 6th order for synchronous machines) are used. In case of constant speed WTs, where the generator is directly connected to the grid, it is often sufficient (for instance, in stability studies of large systems) to model the generator with reduced order models, such as the transient (2nd order) model presented in Section 3.5. In simulations where the switching behavior of the converters is represented, direct *abc* models of the generator may be utilized.

4.1.4 Performance and control systems.

4.1.4.1 Wind turbine with fixed rotational speed and synchronous or asynchronous generators.

In these systems, the generator can be either synchronous or asynchronous. The former is mainly used for isolated operation. In the synchronous case an excitation control system, as well as a speed governor, are required for maintaining the terminal voltage and frequency. Asynchronous generators are almost exclusively used in the case of grid connected WTs. Their main advantage is the simple and cheap construction. On the other hand they require compensating equipment (usually switchable capacitor banks), as well as cut-in connection devices (soft-starters). Synchronous generators are not used today in commercial constant speed WTs, intended for grid-connected operation. Blade pitch control is not present in all the systems, although it tends to be present in turbines beyond the rating of 500 kW.

Steady State Models

From $C_p-\lambda-\beta$ curves and operating ratings of wind turbine and generator, the curves of Figure 4.4 can be found. The operating point of the wind turbine is the intersection of the wind turbine characteristics and the generator characteristics. In the following figure, the case of an asynchronous generator is shown. A synchronous generator would be represented by a straight line, perpendicular to the horizontal (speed) axis.

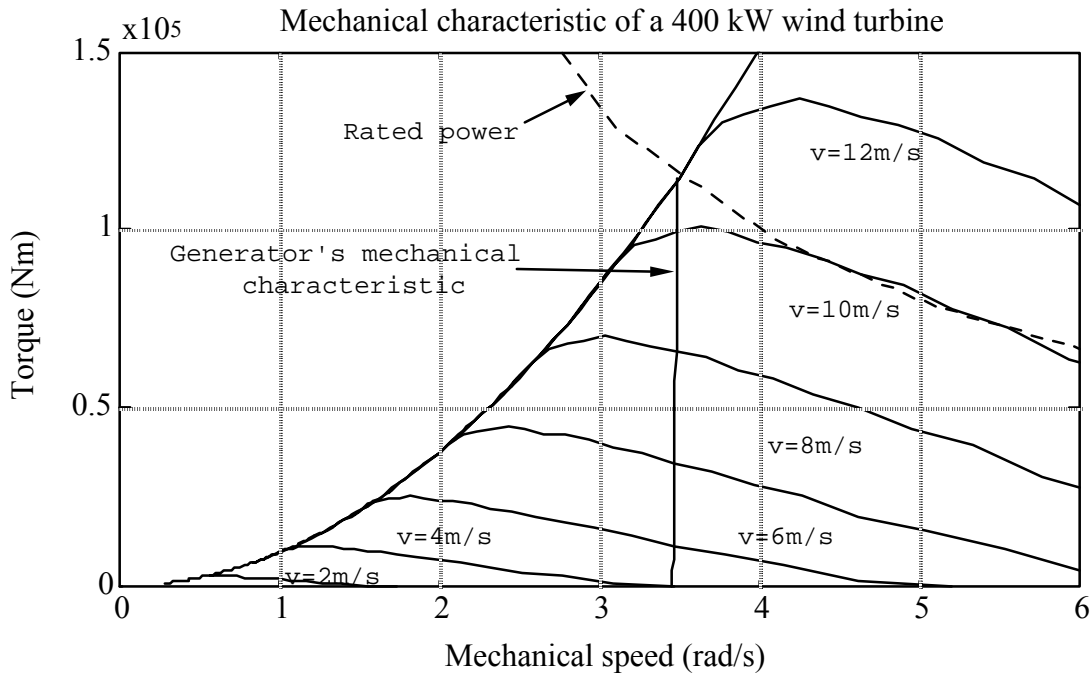


Figure 4.4

Dynamic Models.

The models used for representing constant speed WTs are composed of the subsystem models presented in previous sections, typically, the rotor aerodynamic model, the drive train mechanical equivalent and the generator model. In addition, control systems must be taken into account when present (pitch controller, excitation controls of synchronous generators etc.).

In transient stability studies standard models for generator, either synchronous or asynchronous, are used. In the aerodynamic modeling, accounting for the mean torque variations is sufficient, while a two or three mass model of the drive train is usually used, [18]. In Figure 4.5 the critical clearing times between a more detailed model (5 masses in the drive train) and a simpler one (two masses) are compared. The simulated fault scheme is shown in Figure 4.6. As we can see, the differences are negligible.

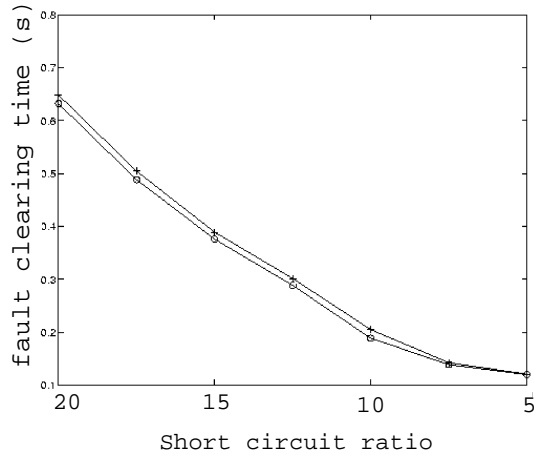


Figure 4.5 Stability limits for two masses (o) and five masses (+) systems

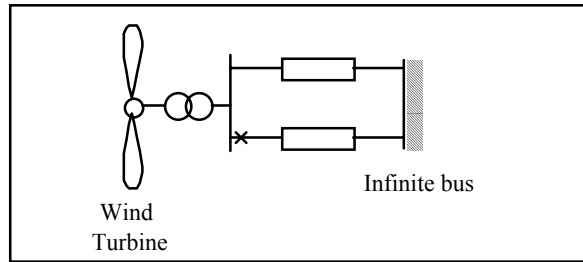


Figure 4.6 Test system for comparison between models

In the case of isolated systems, suitable models must be used for the voltage and frequency regulators, which are usually rather simple. Such models for both systems are shown below.

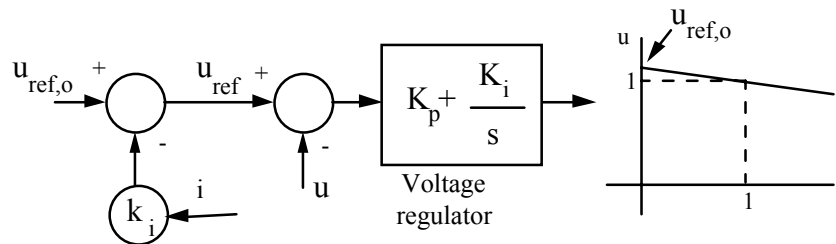


Figure 4.7 Excitation model for synchronous generator.

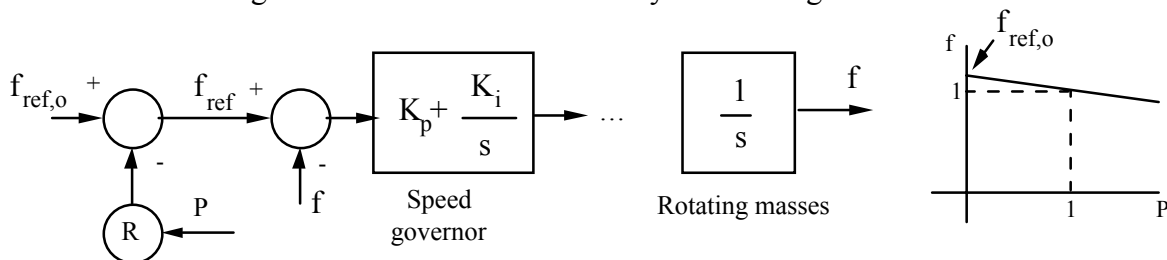


Figure 4.8. Speed control for wind power plant.

Pitch controls, if present, must be properly taken into account, since they directly affect the input mechanical, i.e. the power delivered by the turbine. As the angle β increases, the

lower curves of Figure 4.2 must be used, and a smaller coefficient C_p is obtained. Hence, in the case of isolated systems, the speed governor/frequency control function can be implemented via the pitch controller. Figure 4.9 represents a pitch controller regulating the WT output power. The PI regulator provides a reference pitch velocity, bounded to prevent the overloading of the mechanism. The output, also bounded, is the reference pitch angle. The second order system represents the actuator and blade dynamics.

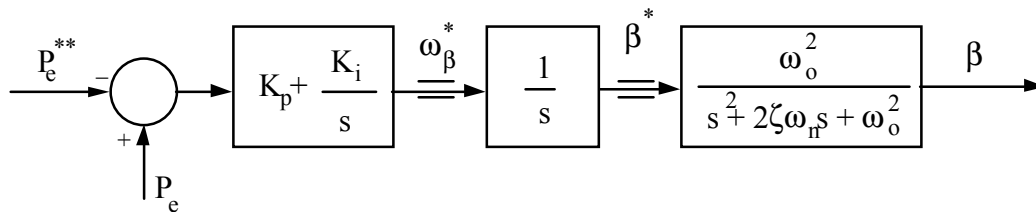


Figure 4.9. Pitch control.

4.1.4.2 Variable Speed Wind Turbines

Control systems of variable speed WTs allow a great variety of strategies to follow. A common one is to optimize aerodynamic efficiency, exploiting the maximum power available at each wind speed. In Figure 4.10 the dotted line joining the maxima of the power curves shows the locus of the optimal operating points, which correspond to different mechanical speeds. In low wind conditions, this curve is tracked, seeking the maximum energy yield from the turbine. At higher winds, however, certain operating limits come into play, such as the mechanical speed limit and the rated torque and power limit of the system. In this region, the control strategy must be accordingly modified, in order not to exceed these limits. This may be achieved using the generator torque control to limit the rotor speed in a stall controlled turbine, or by performing the speed control function via the pitch regulator and setting the generator torque reference at the rated value, in a pitch controlled turbine. In general, variable speed machines have a power reference input, which permits the regulation of their output power (but only at a value lower than the maximum wind power available).

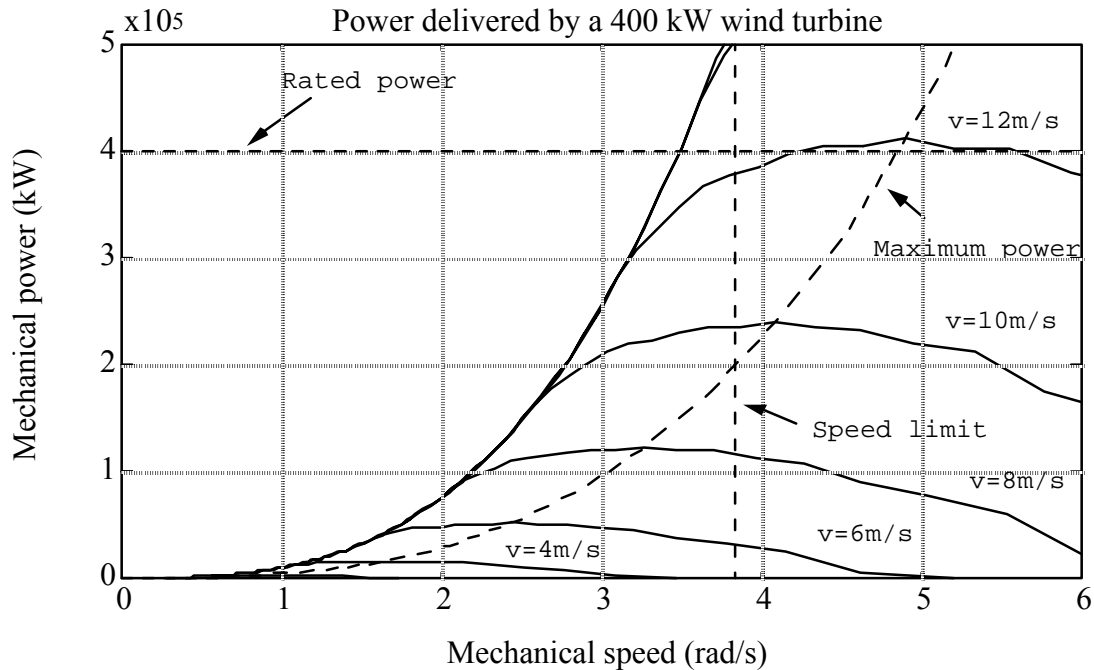


Figure 4.10. Maximum power strategy

For modelling purposes, as in the case of constant speed machines, the rotor aerodynamics, the drive train, the generator and converters and all present controls must be taken into account. In Section 3.6, the modelling of the converter interfaces has been discussed. In the following, of all possible variable speed configurations, discussed in the previous chapters, the doubly-fed asynchronous generator is picked as an example, to illustrate the modelling of the electrical part and the controls.

Modelling Example: The Doubly-Fed Asynchronous Generator

These systems use asynchronous machines with slip-ring rotors. The stator is directly connected to the grid. The rotor is supplied via two frequency converters, one connected to the grid side, and other to the rotor side. There is a DC link between both converters. Additionally there is a pitch control.

For allowing under and over synchronous operation, it is necessary to use four quadrant converters. Doubly fed asynchronous machines with IGBT frequency converter systems exhibit particularly favourable operating characteristics with regard to grid reactions.

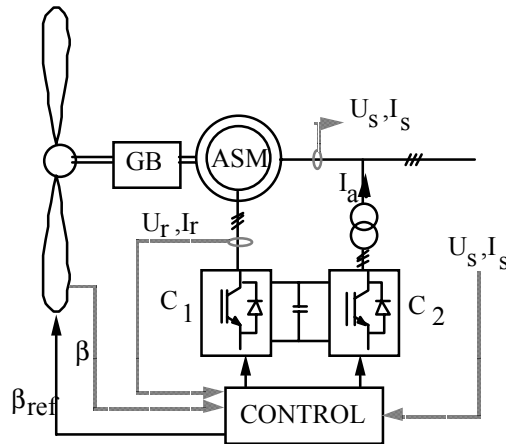


Figure 4.11. Doubly-fed asynchronous generator.

Steady State Behavior

In the system of Figure 4.11, power can be delivered to the grid through the stator and the rotor, while the rotor can also absorb power. In a doubly fed induction generator, the relationship between mechanical, rotor and stator powers are, neglecting losses:

$$P_r = -s \cdot P_s$$

$$P_m = (1-s) \cdot P_s$$

where

P_m is the mechanical power delivered to the generator.

P_s is the power delivered by the stator.

P_r is the power delivered by the rotor.

s is the slip.

Below the synchronous speed:

$s > 0$	$P_r < 0$	the rotor absorbs power
	$P_m < P_s$	a fraction of the stator power enters the rotor circuits

Above synchronous speed:

$s < 0$	$P_r > 0$	the rotor produces power
	$P_m > P_s$	power delivered to grid through the stator and rotor circuits

The range of variation of the slip s determines the size of the converters and therefore it is a design parameter. Mechanical and other restrictions limit the maximum slip well below 1.0. For instance, a practical speed range could be between 0.7 and 1.1. Hence, the required size of the converters is significantly reduced, which is an important advantage of this system.

Dynamic Model

The control of this device is provided through the converters C_1 and C_2 (see Figure 4.13). The tasks that they must perform are:

1. Converter C_1 controls rotor voltage. This magnitude allows to control the electromagnetic torque, and must follow the reference provided by the control system. This converter can also provide reactive power for the magnetization of the machine, reducing the reactive power requirements on converter C_2 .
2. Converter C_2 maintains the grid voltage and the exchange of reactive power with the network.

In the model, the converters are assumed ideal, and the DC link between them has constant voltage. A simple electrical model of the whole system is given in Figure 4.12.

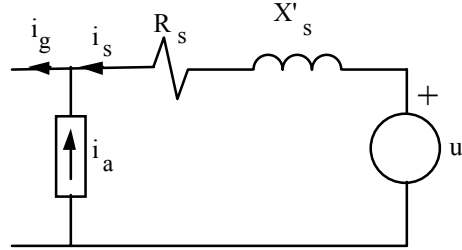


Figure 4.12. Generators and converters, as seen from the grid.

In this figure, i_a is a current source that represents the grid-side converter C_2 , and u' is a voltage source that represents the rotor voltage control, performed by the converter C_1 . The values of the source u' and the inductance X'_s are given later on.

The equations that give the value of the current source i_a are:

$$u_{ds} = -\frac{X_a}{\omega_{base}} \frac{di_{da}}{dt} + X_a i_{qa} + u_{da}$$

$$u_{qs} = -\frac{X_a}{\omega_{base}} \frac{di_{qa}}{dt} + X_a i_{da} + u_{qa}$$

where

u_{ds} u_{qs} d, q components of the converter AC voltage

u_{da} u_{qa} d, q components of the grid voltage

i_{ds} i_{qs} d, q components of the stator current

i_{da} i_{qa} d, q components of the converter AC current

X_a inductive impedance of the converter output branch (e.g. the transformer leakage impedance), added for smoothing of the current and to facilitate control

From the preceding equations we obtain:

$$\frac{di_{ad}}{dt} = \omega_{base} \left(\frac{u_{da} - u_{ds}}{X_a} + i_{da} \right)$$

$$\frac{di_{aq}}{dt} = \omega_{base} \left(\frac{u_{qa} - u_{qs}}{X_a} - i_{qa} \right)$$

Numerical integration of these equations gives the instantaneous values of i_{da} and i_{qa} .

The model of a doubly-fed asynchronous generator has minor differences from the standard asynchronous generator model. The equations that give the stator voltage are

$$\begin{aligned} u_{ds} &= -R_s i_{ds} + X'_s i_{qs} + u'_d \\ u_{qs} &= -R_s i_{qs} - X'_s i_{ds} + u'_q \end{aligned}$$

where

$$\begin{aligned} u'_d &= \frac{\omega_s L_m}{L_{rr}} \psi_{qr} \\ u'_q &= -\frac{\omega_s L_m}{L_{rr}} \psi_{dr} \\ X'_s &= \omega_s \left(L_{ss} - \frac{L_m^2}{L_{rr}} \right) \end{aligned}$$

The state equations of the generator rotor voltages are:

$$\begin{aligned} \frac{du'_d}{dt} &= \omega_{base} \left(-\frac{R_r}{L_{rr}} u'_d + \frac{\omega_s R_r L_m^2}{L_{rr}^2} i_{qs} + \omega_s s u'_q - \frac{\omega_s L_m}{L_{rr}} u_{qr} \right) \\ \frac{du'_q}{dt} &= \omega_{base} \left(-\frac{R_r}{L_{rr}} u'_q + \frac{\omega_s R_r L_m^2}{L_{rr}^2} i_{ds} - \omega_s s u'_d - \frac{\omega_s L_m}{L_{rr}} u_{dr} \right) \end{aligned}$$

where

- ω_s electrical stator frequency, in rad/s.
- L_{rr} , L_{ss} self inductances of rotor and stator windings.
- L_m magnetizing inductance.
- R_s , R_r are the stator and rotor resistances.
- $\psi_{dr,qr}$ are the d, q componets of rotor flux.

Comparing with the standard 2nd order model of the induction machine, used in stability studies, we can see that the terms u_{dr} and u_{qr} do not disappear, because the rotor is not short circuited.

The electromagnetic torque is given by

$$T_e = \frac{u'_d i_{ds} + u'_q i_{qs}}{\omega_s}$$

A usual simplification is to assume $\omega_s = 1$. In this case, the dynamic equations are

$$\begin{aligned} \frac{du'_d}{dt} &= \omega_{base} \left(-\frac{R_r}{L_{rr}} u'_d + \frac{R_r L_m^2}{L_{rr}^2} i_{qs} + s u'_q - \frac{L_m}{L_{rr}} u_{qr} \right) \\ \frac{du'_q}{dt} &= \omega_{base} \left(-\frac{R_r}{L_{rr}} u'_q + \frac{R_r L_m^2}{L_{rr}^2} i_{ds} - s u'_d - \frac{L_m}{L_{rr}} u_{dr} \right) \end{aligned}$$

and the electromagnetic torque is

$$T_e = u'_d i_{ds} + u'_q i_{qs}$$

If this simplification is not justified, the value of ω_s should be calculated from stator voltage variation.

Control systems

Torque Control

This control acts on the rotor side converter C_1 . Its purpose is to drive the system to the operating point chosen by the adopted control strategy. This may be achieved by setting a speed reference that the system must follow. The speed error then determines the reference current i_{rq} by means of a PI regulator.

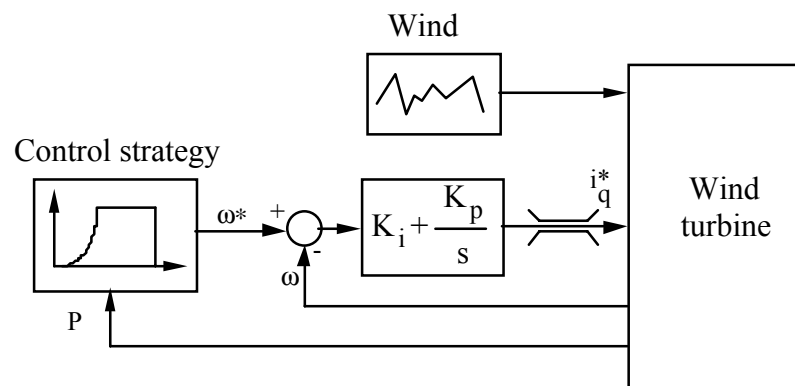


Figure 4.15. Torque control

Torque is proportional to i_q . The expression of the torque, using a reference frame with the direct axis aligned with the stator flux linkage vector ψ_s , becomes

$$T_e = -\frac{L_m}{L_{ss}} \psi_{ds}^m i_{qr}^m$$

The actual implementation can take many forms and strategies. A typical one is described, whose inner control loop is shown in Figure 4.16. The torque is modified by acting on the value of i_{qr}^m . This magnitude is the q component of the rotor current, but in the new reference. The magnitude i_{dr}^m is not used for the torque control and it is usually set to zero in order to minimize the current – the magnetizing current is drawn by the stator, but reactive compensation is possible through the grid-side PWM converter.

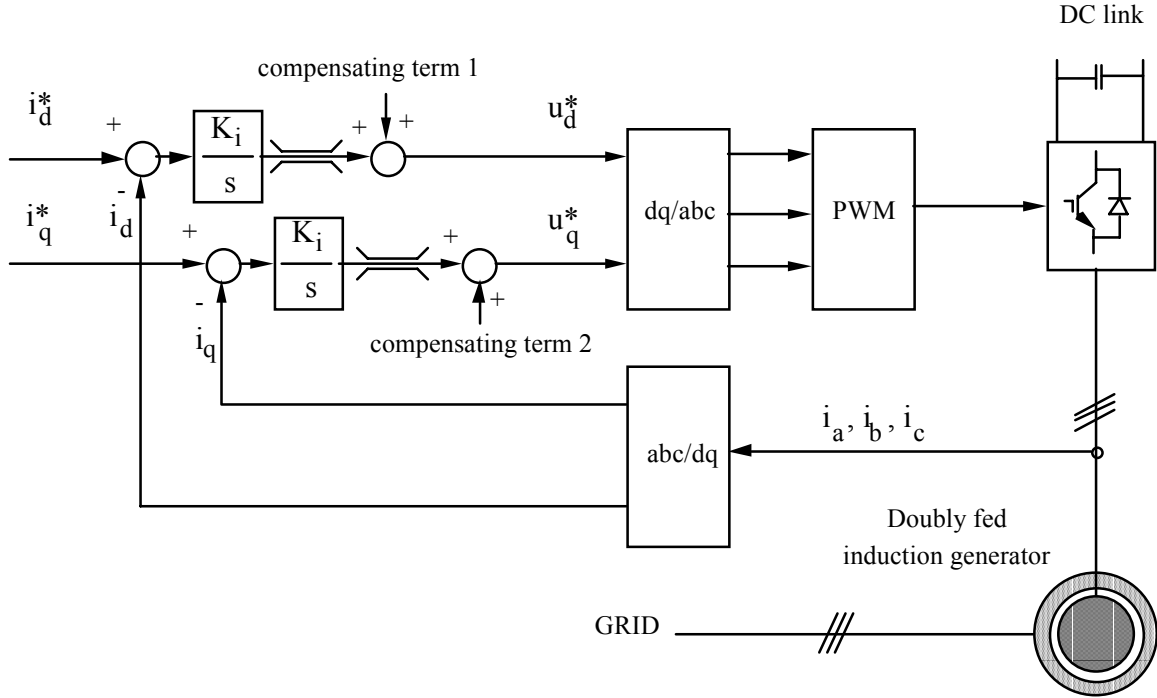


Figure 4.16. Speed control inner loop.

These control loops are modelling the following state equations:

$$u_{dr}^m = -R_r \dot{i}_{dr}^m + sL_{rr}\sigma i_{qr}^m - \frac{1}{\omega_b} L_{rr} \sigma \frac{di_{dr}^m}{dt}$$

$$u_{qr}^m = -R_r \dot{i}_{qr}^m - sL_{rr}\sigma i_{dr}^m - s \frac{L_m}{L_{ss}} \psi_{ds}^m - \frac{1}{\omega_b} L_{rr} \sigma \frac{di_{qr}^m}{dt}$$

where

$$\sigma = 1 - \frac{L_m^2}{L_{rr}L_{ss}}$$

The compensating terms are included to improve the system dynamic response. Their expressions are:

Compensating term 1	$sL_{rr}\sigma i_{qr}^m$
Compensating term 2	$sL_{rr}\sigma i_{dr}^m - s \frac{L_m}{L_{ss}} \psi_{ds}^m$

The value of the source u' of Figure 4.14 depends directly on the rotor flux, whose expression in the new reference is given by:

$$\psi_{dr}^m = \left(L_{rr} - \frac{L_m^2}{L_{rr}} \right) i_{dr}^m + \frac{L_m}{L_{ss}} \psi_{ds}^m$$

$$\psi_{qr}^m = \left(L_{rr} - \frac{L_m^2}{L_{rr}} \right) i_{qr}^m + \frac{L_m}{L_{ss}} \psi_{qs}^m = \left(L_{rr} - \frac{L_m^2}{L_{rr}} \right) i_{qr}^m$$

Therefore, variations of the rotor current are reflected on the value of u' .

Control of Reactive Power

This control is provided by the converter C_2 of Figure 4.13. This converter regulates the reactive power exchanged with the grid. The following equations relate the converter voltage and current at the grid side. In order to simplify the control, the reference frame is changed, placing the direct axis in coincidence with u_{ds} , obtaining

$$u_{ds}^s = -\frac{X_a}{\omega_{base}} \frac{di_{da}^s}{dt} \cdot i_{qr}^m + X_a i_{qa}^s + u_{da}^s,$$

$$0 = -\frac{X_a}{\omega_{base}} \frac{di_{qa}^s}{dt} \cdot i_{qr}^m - X_a i_{da}^s + u_{qa}^s,$$

The superscript s denotes the new reference frame. The expression of apparent power supplied by this converter is

$$s = u_d^s \cdot i_{da}^s + j u_d^s i_{qa}^s$$

Therefore control on i_{da}^s is an active power control. The stored energy in the DC link capacitor cannot change, since this would imply oscillations of the DC voltage. For this reason, the reference i_{da}^s is selected so as to make the input (or output) power at the rotor side equal to the output (or input) power at the grid side

$$i_{da}^{s*} = \frac{u_{dr} \cdot i_{dr} + u_{qr} \cdot i_{qr}}{u_d^s}$$

By means of i_{qa}^s it is possible to control the reactive power exchanged with the network. If a reference reactive power Q^* is specified for the wind turbine, then

$$i_{qa}^{s*} = -\frac{Q^*}{u_d^s} - i_{qs}^s$$

Pitch Regulation

The blade pitch angle regulates the active power delivered by the turbine, as shown in figure 4.2. As the angle β increases, the lower curves must be used, and a smaller coefficient C_p is obtained. This systems is used to limit the power delivered to the grid under high wind speed conditions. Figure 4.9 represents the control of the power obtained from the wind. The PI regulator provides a reference velocity, bounded to prevent the overloading of the mechanism. The output, also bounded, is the reference pitch angle. The second order system represents the mechanical device.

Control Strategy

The objective of the control is to regulate the rotor angular velocity for achieving the optimal coefficient C_p . Since $\lambda = \omega R/v$, for a given wind velocity v , the maximum power is obtained for an angular velocity of $\omega = \lambda v/R$. This value, in p.u., is used as the reference in the speed control of Figure 4.15. Under strong wind, the optimal speed could

exceed the upper mechanical speed limit and therefore it should be limited, for instance to 110 % of the synchronous value. Rotor current control is tuned to obtain the fastest possible response with a reasonable damping. The PI speed regulator of Figure 4.15, however, is set for a relatively slow response, because fast control would produce torque fluctuations which would be transmitted towards the output. When the generator reaches rated power, the pitch control starts acting, limiting the power produced by the wind.

It must be pointed out that this control strategy requires a wind velocity input in order to calculate the reference mechanical speed, which must be provided by an anemometer. It must be noted, however, that in such a case, problems related to the anemometer's accuracy, reliability and dynamic response, or the correlation between measured and actual wind speed, are important issue and may compromise the effectiveness of the control. It is also possible to regulate the turbine from a power reference, instead of trying to get the maximum power. This could be done by means of a third loop which measures the power error and modifies the reference velocity.

Asynchronous generator with variable slip control

An interesting configuration, utilizing a wound-rotor induction machine, is illustrated in Figure 4.17. This system is considerably simpler than the doubly-fed induction generator, but its slip control range is limited (typically up to 10%), due to the fact that the rotor slip power is not returned to the grid, but consumed as losses on the external rotor resistors. In general, the principle of limited slip variation allows a smoother operation, improving the general performance and output power quality of the wind turbine. Obviously, alternative designs, other than the one shown in Figure 4.17, can be also used.

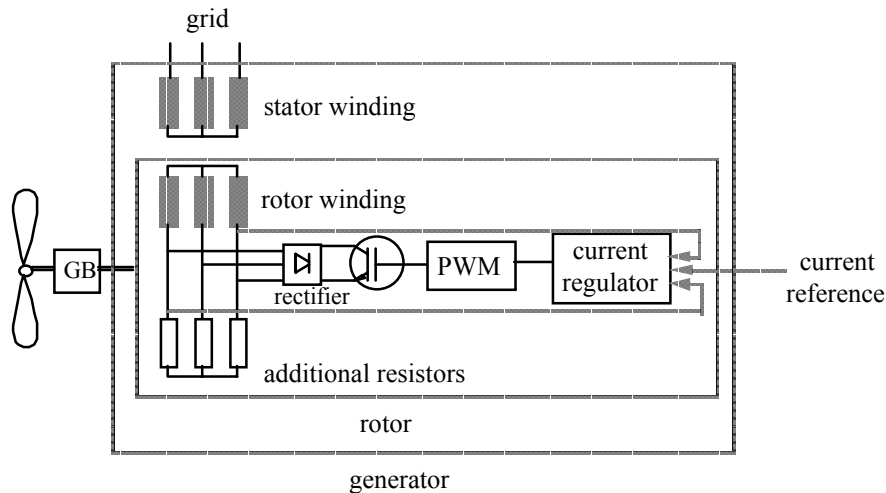


Figure 4.12. Asynchronous generator with variable slip control.

The dynamic behaviour and the control systems of this configuration are similar in principle to the doubly-fed induction generator, but much simpler. It must be noted, however, that there is no converter at the grid side and hence no control of the reactive power is possible. Also the limits of the slip variation are restricted and therefore the regulation/optimisation of the turbine power is not possible.

4.1.5 Wind Farms Aggregation (Equivalents)

Most of the existing tools to assess the interaction between wind turbines and the existing electrical grid are based on detailed models that are able to simulate the transient behaviour of individual WECS and the whole park. The main disadvantage of these detailed models is related to the computational burden, which may render unpractical the study of a wind park composed by 20 or more WECS.

This is an important issue, since the inclusion of the fast dynamics when studying the interaction between a wind park and the grid does not always add relevant information, compared with the use of reduced order models. Therefore, the need arises for wind park dynamic equivalents which are able to retain the relevant dynamics with respect to the utility grid [19-22]. Moreover, these equivalents should take into account the effects of wind speed fluctuations.

A first step towards establishing such dynamic equivalents is to apply the methodologies currently available for the order reduction of power systems. It is worth mentioning that these techniques actually reduce the order of the system, but do not perform aggregation of WECS. In broad terms, this means that, for each one of the existing WECS, it is necessary to solve less and simpler differential equations. A survey of available power system order reduction techniques and their application to a linearized wind park full order model is outlined in the next section.

This preliminary analysis has showed that the technique known as singular perturbations was the best suited for the purpose of achieving a reduced order model which describes with a reasonable degree of accuracy the transient behaviour of the wind park in what concerns the interaction with the electrical grid. A step further in the simplification of the reduced order model was accomplished by applying aggregation techniques to the previously developed singular perturbations wind park model. A model in which less and simpler equations for less WECS (depending on wind conditions, may be only for one WECS) has therefore been achieved.

Order-Reduction Preliminary Analysis

Some of the methodologies currently available to reduce the order of power systems models have been applied to the specific case of wind parks. As the main objective of this step was to gain some insight regarding the behaviour of each technique, a steady-state preliminary analysis using a linearized wind park model has been carried out [23].

Modal truncation is the first reduction scheme that has been applied to electric power systems. This technique is based on the pole location of the linear system [24]. The state variables are transformed in modal variables and the fast decay poles and/or those associated with high frequencies are neglected, thus enabling a reduction in the order of the system.

Balanced reduction techniques take a slightly different approach, because they are based in the input/output behaviour of the system [25]. Actually, the original state-space system is transformed into a new representation, which has the property that each state-space

variable is both controllable and observable. In order to achieve a reduced order model, states that are strongly influenced by the inputs and strongly connected to the outputs are retained, whereas states that are weakly controllable and observable are truncated.

Another method used in power systems order reduction is the so called optimal Hankel-norm approximation [26]. This criterion tries to achieve a compromise between a small worst case error and a small energy error.

The technique known in the literature as singular perturbations decomposes the system according to its fast and slow dynamics and then lowers the model order by first neglecting the fast dynamic phenomena [27]. The effects of fast dynamics are then reintroduced as "boundary layer" corrections, calculated in separated time scales, which leads to correct static gains.

Both Hankel-norm and balanced reduction methods, although producing very good approximations of the transient response, have the drawback of high reduction errors at low frequencies, due to the intrinsic mismatch between the DC gains of the full and reduced order models. Therefore, these methods are not suitable to steady-state applications.

The applied modal based reduction techniques make the discarded dynamic behaviour static, so that the DC gain of the reduced model is equal to that of the original model. Therefore, this method, which actually neglects the fast dynamic phenomena, is thought to be the best suited to steady-state applications, but a good performance in what concerns the transient behaviour is not expected. Moreover, due to its inherent lack of a clear criterion for determining the proper order of the reduced-order model, it becomes strongly dependent on the specific system to which it is applied. In fact, when the issue of neglecting the so called fast poles is to be assessed, one has to be extremely cautious and a pre-analysis of the characteristics of the system is required.

Singular perturbations seems to be a more prominent reduction technique. Due to the fact that the effects of fast dynamics are reintroduced in the reduced system, this technique seems to be more general, namely in what concerns the prediction of both steady-state and transient behaviour of the systems.

Singular perturbations has shown to be the most promising reduction-order technique for the development of the dynamic equivalent. In addition to the excellent agreement between full and reduced order results, the following advantages should be mentioned:

- the order reduction methodology retains the physical meaning of the variables;
- the method contains the procedures to systematically improve the answers of the simplified model.

Singular Perturbations Background

Singular perturbations approach provides a tool to overcome the lack of provision to improve the quasi-steady-state approximation that characterize conventional reduction-order techniques.

Let us consider two time variables [28]: t , which we assume to be properly scaled for the slow phenomena and τ , which we state that is related with the fast phenomena. The ratio of these time scales is a small positive parameter ε , which allows the definition of the new time variable τ as:

$$\tau = \frac{t - t_0}{\varepsilon} \quad (1)$$

The smaller ε is, the larger τ will be for a given $(t-t')$ interval. This means that the fast phenomena will have enough time to reach their steady-state, but on the other hand, allows that the interval $(t-t')$ may be sufficiently short to consider the slow variables as constant.

If the operating experience, or some empirical estimates, indicates that the dynamics of the fast states z are $1/\varepsilon$ times faster than the slow states x , one can write:

$$\begin{aligned} \frac{dx}{dt} &= f(x, z, t); x(t_0) = x_0 \\ \varepsilon \frac{dz}{dt} &= g(x, z, t); z(t_0) = z_0 \end{aligned} \quad (2)$$

in which f and g are of the same order of magnitude.

In the limit $\varepsilon \rightarrow 0$ the quasi-steady-states (also known as slow sub-system) can be defined in the t time scale by:

$$\begin{aligned} \frac{dx_s}{dt} &= f(x_s, z_s, t); x_s(t_0) = x_0 \\ 0 &= g(x_s, z_s, t) \end{aligned} \quad (3)$$

To obtain the fast parts of x and z we now rewrite the system in the fast time scale τ :

$$\begin{aligned} \frac{dx}{d\tau} &= \varepsilon f(x, z, t_0 + \varepsilon\tau) \\ \frac{dz}{d\tau} &= g(x, z, t_0 + \varepsilon\tau) \end{aligned} \quad (4)$$

Let us again examine the limit as $\varepsilon \rightarrow 0$: x is constant in the fast time scale, the only fast variations are the deviations of z from its quasi-steady-state. If one denote these fast variations by $z_f = z - z_s$ and again letting $\varepsilon = 0$, will obtain the so called fast sub-system as:

$$\frac{dz_f}{d\tau} = g(x_0, z_{s0} + z_f(\tau), t_0); z_f(0) = z_0 - z_{s0} \quad (5)$$

The approximations for x and z are then given by:

$$\begin{aligned} x(t) &\equiv x_s(t) \\ z(t) &\equiv z_s(t) + z_f\left(\frac{t-t_0}{\varepsilon}\right) \end{aligned} \quad (6)$$

Application of Singular Perturbations to the Wind Farm Model

The singular perturbations theory outlined in the previous section was applied to the case of a wind park detailed model, whose fundamentals can be found in [29].

The first step consists in the separation of the time variables in slow variables and fast variables, in order to be able to solve them in the appropriate time scales. The variables associated with the induction generator rotors (electromotive forces and rotor speeds) were considered as slow variables, the remaining ones (stator currents, terminal voltage and branch currents) were assumed as fast variables. The main reasons for this decision are listed below:

- operating experience with the detailed model;
- empirical estimates derived from the fact that rotor transients are related with mechanical time constants, which are slower than electrical ones;
- analogy with the application of the same theory to the case of synchronous machines [30,31];
- theoretical validation [30,31].

Another important issue is the definition of the small parameter ε . It is possible to prove [30] that the physical parameter which allows the separation of the variables into slow and fast variables is the synchronous angular frequency $\omega_s=100\pi$ rad/sec. Therefore, we have considered $\varepsilon=1/\omega_s$.

Under these conditions, to obtain the slow sub-system the wind park model has to be rewritten to comply with the formulation given by equations (3). It should be mentioned that states x_s and z_s do not represent the real variables, but actually they are associated with a different system in which $\varepsilon=0$. Also, the “initial conditions” for the z_s states are fixed by the initial conditions for the states x_s and by the algebraic relationship in (3). This difference between the initial conditions of the quasi-steady-state variables and the initial conditions of the real variables explains the necessity of the boundary layer correction (5).

In order to recover the lost dynamics and obtain the fast sub-system, the system must be analyzed in a time scale compatible with the fast variations. Therefore, the time scale change (1) has to be performed and the system has to be rewritten following the rules implicit in equation (5).

Finally, the approximations for x and z are obtained from equations (6).

Aggregation methodology

Further simplification of the reduced order singular perturbations model outlined in the previous section can be achieved through the use of aggregation techniques.

As far as steady-state and transient studies are concerned, a wind park is similar to a conventional thermal power plant composed of several identical generating units. To assess its behaviour it is normal practise to use aggregated models in which the units are replaced by a single equivalent unit [32,33,34].

The same methodology is applied to the case of the wind park singular perturbations model, thus allowing the development of an aggregated wind park model. The fundamentals of the aggregated model can be symbolically expressed by the following set of equations:

$$S^{eq} = \sum_{i=1}^n S_i ; C^{eq} = \sum_{i=1}^n C_i \quad (7)$$

$$V + \delta v^{eq}(t) = V + \frac{1}{n} \sum_{i=1}^n \delta v_i(t) \quad (8)$$

$$x_i^{eq}(0) = \frac{1}{n} \sum_{i=1}^n x_i(0) \quad (9)$$

where n is the total number of WECS composing the wind park, the superscript eq refers to the single equivalent WECS and the meaning of the variables is as follows:

S – nominal power;

C – capacitance of the reactive power compensation system;

V – mean wind speed;

v – wind associated turbulence;

$x(0)$ – initial conditions of the state variables.

The aggregated model is actually a dynamic equivalent in the classic sense: the concept of equivalent wind unit comes as a result of the aggregation of the characteristics of the individual wind units in a single unit with equivalent characteristics. Furthermore, the relevant dynamics concerned with the interconnection of the park to an existing utility grid is saved.

Conclusions

In order to evaluate the performance of both the reduced order non-aggregated and aggregated singular perturbations models in describing the wind park steady-state and transient behaviour, some simulations have been carried out and the results compared with a wind park full order detailed model.

In what concerns the non-aggregated model, the results achieved with the slow sub-system model did confirm the expectations: a good performance of the slow variables, and a poor agreement, due to the lack of the stator related transients, in what concerns the fast variables. To recover the fast part, the singular perturbations boundary layer correction has been applied, thus making apparent the excellent agreement between the results provided by the full-order and reduced-order models.

Another set of simulation results demonstrated that the aggregated singular perturbations model is capable of reproducing with a high degree of accuracy the transient behaviour of the park, providing that the wind conditions as seen by the individual WECS within the park are similar.

An important conclusion derived from the simulations performed with the aggregated singular perturbations models is that when the area occupied by the park is likely to enable very different wind inputs in the WECS, a dynamic equivalent composed by a single equivalent WECS may not be enough to represent the dynamic characteristics of the park, namely in what concerns its interconnection with a utility grid. In these conditions, the WECS should be aggregated taking account for the wind conditions within the park, and therefore a two, or may be more, WECS dynamic equivalent is required to properly simulate the transient behaviour of the wind park. However, in dynamic stability studies, wind variations are less relevant when studying the first seconds after a fault.

4.2 Small Hydro Turbines

4.2.1 Introduction

In this section a model for depicting the dynamics behavior of reservoirs is presented and its usefulness demonstrated in the design of automatic controllers for small hydro plants [35]. For plants equipped with propellor type turbines the regulation of the head is very desirable under run of the river mode operation and modification to usually used governors is applied to perform the head control.

The power generated by a hydroelectric plant can be calculated from the simple formula:

$$P_m = C_o n Q_o H$$

Where

- C_o is the power conversion factor,
- n plant's efficiency,
- Q_o the flow rate and
- H the head.

By adjusting the wicket gate opening and/or the pitch angle on the turbine propellers changes are made to the effective orifice opening in the reservoir wall, thus providing

control over the release flow rate Q_o . Unfortunately, sharp variations in Q_o also cause changes in turbine's efficiency η and through the reservoir dynamics changes to the head H . The control problem is to minimize fluctuations to the power output P_m of small installations, even when rapid fluctuations in stream flow occur.

4.2.2 Reservoir Dynamics

For the modeling of the reservoir dynamics we assume run of the river rather than the conventional constant power output mode of operation.

For variations in

Head $H(t) = \bar{H} + h(t)$ (4.2.1)

Orifice opening $A(t) = \bar{A} + a(t)$ (4.2.2)

Inflow rate $Q_I(t) = \bar{Q} + q_I(t)$ (4.2.3) and

Release flow rate $Q_o(t) = \bar{Q} + q_o(t)$ (4.2.4)

We obtain the bilinear system

$$C \frac{dh}{dt} + a_H h(t) + \beta_H h(t)a(t) + a_A a(t) = Q_I(t) \quad (4.2.5)$$

where

$$C = \frac{\partial S}{\partial H}, a_H = \frac{K_d \bar{A}}{2\sqrt{\bar{H}}}, \beta_H = \frac{K_d}{2\sqrt{\bar{H}}}, a_A = K_d \sqrt{\bar{H}}$$

$$K_d = C_d \sqrt{2g},$$

S = reservoir storage

C = the orifice discharge coefficient

g = the gravitational constant

G = the wicket opening

N = the rotational (shaft) speed.

In many cases $\bar{A} \gg 1$ and as a result $\beta \ll \alpha_H$ which would render the bilinear term in (4.2.5) negligibly small and we obtain the linear model

$$C \frac{dh}{dt} = -a_H h(t) - a_A a(t) + Q_I(t) \quad (4.2.6)$$

The main control variable in this model is the change in effective orifice opening denoted by $a(t)$. The action of either the wicket gates and/or the propeller blade pitch angle provide this control. The control strategy is simple that of keeping the head variations $h(t)$ as small as possible by the appropriate choice of the control $a(t)$. Unfortunately the inflow

rate variations Q_1 are usually uncontrolled and very difficult to measure or predict and are consequently treated as input noise in this analysis of the system.

As with the linear version given in equation (4.2.6), the bilinear system of (4.2.5) has the time constant

$$T_d = \frac{C}{a_H}$$

It is also interesting to note that

$$T_d = \frac{\partial S}{\partial H} \frac{\partial H}{\partial Q_o} = \frac{\partial S(\bar{H})}{\partial Q_o}$$

Which coincides with the classical definition of a reservoir time constant.

4.2.3 A Simple Head Controller

Head control

The required head control can be provided by a simple and inexpensive modification to a conventional speed governor. One possible controller is illustrated in the schematic diagram of Figure 4.16. A mechanical float with linear transducer is used to measure head variations and the control loop is closed through an integrator-compensation unit to the conventional governor.

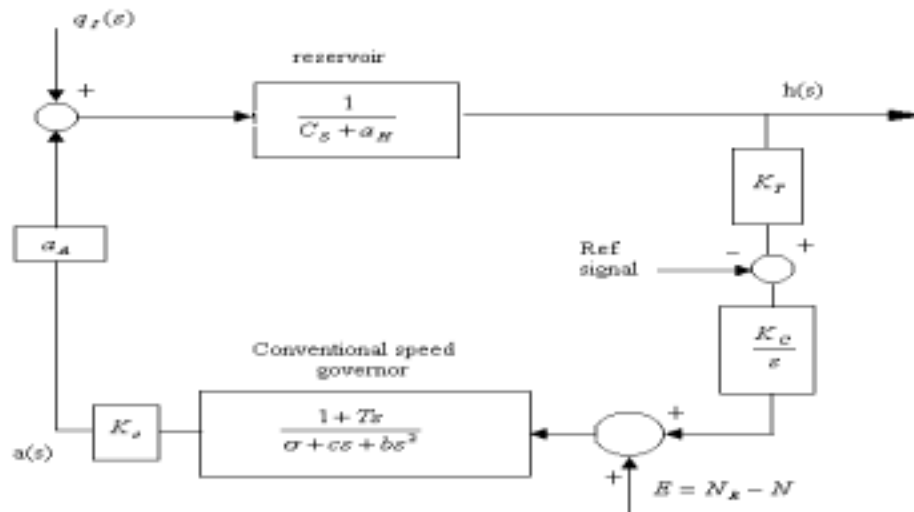


Fig. 4.16 The head control loop

To avoid excessive mathematical detail, the linear system model of equation (4.2.6) is employed to represent the reservoir dynamics in the functional block diagram of figure 4.16. The proposed controller, therefore, has the transfer function

$$h(s) = \frac{s(\sigma + cs + bs^2)}{M(s)} Q_I(s) - \frac{sa_A K_o (1 + sT)}{M(s)} E(s) \quad (4.2.7)$$

Where the polynomial

$$M(s) = Cbs^4 + (Cc + a_H b)s^3 + (C\sigma + a_H c)s^2 + (a_H \sigma + a_A K_o K_T K_c T)s + \sigma_A K_o K_c K_t \quad (4.2.8)$$

where

$$c = \frac{1}{K} + \sigma T + \delta_T T, \quad b = \frac{T}{K}$$

K = the hydraulic servomotor gain

σ = the permanent servo droop setting

T = the servo dashpot time constant

δ_T = the temporary servo droop setting

N_R = the servo speed reference signal

$E = N_R - N$ the speederror signal

K_T = the forebay (head) float transducer gain

K_C = the head controller gain

K_o = the gate position – orifice opening conversion factor

And the feedback reference signal

$$\varepsilon(s) = \frac{\bar{H}}{K_T}$$

Note that from (4.2.7) step changes in either the inflow rate variation Q_I and/or the speed error $E = N_R - N$ will produce no steady state error in the head variation h for a stable system. Stability for the system is assured if the polynomial $M(s)$ of (4.2.8) have negative real parts to all roots.

In the controller's operation the external speed setting N_R no longer control the power output of the plant. As a result, the head control loop should be disabled during “start-up” or “shut down” operations. In fact, with the head controller operative, the power output will fluctuate only with inflow rate fluctuations, i.e.

$$\Delta P_m = \frac{CK(\bar{H})^{3/2}}{a_A} \Delta Q_I$$

For $|h(t)|$ small.

An hydraulic system is normally employed in the wicket gate and/or propellor blade pitch angle actuating system. In most cases this implies physical constraints to the actuating mechanism and therefore to the effective orifice opening; i.e. $0 < A < A_{max}$.

4.3 Power Electronics Based Micro-Sources [Micro-turbines & Fuel cells]

Emerging technologies have made economically attractive the use of Fuel Cells and Micro Turbines in electric power production. Their relative small size, typically below 300 kW, makes them a good candidate to play a role in what has been defined distributed resources. They can be placed at key locations within an existing electric distribution network locally increasing the available power and enhancing the overall system reliability since these units can provide power to customers even in a event of loss of power from the main grid.

In all cases, the electricity is available at a DC stage. The interface with the electrical grid is achieved by means of power electronics. An inverter is responsible for the conversion from DC to the desired AC voltage magnitude and angle. For the Fuel Cell technology, the electricity is already produced at the device terminals in DC form. Electric power from Micro Turbines comes from the high speed permanent magnet generator coaxially installed on the same shaft of the turbine. The result is that electricity is produced typically at few kHz, and is subsequently rectified to a DC quantity. Figure 4.17 gives the broad view of a micro sourced generator where we have the prime mover responsible to sustain the voltage at the DC bus, and then there is the inverter interface to the electrical grid.

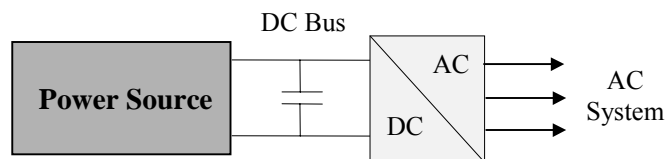


Figure 4.17. Interface Inverter System

Micro Sources

Typical macro sources used as prime movers to obtain DC electric power are Fuel Cells and Micro Turbines. Each of them has a way to control the output power by means of a fuel valve. This valve, in turn, is regulated by a governor whose goal is to maintain the DC bus voltage as constant as possible. This governor is a single input, single output block. Its input is the measure of the DC voltage, while the output is the position of the fuel valve. This position is limited by an upper (full throttle) and lower (shut off) limits. The fact that the prime mover is somewhat limited in its output performance will result in constraints in the response of the prime mover to step changes in output power requests.

It is worth spending some time to understand the way a change in the command propagates through the power source, depending on the nature of the prime mover.

Micro-Turbine

The full diagram for the prime mover based on Micro Turbine technology is represented in Figure 4.18. Here, it is possible to follow the air mass flow as it enters the compressor after having gone through the permanent magnet generator casing. This is done to achieve some sort of cooling on the electric coils of the stator that are subject to the load current. The rise in pressure is obtained by only one stage of a centrifugal compressor, borrowed from the turbocharger technology well tested in automotive industry. After this stage, the air goes through a heat exchanger called recuperator that rises the temperature of the high pressure air at expenses of the exhaust gases before they are discharged in the environment. This feature dramatically improves the efficiency of the unit. At this point the air enters the combustion chamber, where it is mixed with the fuel (typically natural gas) and burned in a continuous process. The high temperature gases are then expanded in the turbine (here again, of radial design) where the useful work is extracted and converted into mechanical form.

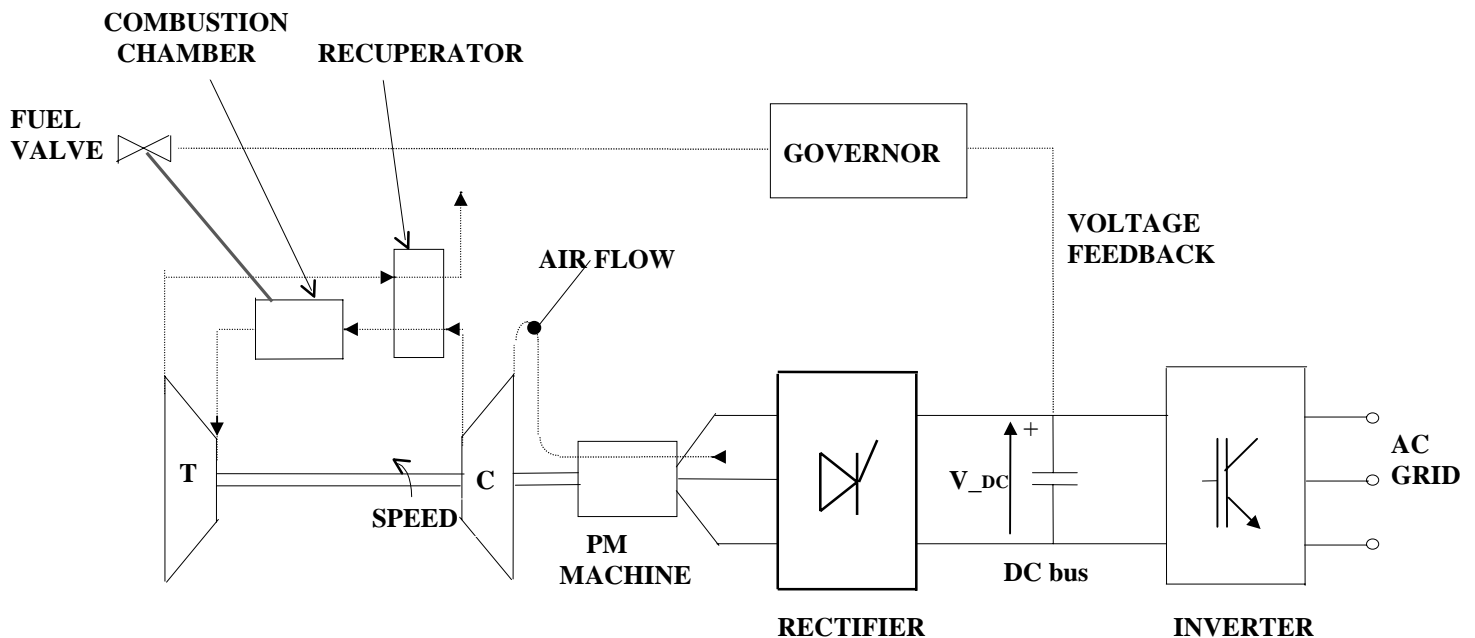


Figure 4.18. Micro-Turbine Block Diagram

The output mechanical power is regulated solely by the fuel mass flow. As the more fuel enters the combustion chamber, more heat is generated and more power is converted in mechanical form. It is important to notice that a step change in the fuel valve position will not result in an instantaneous increase of power. Actually, at the time of the change, the output power decreases. This is due to the fact that the speed of the turbine had not time to change, and the consequently the air flow entering the combustion chamber didn't have time to increase. The increased fuel rate generates a non ideal stoichiometric ratio between fuel and air, instantaneously lowering the power available at the shaft. As the turbine-compressor block increases speed, more air is drawn into the combustion chamber, allowing for all the extra fuel to be burned, and in turn for an higher power output.

Figure 4.19 shows the Micro Turbine response to a step change in the fuel valve. Time constants may be as high as 10 seconds, and this is a property of this prime mover that does not make it exactly ideal for AC system interface.

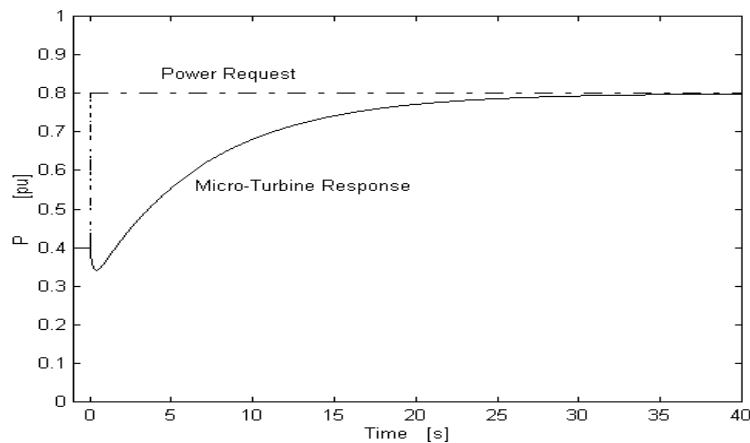


Figure 4.19. Micro-Turbine Step Change Response

The only remaining detail that is worth mentioning is that the electric power available at the terminals of the permanent magnet machine is produced at a frequency that is directly proportional to the Micro-Turbine speed. Generally, there is no control loop to regulate the speed and therefore there is no mean to set the output frequency to a desired value. Furthermore, the thermodynamics of the compressor and turbine block require the mechanical speed of the shaft to be some tens of thousand of revolutions per minute, which makes the frequency of the output electric quantities to be in the range of few kHz. Network interface requires a tight control of the frequency, therefore the conversion to an intermediate DC stage before conversion to the desired constant frequency is mandatory.

Fuel Cell

The Fuel Cell technology-based prime mover diagram is shown in Figure 4.20. As in the micro-turbine, we can recognize the DC bus voltage measurement that is fed in a controller, whose output regulates the position of a fuel valve. Fuel Cells are capable to produce low voltage at the sides of a membrane.

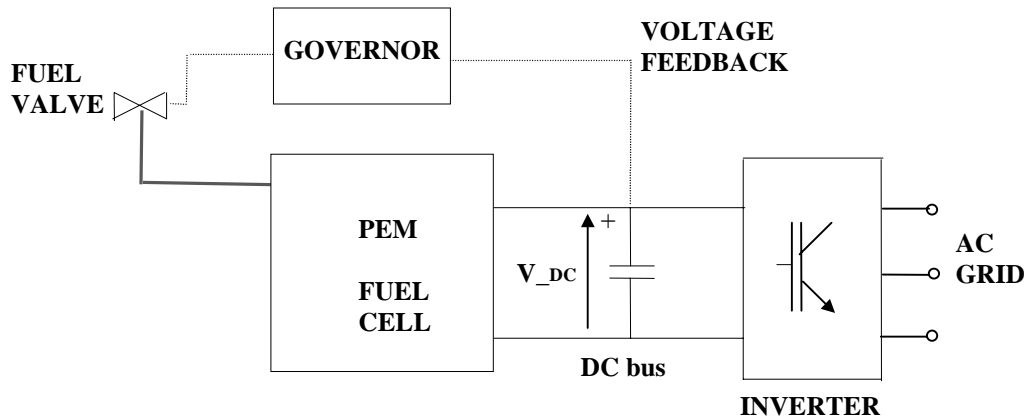


Figure 4.20 Fuel Cell Block Diagram

The breathing Proton Exchange Membrane (PEM) can be crossed only by ions charged with one sign, while it is totally impermeable to the charges of the other sign. The sides of the membrane result charged like the plates of a condenser. The charges can reach the other side of the membrane by flowing through the external circuit, which is the electrical load. Once the charges arrive from the load, they neutralize the ones already existing on the other side of the membrane.

The result of this process is that charges of opposite sign must be constantly created at either side of the membrane. The accumulation of charges comes from a ionization process driven by a chemical reaction. This reaction is highly sensitive to parameters such as concentration of the reactants and products of the reactions, temperature and pressure.

Each membrane has a determined maximum voltage that it can produce given by the charges per unit of surface that are present, while the current is determined by the total amount of charges, which is determined by the total surface of the membrane. Typically, one membrane can produce less than a Volt between its sides. It is required to stack tens of these membranes to obtain an output voltage level that can be suited for AC system interface.

A step change in the input reactant element will not be noticed as a sudden increase in charges at the sides of the membrane. Typically, there is a sudden but contained rise in output power that takes place in 2-3 seconds, while the newly desired output power level is reached as the membrane reaches its thermal equilibrium, which may take up to a minute. Figure 4.21 shows the response of the Fuel Cell to a step change command in the desired output power.

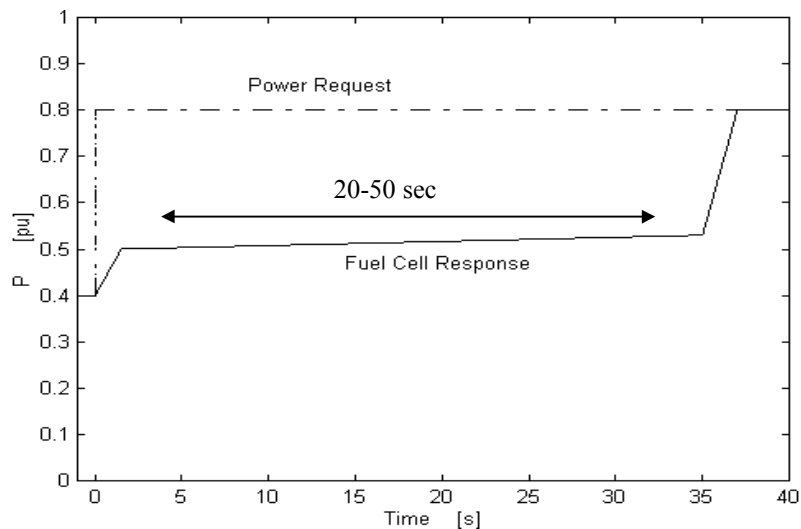


Figure 4.21. Fuel Cell Step Change Response

This characteristic makes the Fuel Cell a poor candidate for a direct AC grid interface, where loads require power instantaneously, as the breaker closes the circuit with a new load.

Instantaneous Power Issue

The introduction of a micro-source within an existing power system assumes that there may be a cluster of small generators located in electrical proximity, interconnected through on-site feeders and operation can be isolated or connected to a transmission/distribution grid.

Micro sources have a slow response to changes in commands and also do not provide any kind of internal form of energy storage. These inertia-less systems are not well suited to handle step changes in the requested output power. It must be remembered that the current power systems have storage in the mechanical energy of the inertia of the generators. When a new load comes on line the initial energy balance is satisfied by the inertia of the system: this results in a slight reduction in system frequency.

The power electronics interface between the DC bus and the AC grid has fast response and is inertia-less, this due to the fact that the matrix of switches of the inverter does not have any sort of energy storage capability. The step sized power demand in the AC system should be instantaneously matched by an identical supply of power from the micro source prime mover.

Distributed resources have a problem in instantaneous power tracking. Figure 4.22 shows that a poor load tracking is penalized with a difficulty in holding the local voltage to the desired value. Here a load comes on-line and the micro-source ramps up to pick up the whole quota of extra power request. The missing transient power that the micro-source is

not fast enough to provide is taken from the connection with the grid that supplies only a part of the local requested power during steady state. The voltage is not affected too much in its magnitude since the power is instantaneously given to the load in its full amount.

The requested power from the load coming on-line is a step function, while the inertia-less micro source always takes a finite amount of time to ramp up to the newly requested value.

Figure 4.23 shows a load coming on-line in an islanded mode, with no connection from the grid. Since the unit cannot change its output power instantaneously, the power that goes instantaneously to the new load is taken from the other loads. This process takes place at the price of a reduction of the regulated bus voltage magnitude. As the power injected from the micro source increases to cover completely the newly connected load, then the voltage is restored to the customary value.

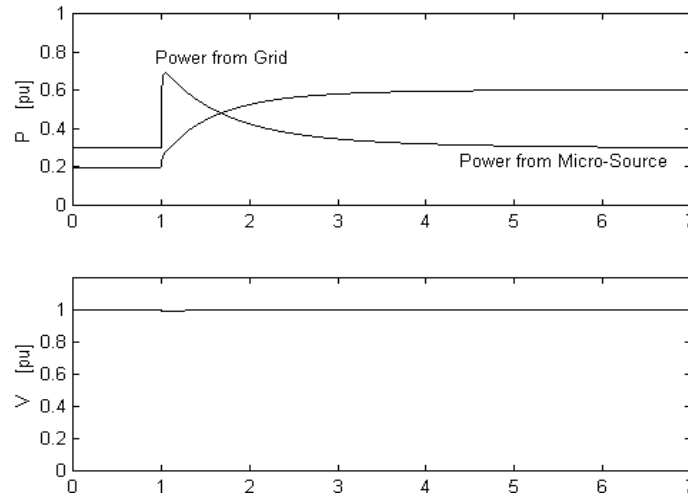


Figure 4.22. Load Coming On-Line with Grid Connection

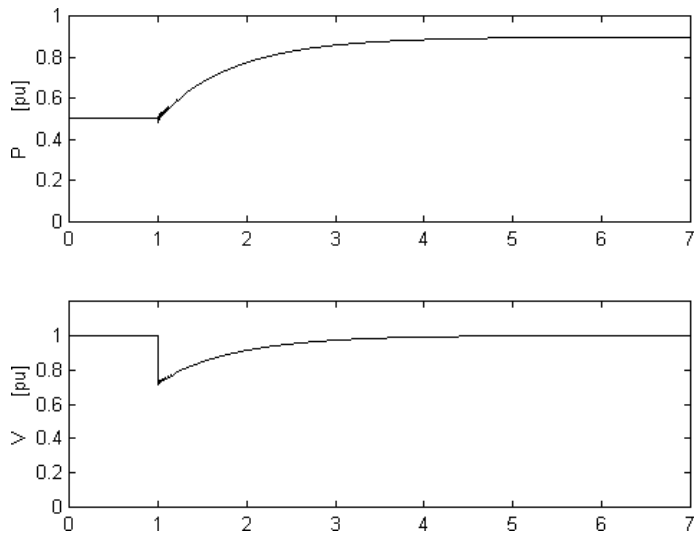


Figure 4.23. Load Coming On-Line without Grid Connection

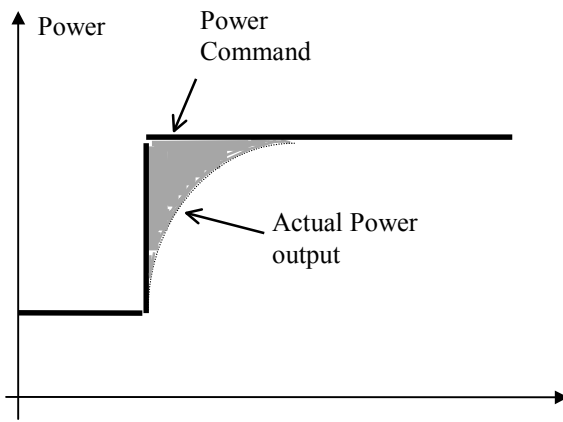


Figure 4.24. Missing Transient Energy t

Figure 4.24 shows that there is a missing quota of energy from the difference of the power that the load is requesting and the power that the unit is able to provide shown by the shaded area.

If the connection to the main grid is active, then the missing quota can be provided by the utility. It will be seen from the grid terminals as a temporary, pulse-like power request. Utilities do not like these topology of events, since they are hard to service.

If the connection to the grid is missing due to a malfunction or a to geographical constraint that makes it impracticable, then the need for some sort of storage is manifest. Voltage drop could be large even for small loads coming on line. Storage is requested to satisfy the instantaneous power balance as a new load comes on-line without penalizing the quality of other network quantities, such as bus voltage magnitudes. Storage can be provided on the DC as well on the AC side at the point of including rotating machines in the Micro-grid.

The capacitor bank that we see in Figure 4.18 located on the DC bus is only sized to smoothen the voltage ripple, but by all means it is not able to store and provide the transient amount of energy that is missing as of Figure 4.24. Storage can take place in different forms, but the most practical is the DC battery placed in parallel to the already existing DC bus terminals of the distributed resource.

Customers may indicate the sensitivity of each of their load clusters, setting the boundaries for the largest voltage dip that they can tolerate. It is possible to optimize the size of the battery knowing the physical location and sensitivity of the local loads, setting the stage for the hybrid system constituted by the combination of the distributed resource with the storage capability of the battery bank. Such a hybrid system allows for many degrees of freedom providing a solution to customers with different system needs and priorities in their loads.

To complete the picture it is important to notice that at a given time, there may be more distributed resources located in electrical proximity to each other. Power sharing during island mode must be addressed since it is critical to system performance and survival in such times. Control of the inverters that perform the grid interface should be based only on information available locally. In a system with many micro-sources, communication of information between systems is impractical. Communication of information may be used to enhance system performance, but must not be critical for system operation. Essentially this implies that the inverter control should be based on terminal quantities only.

To summarize, the introduction of micro-source within the context of an already existing grid can provide control of local bus voltage, control of base power flow thus reducing the power demand from the main grid feeder, and ultimately frequency control associated with load sharing within units located in the micro-grid.

4.4 Photovoltaic Systems (PVs)

The typical structure of a grid connected photovoltaic generator is shown in Figure 4.25. Its main subsystems are the PV array, the DC/DC and DC/ACs converters and the associated (converter and overall system) controls [36-39]. A storage device is absent in large grid-connected installations (except maybe for small critical loads of the plant, such as start-up controls, computers etc.).

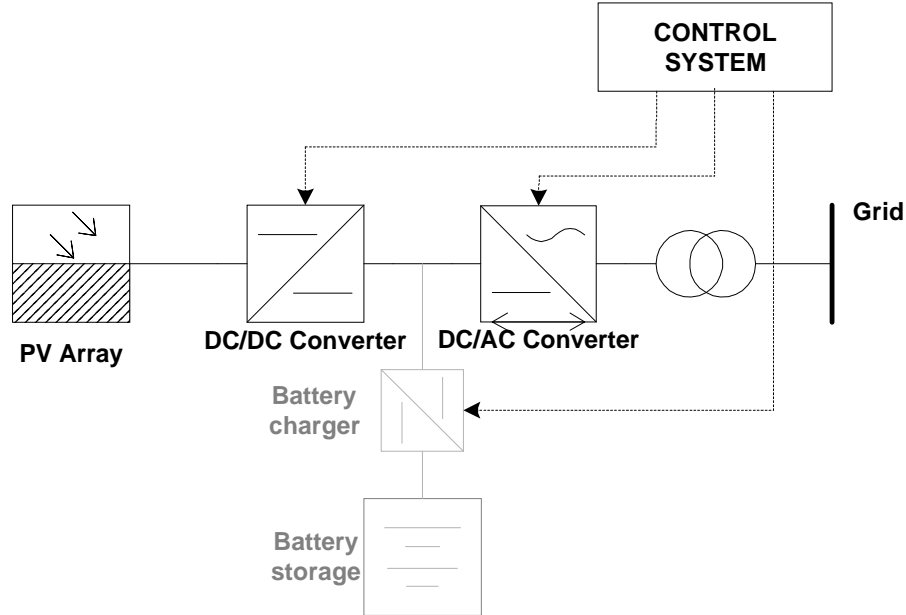


Figure 4.25. Typical structure of a grid connected PV generator.

In Figure 4.26 the electrical equivalent circuit of a PV cell is shown. Its main elements are the dc photocurrent I_L source and the shunt diode D. The series resistance R_s represents the internal losses due to the current flow, whereas the shunt resistance R_{sh} corresponds to the leakage current to the ground and it is commonly neglected. In an ideal cell $R_s = R_{sh} = 0$, which is a relatively common assumption. The equivalent circuit of a PV module, which consists of a combination of series and parallel connected cells is the same.

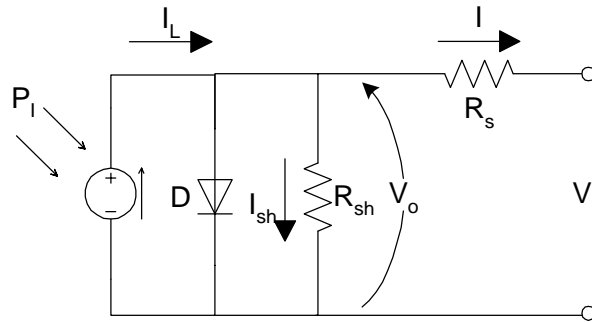


Figure 4.26. PV cell equivalent circuit.

The equations describing the equivalent circuit of Figure 4.26 are the following:

$$V = V_o - R_s I$$

$$I = I_L - I_D \left[\exp\left(\frac{qV_o}{AkT}\right) - 1 \right] - I_{sh}$$

$$I_{sh} = \frac{V_o}{R_{sh}}$$

$$I_L = I_{sc1} \left(\frac{P_I}{1000} \right)$$

- where V , I are the output voltage and current
 q the electron charge ($1.6 \cdot 10^{-19}$ Cb)
 k the Boltzmann constant ($1.38 \cdot 10^{-23}$ J/K)
 T the temperature in K
 A the quality factor (constant)
 I_D the reverse saturation current of the diode
 I_L the photocurrent, dependent on
 P_I the insolation level in W/m^2
 I_{sc1} the short circuit current at $1000 W/m^2$ solar radiation

Multiple PV modules are connected in series and in parallel to form the PV array. Similar equations hold for the whole array, provided that all modules are identical and subject to the same insolation.

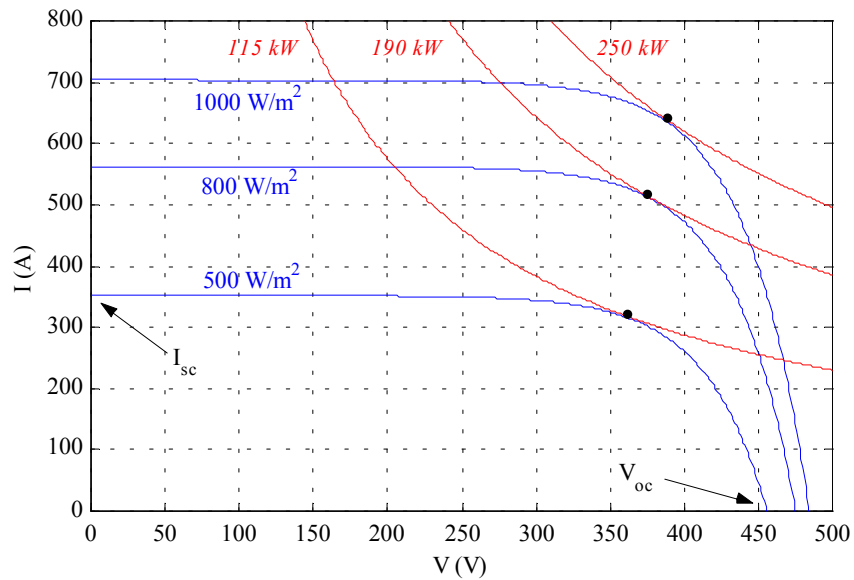


Figure 4.27. Typical PV array V-I characteristics.

In Figure 4.27 the V-I characteristics of a 250 kW array are shown at three solar radiation (P_I) levels. On the same diagram three constant power curves (red lines) have been drawn. It is clear that, for a given insolation, the array produces maximum power only when operating near the knee point of the corresponding V-I curve (maximum power point). The task of tracking the maximum power point (MPPT) is usually performed by a DC/DC converter at the output of the array, which regulates the voltage to the desired

value. Since no moving parts are employed in this process, the response of the MPPT can be considered instantaneous for system studies.

A device that may affect the response of the PV generator output in case of solar radiation changes is the sun-tracking system of the panels, which adjusts the orientation of the panels with respect to the sun, a task performed by the use of properly controlled servomotors. However, these are relatively slow acting devices and may be ignored in transient stability studies.

As discussed in Section 3.5, the remaining of the system components (dc bus, inverter and grid-connection devices) are of similar nature and characteristics as for other dispersed generators (e.g. variable speed wind turbines) and similar are the modeling requirements, too.

4.5 Superconducting Magnetic Energy Storage Systems (SMESS)

4.5.1 Introduction

In systems that are transient stability limited, SMES real-power modulation based on fault-dependent control schemes can provide considerable power transfer enhancement. Fast high-power energy is provided to the system either in a braking or a generating mode in a matter of milliseconds. The amount of power and energy that is required for transient stability enhancement is highly system dependent. In many cases, power modulation will only be required for a few seconds after the fault occurs. This provides support long enough for the system to ride through first-swing instability or for traditional remedial action schemes to take effect. Such brief demands limit the stored energy requirement.

Because SMES can be charged and discharged rapidly, it can be accurately modeled as a source of real and reactive power injection in electromechanical stability studies [40]. Converter controls can be operated so that power injection is relatively independent of bus voltage. Also, modern forced-commutation converters allow for independent control of the real or reactive injections, provided the combined injection is within the hardware rating. Therefore, the effect of the power converter is small, and thus the power injection can be assumed to equal the output of the stability controller.

A SMES power-swing damper uses feedback through a compensating controller to modulate SMES real power, reactive power, or a combination of real and reactive power. The design of the modulation control requires a detailed understanding of the stability characteristics of the system and how these characteristics are affected by SMES power injection. The relative merit of real versus reactive modulation is dependent on the location of SMES and the nature of the oscillation.

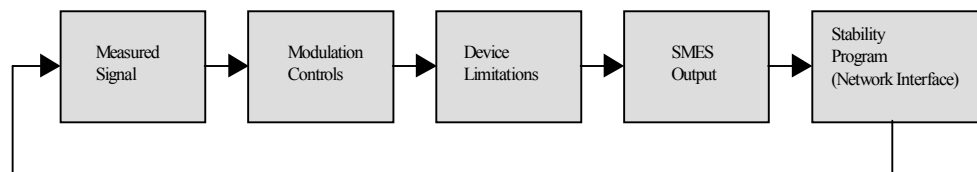


Figure 4.28. General SMES model block diagram.

Provisions should be available for the user to model different device limitations that may be appropriate to the particular study being performed. For example, limits of the maximum and minimum outputs may be entered as a function of state-of-charge on the device. Also, studies of simultaneous real and reactive modulation may require conditional limits (i.e., the reactive power capacity calculated as a function of real power output). Similarly, limitations on rate-of-change or delayed response times (to model the effect of the power converter system) may also be included. An example of implementing device limitations is given in Figure 4.29. Depending on the needs of the user, the limits can be fixed, or implemented as a function of other variables [41].

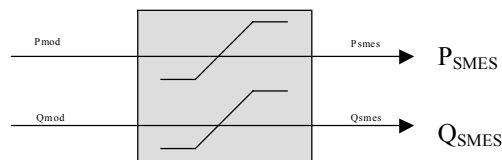


Figure 4.29. General structure of device limitation implementation example.

4.5.2 SMES Operation and Control

The main SMES structures are based on voltage source inverters (Fig. 4.30) [40,42]. The voltage source inverter generates a controllable ac voltage source $u=V\sin(\omega t-\psi)$ behind a leakage reactance. The voltage difference across the coupling transformer reactance produces active and reactive power flows with the network. The chopper is used to maintain a constant dc voltage across the capacitor; in the end, the active power exchanged with the power system comes from the superconducting coil.

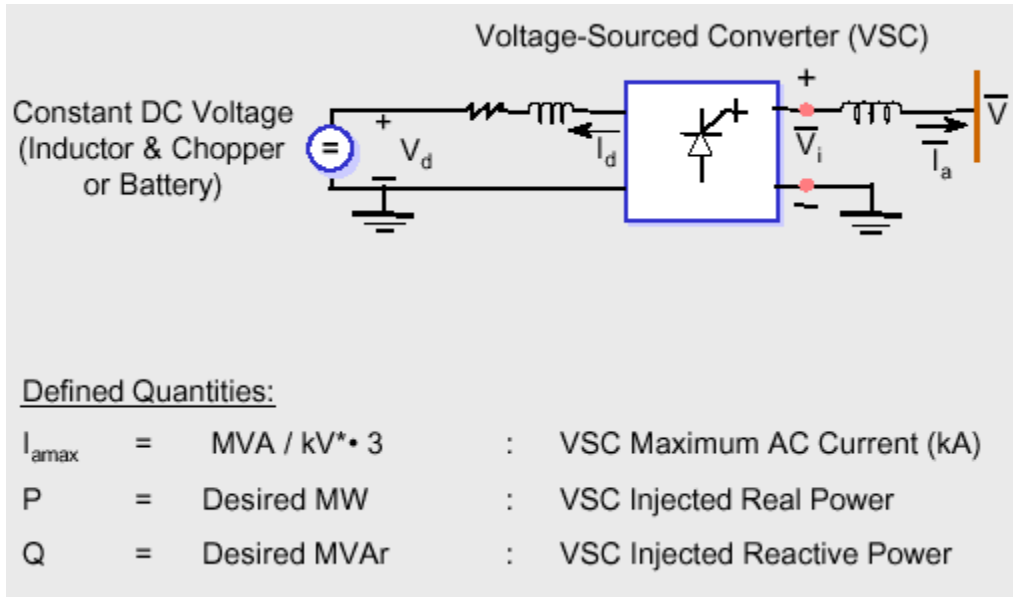
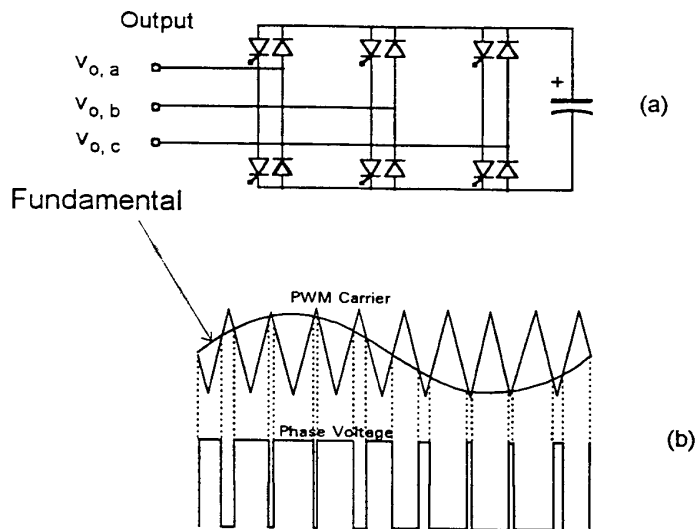


Figure 4.30: SMES operating principle

Figure 4.31 shows the basic voltage source inverter and chopper structures respectively. The most common method used for controlling the AC voltage generated by the inverter is the pulse-width modulated inverter, since the dc voltage is constant.



**Figure 4.31: (a) voltage source inverter using GTO thyristors
(b) pulse width modulated**

Figure 4.32 shows the chopper operating principle. The dc voltage can be applied across the superconducting coil and modifies the current in that coil. At the same time the superconducting current goes through the dc capacitor and modifies the dc voltage.

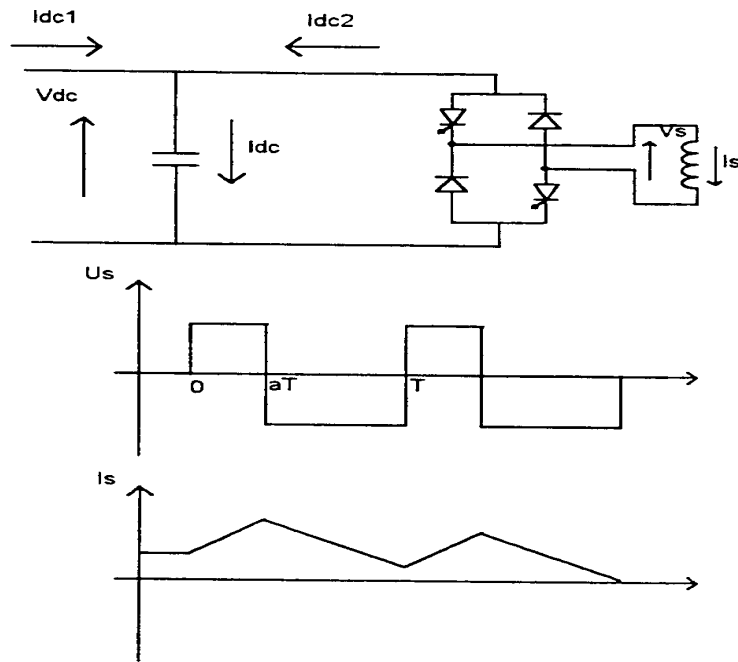


Figure 4.32: Chopper operating principle

With a constant dc reference voltage the following control principles apply:

- changing the ratio m defined by the PWM, enables the converters to adjust the magnitude of the ac voltage and thus the exchange of reactive power with the network,
- changing the phase shift ψ between the network voltage and the voltage generated by the converter makes possible an exchange of active power. The DC voltage is controlled to a given reference value by an exchange of active power between the superconducting coil and the chopper.

Figure 4.33 shows the SMES V-I characteristics. Under steady-state conditions ($I_p=0$), the real power output of the SMES is zero and the SMES can only exchange reactive power with the network. The operating area is defined by the maximum capacitive and inductive currents, the maximum reference voltage (inverter rating) and the minimum operation voltage for the inverter.

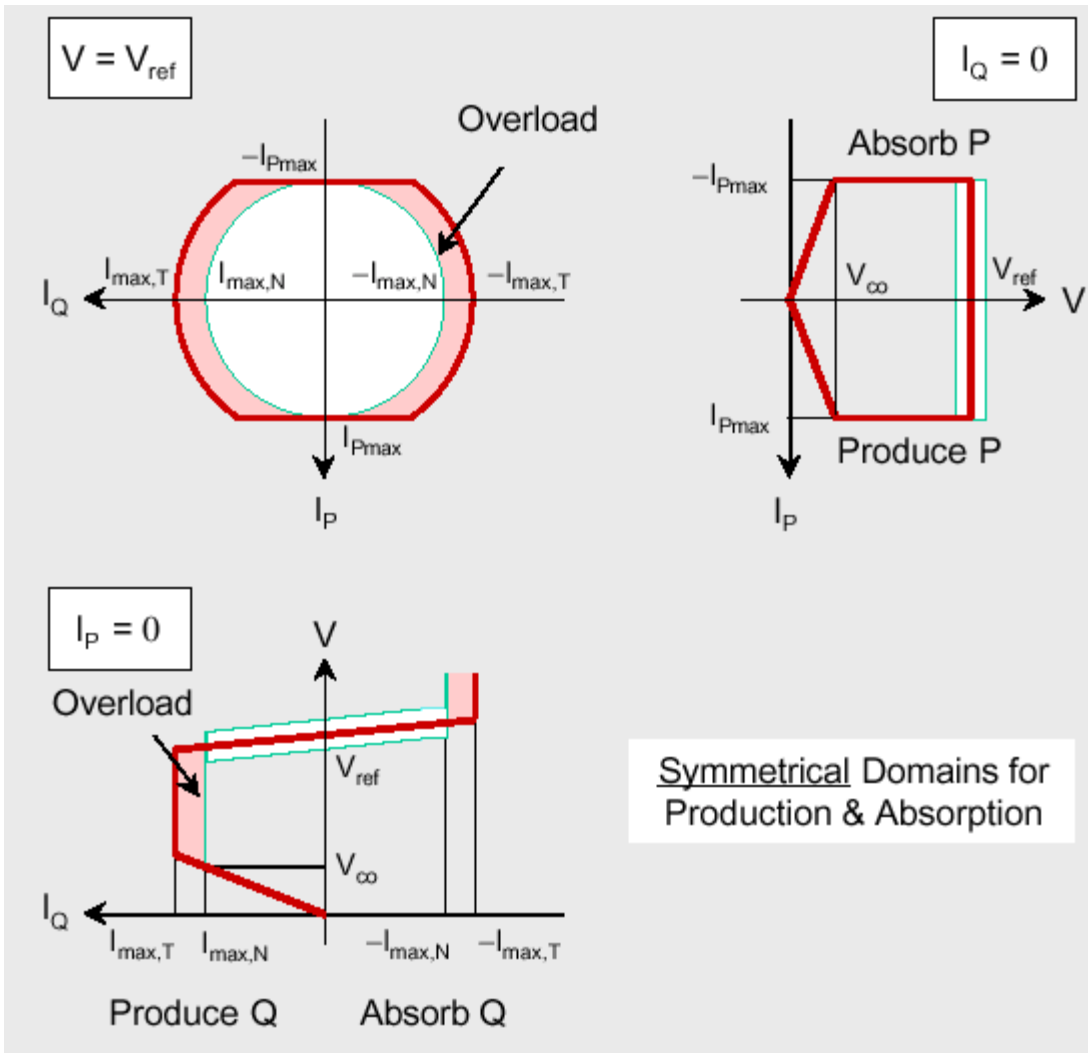


Figure 4.33: SMES V-I characteristics

Figures 4.34 to 4.38 show a dynamic SMES model with a block diagram representation [42]. Figure 4.34 provides the dynamic model of the coil, Figure 4.35 for the voltage source converter control, Figure 4.36 the frequency control block diagram together with the converter active current limits (Figure 4.37) and Figure 4.38 the ac voltage control diagram.

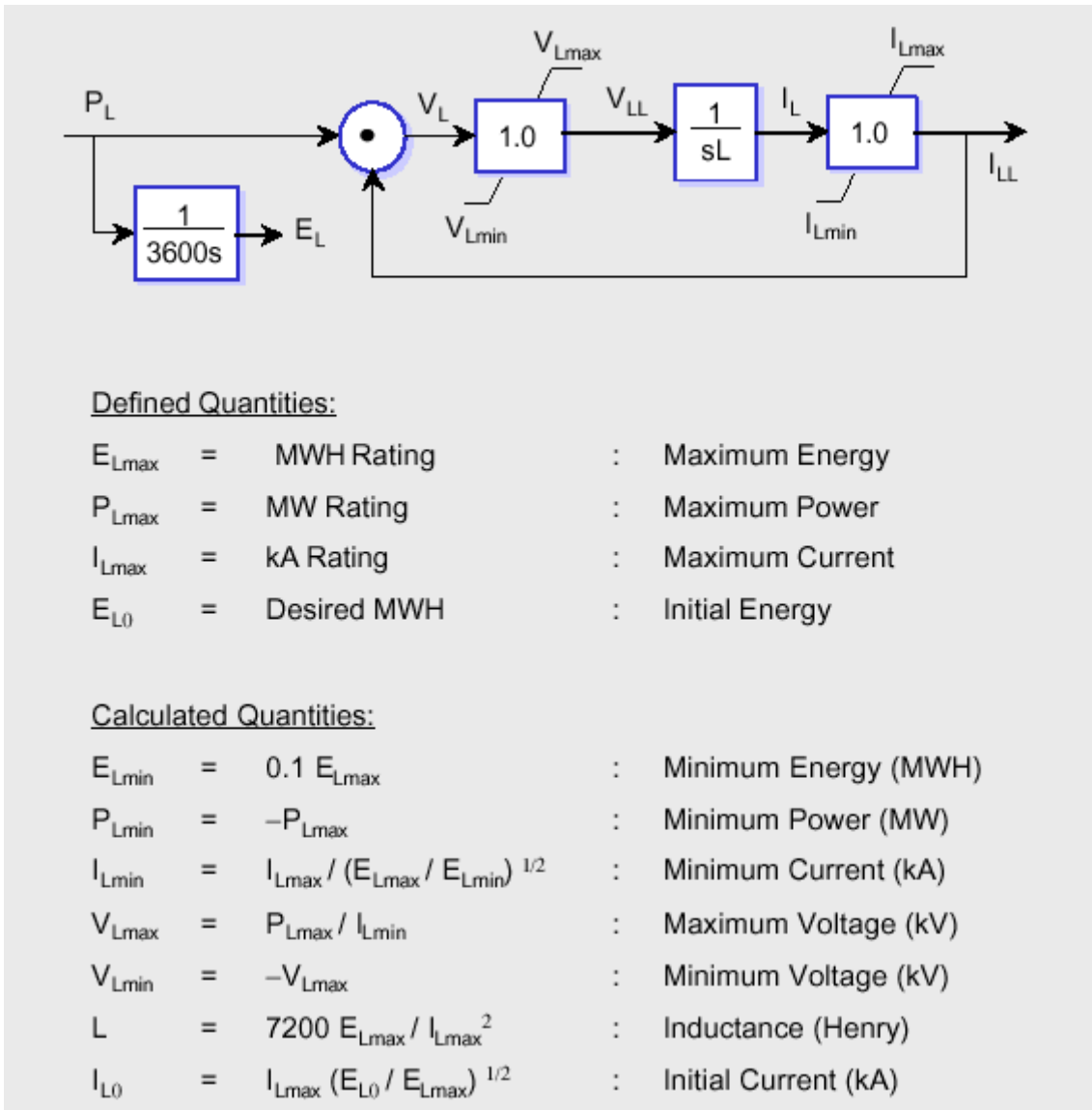


Figure 4.34: Dynamic Model of Inductor

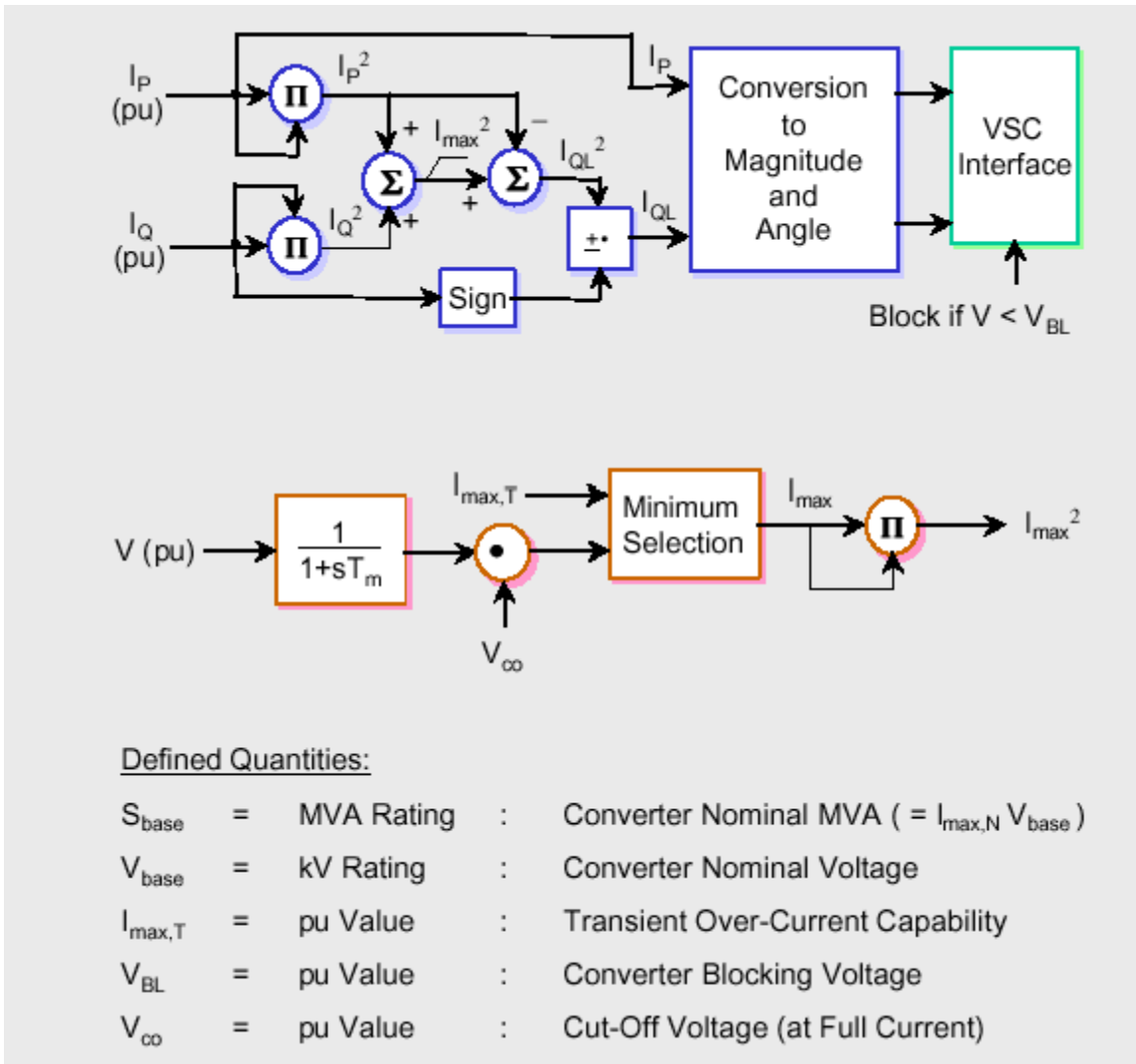


Figure 4.35: Voltage Source Converter Control (SMES/BESS)

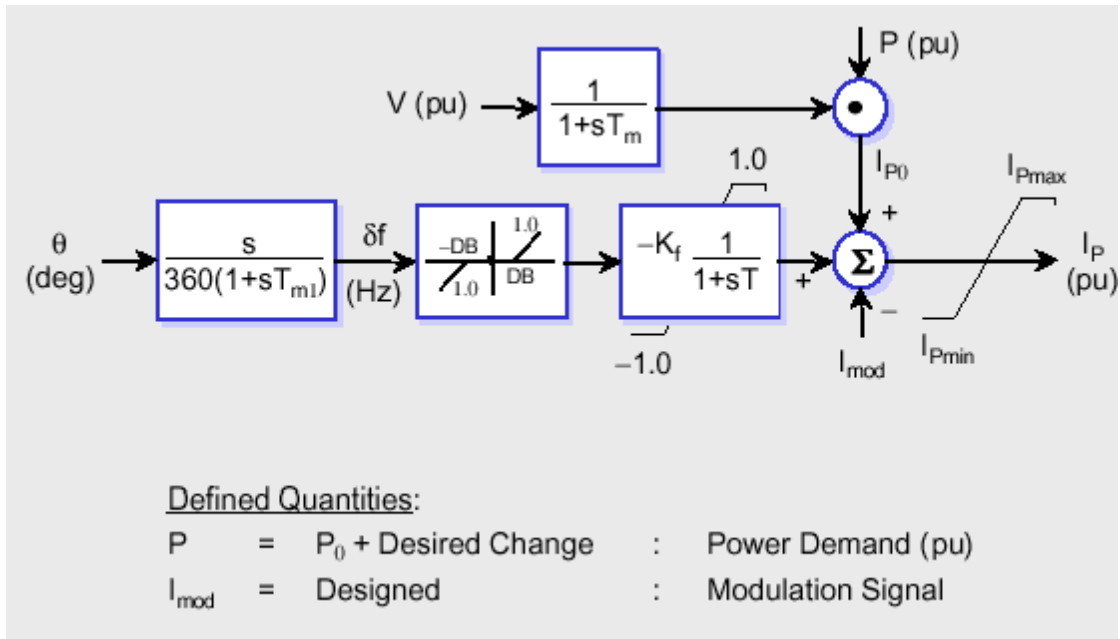


Figure 4.36: Frequency Control Block (SMES/BESS)

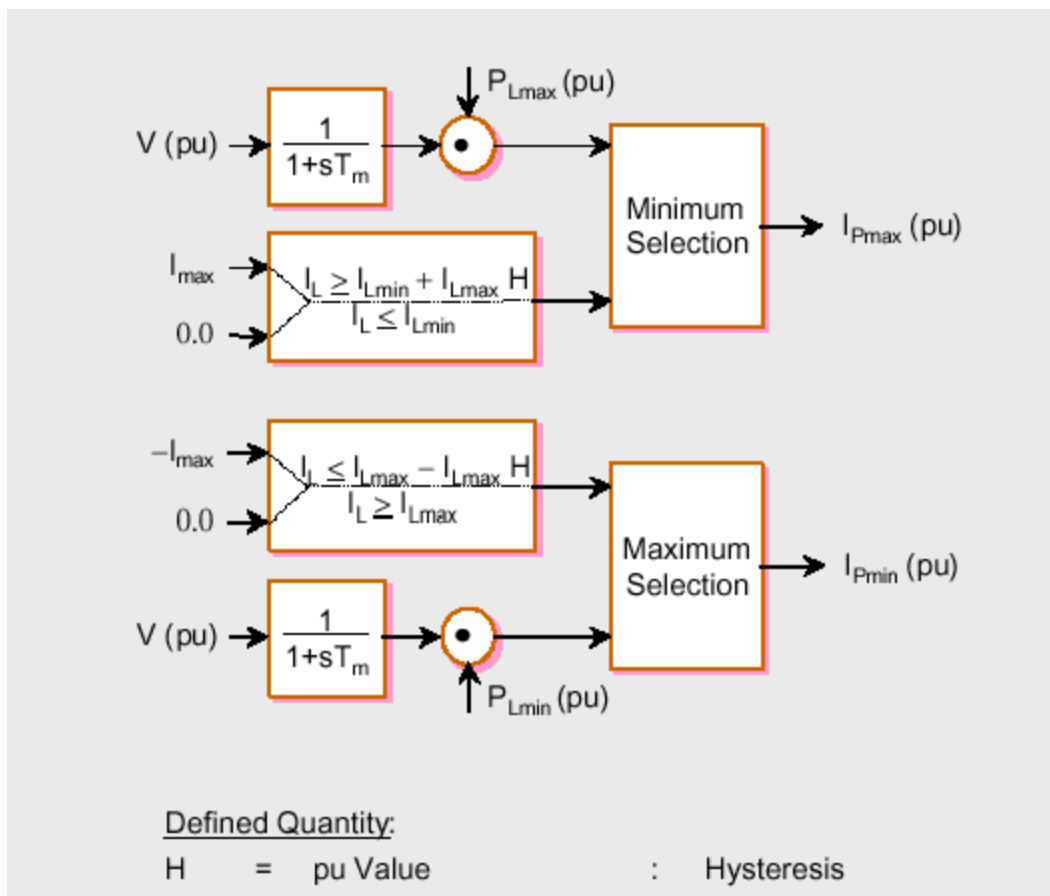


Figure 4.37: Converter Active Current Limits

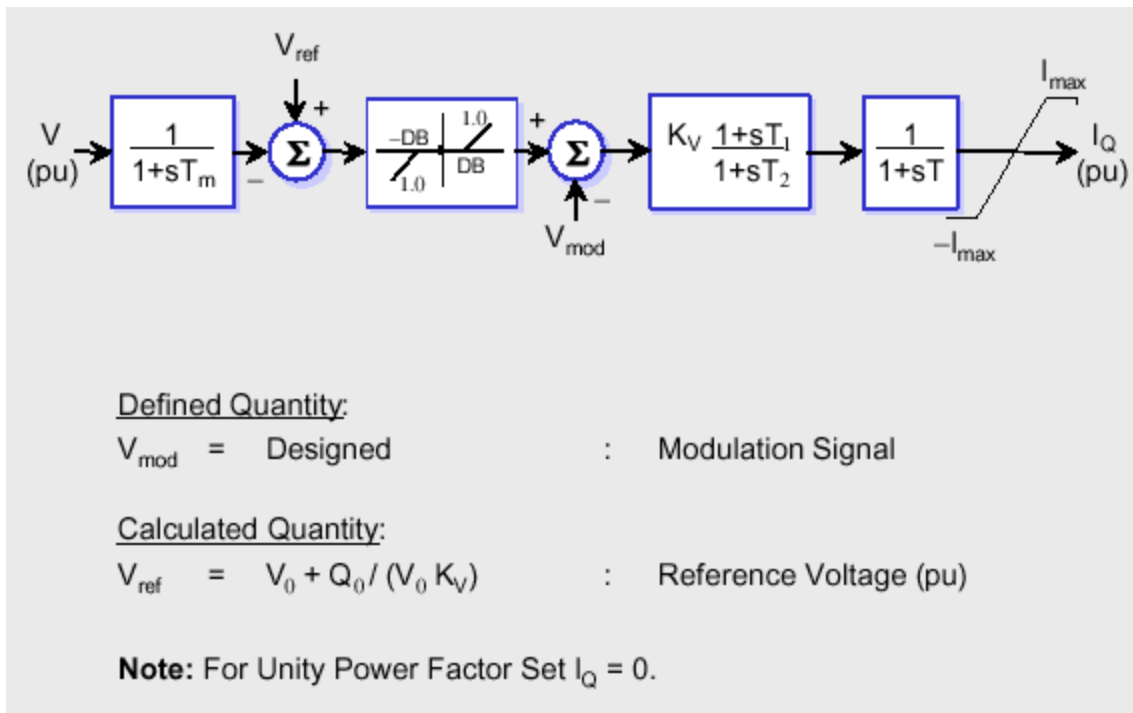


Figure 4.38: AC Voltage Control Block diagram.

Similar models are provided in [40]. Figure 4.39 shows the SMES dynamic model.

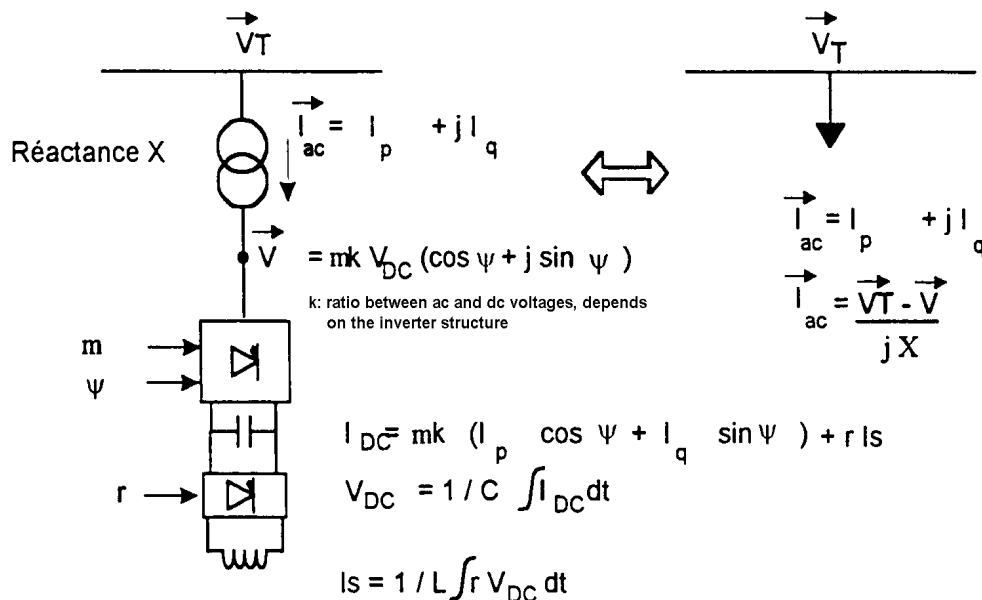


Figure 4.39: SMES dynamic model

The ratio k between ac and dc voltages depends on the inverter structure, m is defined by the PWM, phase ψ is defined by the PWM and ratio r is defined by the chopper. Figure 4.40 gives the control block diagrams for the voltage source converter. The outputs are the parameters ψ and m needed for the PWM technique.

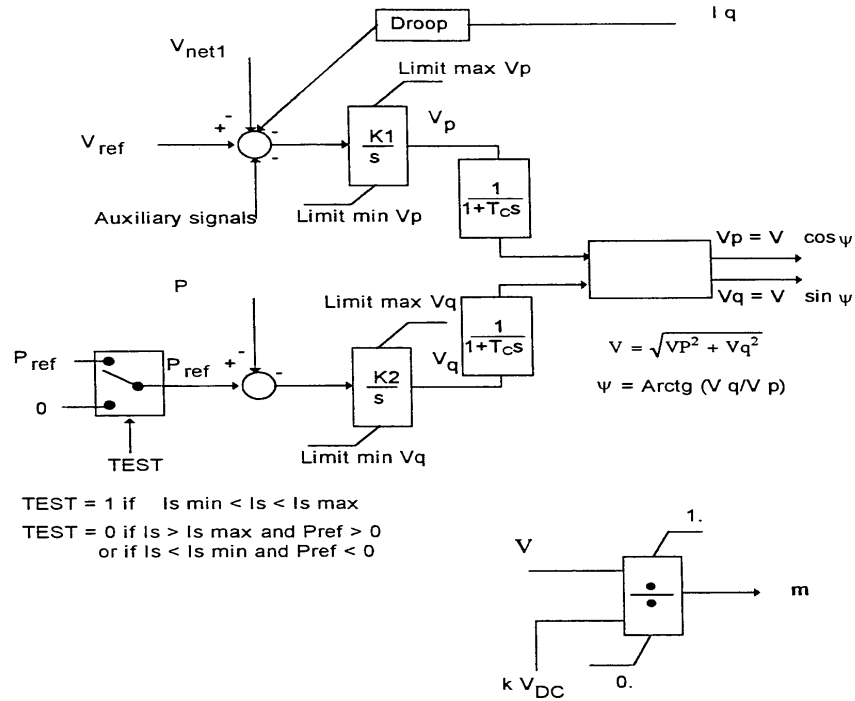


Figure 4.40: Control block diagrams for the voltage source

The component V_p is used to control the ac voltage because an insertion of V_p is in phase with the network voltage and gives rise to a reactive current which has an effect on the voltage magnitude. The component V_q is in quadrature with the network voltage and gives rise to an active current which is used to obtain the active power P_{ref} required by the power system. Depending on the application, the reference P_{ref} can be used to improve the network transient stability or to supply power during a short disturbance (a few seconds).

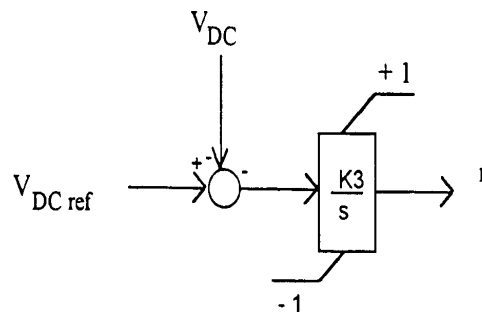


Figure 4.41 Control block diagrams for the chopper

Figure 4.41 describes the dc voltage regulation by the chopper. The reference for the dc voltage is a design constant.

Accordingly, the SMES model comprises:

- ac voltage regulation,
- active power regulation. Pref represents the active power needed by the application. This exchange of active power can take place as long as there is enough energy stored in the superconducting coil. The reference Pref is set to zero if the coil current is under Ismin or above Ismax (minimum and maximum current allowed by the coil). Under steady state conditions the value of Pref must be defined with a very slow time response in order to keep the coil current close to its nominal value
- A first order transfer function for the converter time constant (Tc),
- Voltage limits corresponding to the current ratings of the SMES.

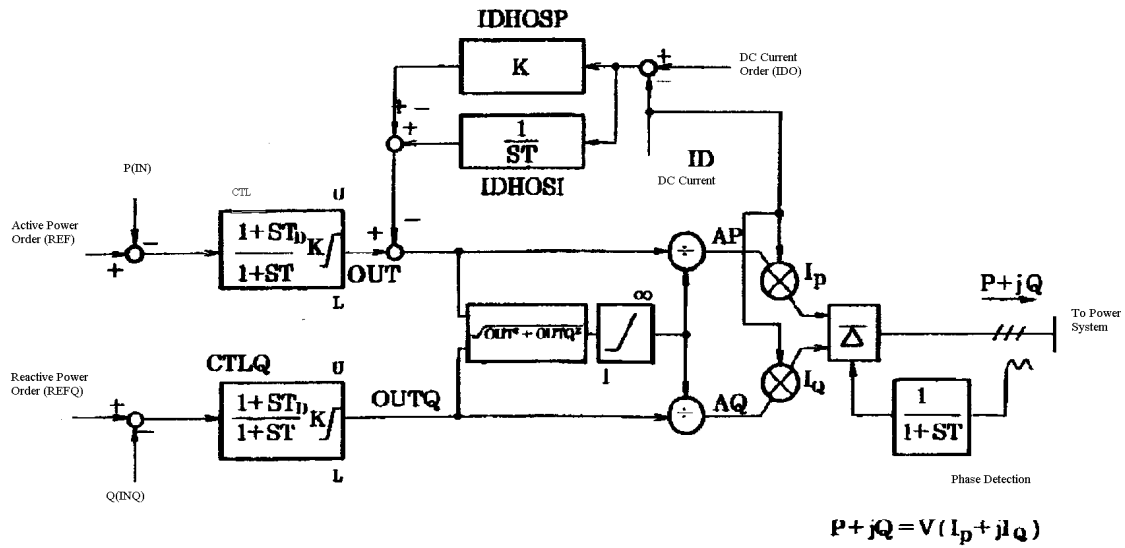
Limit max $V_q = X I_{max}$ (X transformer leakage reactance)

Limit min $V_q = -X I_{max}$

Limit max $V_p = V_T + X I_{qmax}$ ($I_{qmax} = \sqrt{I_{max}^2 - I_p^2}$,
 $I_p = V_q / X$ and limited by I_{max})

Limit min $V_p = V_T - X I_{qmax}$

I_{max} is the current rating; in this case priority is given to the active current.



Controllable Region of AP dependent on DC

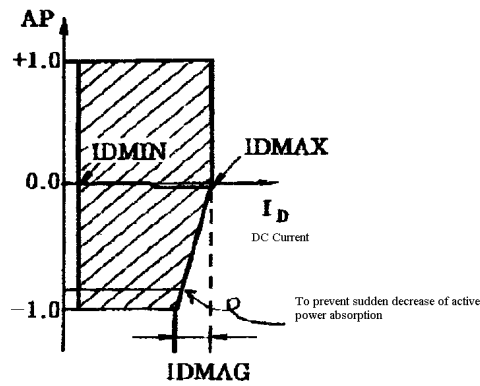


Figure 4.42 SMES model for stability analysis used in CRIEPI's stability analysis program (Y-method).

4.6 Battery Energy Storage Systems (BES)

The fundamental configuration of an equivalent BES system is shown in Fig. 4.43, which contains an equivalent battery composed of parallel/series connected battery cells, a 12-pulse cascaded bridge circuit connected to a Y/ Δ -Y transformer, and a control scheme. The ideal no load maximum DC voltage of the 12-pulse converter is expressed as

$$E_{DO} = E_{DO1} + E_{DO2} = 2 \times \frac{3\sqrt{6}}{\pi} V_t \quad (4.11.1)$$

where V_t is the line to neutral r.m.s voltage.

The terminal voltage of the equivalent battery is obtained from

$$V_{BT} = E_{DO} \cos a - R_C I_{BES} = \frac{3\sqrt{6}}{\pi} V_t (\cos a_1 + \cos a_2) - \frac{6}{\pi} X_{CO} I_{BES} \quad (4.11.2)$$

where X_{CO} = commuting reactance

I_{BES} = DC current flowing into equivalent battery

a_1 = firing delay angle of converter I

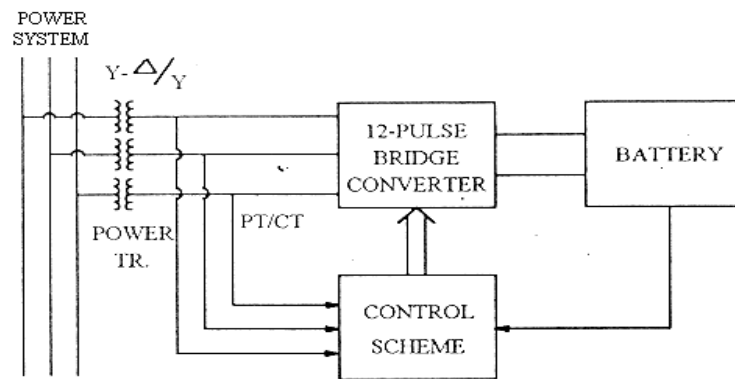


Fig. 4.43. Fundamental Configuration of BES in power system.

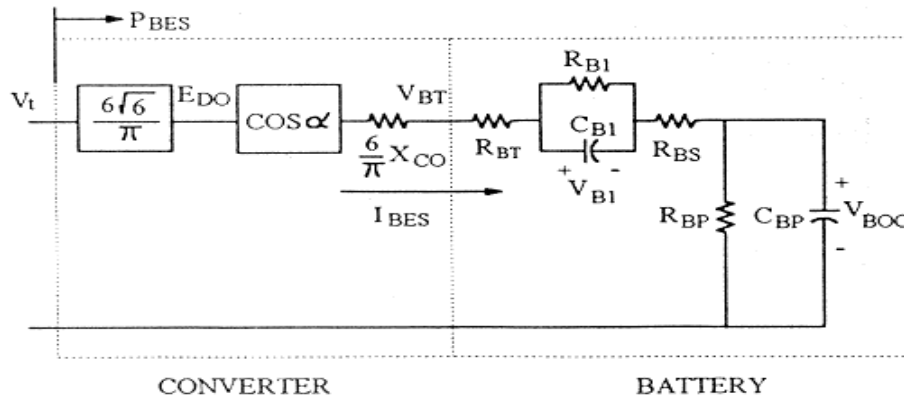


Fig. 4.44. Equivalent circuit of BES.

The equivalent circuit of the BES can be represented as a converter connected to an equivalent battery as shown in Fig. 4.44 with the same cosine value of the firing delay angles in (4.11.2). In the battery equivalent circuit :

V_{BOC} = battery open-circuit voltage
 V_{B1} = battery overvoltage
 R_{BT} = connecting resistance
 R_{BS} = internal resistance
 R_{B1} = overvoltage resistance
 C_{B1} = overvoltage capacitance
 R_{BP} = self discharge resistance
 C_{BP} = battery capacitance

We can obtain the expression of the DC current flowing into the battery from the equivalent circuit analysis as

$$I_{BES} = \frac{V_{BT} - V_{BOC} - V_{B1}}{R_{BT} + R_{BS}} \quad (4.11.3)$$

where $V_{BOC} = \frac{R_{BP}}{1 + SR_{BP}C_{BP}} I_{BES}$ (4.11.4)

$$V_{B1} = \frac{R_{B1}}{1 + SR_{B1}C_{B1}} I_{BES} \quad (4.11.5)$$

According to the converter circuit analysis, active power and reactive power absorbed by the BES are

$$P_{BES} = \frac{3\sqrt{6}}{\pi} V_t I_{BES} (\cos a_1 + \cos a_2) \quad (4.11.6)$$

$$Q_{BES} = \frac{3\sqrt{6}}{\pi} V_t I_{BES} (\sin a_1 + \sin a_2) \quad (4.11.7)$$

There are two control strategies

(1) PQ modulation: $a_1 = a_2 = a$

$$P_{BES} = \frac{6\sqrt{6}}{\pi} V_t I_{BES} \cos a \quad (4.11.8)$$

$$Q_{BES} = \frac{6\sqrt{6}}{\pi} V_t I_{BES} \sin a \quad (4.11.9)$$

(2) P modulation : $a_1 = -a_2 = a$

$$P_{BES} = \frac{6\sqrt{6}}{\pi} V_t I_{BES} \cos a = E_{DO} I_{BES} \cos a = V_{CO} I_{BES} \quad (4.11.10)$$

$$Q_{BES} = 0 \quad (4.11.11)$$

where $V_{CO} = E_{DO} \cos a$ is the DC voltage without overlap.

Since only incremental active power is considered in load-frequency control, we select P modulation. Linearisation of equation (4.11.10) gets the incremental power of the BES:

$$\Delta P_{BES} = V_{CO}^0 \Delta I_{BES} + I_{BES}^0 \Delta V_{CO} \quad (4.11.12)$$

The ΔI_{BES} will be negative when the BES is under continuous charging mode due to the increment of battery voltage ΔV_{BOC} and ΔV_{B1} . Although constant current operating mode is the most efficient for the BES, we should adjust the firing angle a , that is ΔV_{CO} in equ. (4.11.12), to keep the BES in constant power mode for the sake of load-frequency control. The ΔV_{CO} can be decomposed into two components: (a) $E_{DO} \Delta V_f$ to compensate the power deviation caused by ΔI_{BES} , and (b) $E_{DO} \Delta V_s$ to respond the system disturbance. We can obtain:

$$\Delta P_{BES} = V_{CO}^0 \Delta I_{BES} + I_{BES}^0 E_{DO} (\Delta V_f + \Delta V_s) = I_{BES}^0 E_{DO} \Delta V_s \quad (4.11.13)$$

If we let

$$\Delta V_f = \frac{-\cos a^0}{I_{BES}^0} \Delta I_{BES} \quad (4.11.14)$$

Then the use of the BES in LFC (Load Frequency Control) is obtained by a damping signal ΔV_s :

$$\Delta V_s = \frac{K_{BP}}{1 + ST_{BP}} \Delta Signal \quad (4.11.15)$$

Where K_{BP} and T_{BP} are the control loop gain and the measurement device time constant, respectively. The $\Delta signal$ is a useful feedback from the power system in order to provide damping effect. Combination of the above equations, yields the incremental model of the BES shown in Fig. 4.45.

The discharging mode operation of the BES also can be expressed by Figure 4.36. We can use the ignition angle β for the converter in the discharging mode. The power consumption of the BES is

$$P_{BES} = \frac{6\sqrt{6}}{\pi} V_t I_{BES} \cos \beta, \beta = \pi - a = -E_{DO} I_{BES} \cos a = -V_{CO} I_{BES} \quad (4.11.16)$$

A similar result is obtained as:

$$\Delta P_{BES} = -I_{BES}^0 E_{DO} \Delta V_S \quad (17)$$

The incremental BES model shown in Fig. 4.45 can identify charging mode or discharging mode according to the sign of I_{BES}^0 value, that is, the direction of initial current within the BES. Since there are DC breakers to prevent too high currents which would endanger battery service life, the deviation of battery current is limited. There is also a limiter upon ΔV_S due to $V_{CO} \leq E_{DO}$

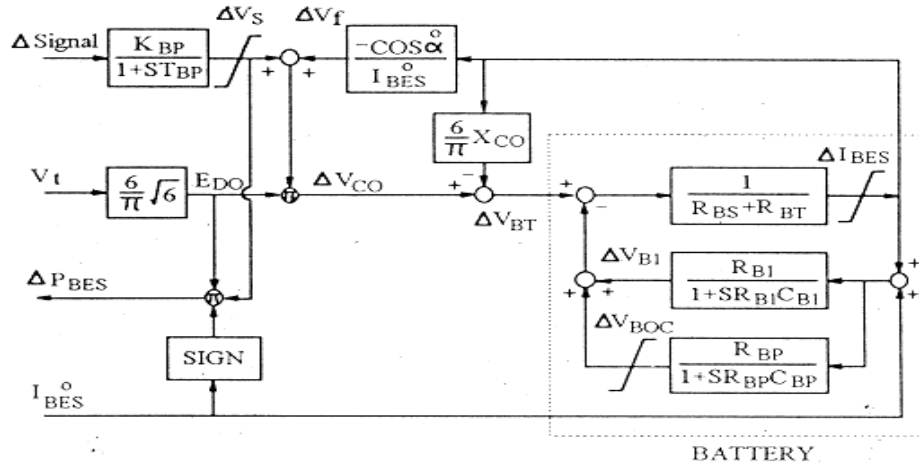


Fig.4.45 **Block diagram of BES incremental model**

For Load Flow studies the BESS can be adequately modeled as a standard PV bus. Care must be taken to ensure that the current ratings of the device, as dictated by the terminal voltage and the device MVA rating are not exceeded. Obviously, when the BESS is charging, the sign of P is negative. Filter ratings ranging from 0.3 to 0.6 pu of the device rating are typical.

Figures 4.46 and 4.47 show a dynamic BES model with a block diagram representation [43]. Figure 4.46 provides the dynamic model of the battery, Figure 4.35 for the voltage source converter control (same as for SMES), Figure 4.36 the frequency control block diagram (same as for BES) together with the converter active current limits (Figure 4.47) and Figure 4.38 the ac voltage control diagram.

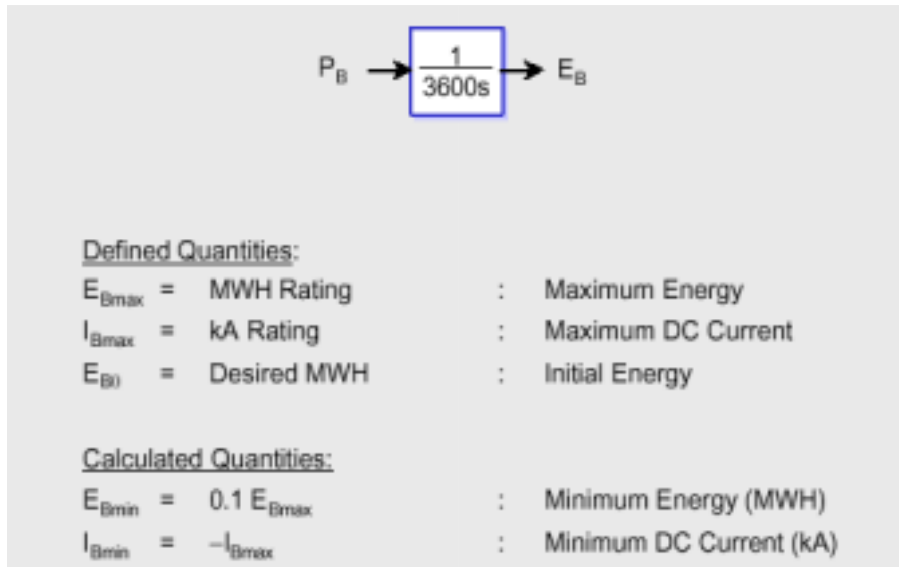


Figure 4.46: Dynamic Model of a Battery

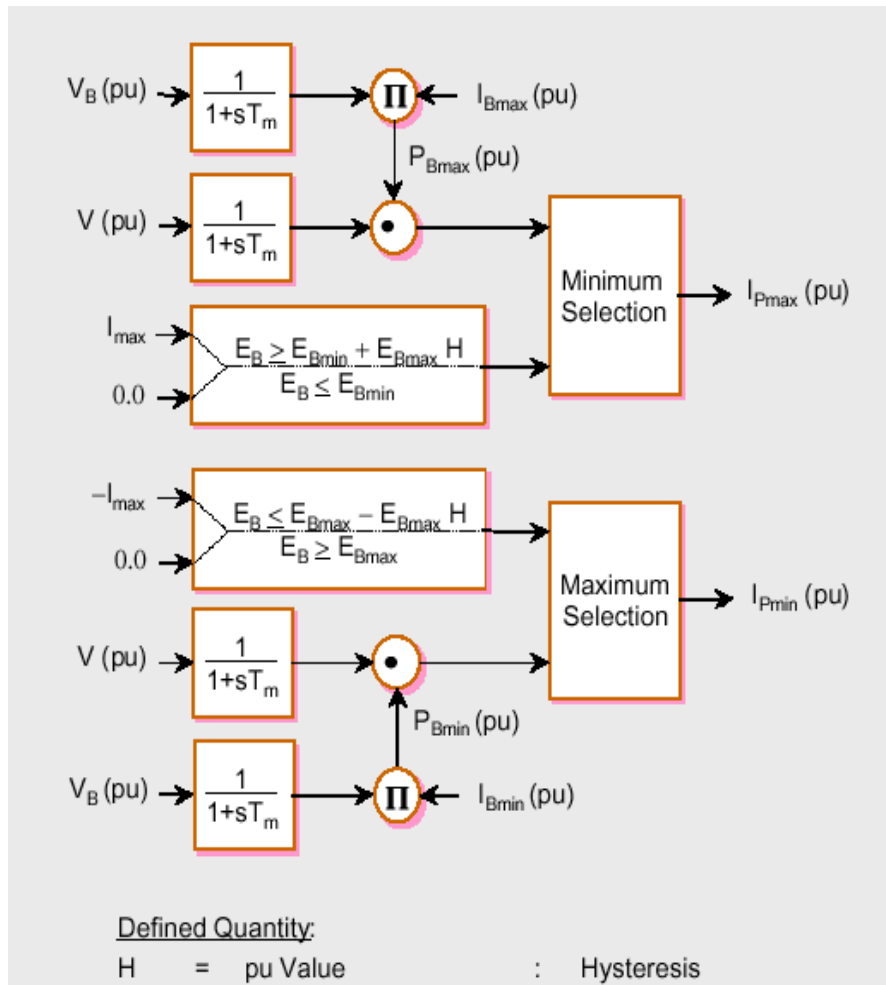


Figure 4.47: Active Current Converter Limits

A similar general purpose dynamic model is developed in [40]. BESS provides a full four-quadrant converter, therefore there are two independent control functions, one for voltage control and one for frequency control (Figure 4.48). These control functions provide active and reactive power output settings to the power converters, which are then translated to voltage angle and voltage magnitude commands, respectively. When these instructions result in currents that exceed the current capability of the PCS, limits must be applied.

The active power control may have the operating objective of regulating frequency, power flow or a combination of the two, as shown in Figure 4.49. For a general purpose model, the input signals for the active power control are active power (P) and frequency (F).

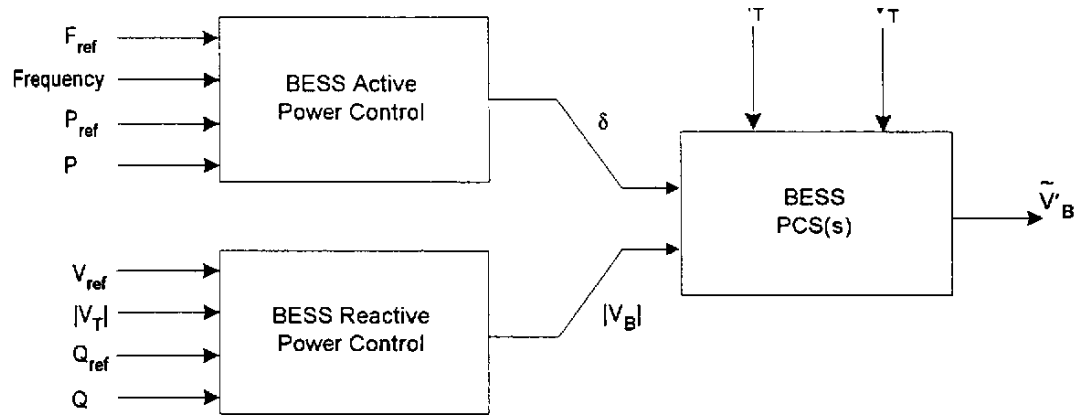


Figure 4.48. Functional Blocks of BESS model

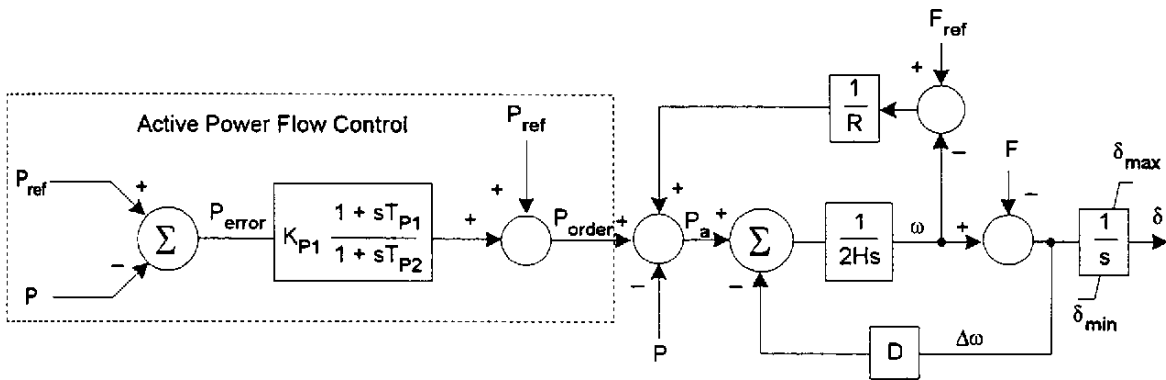


Figure 4.49 Active Power Control

The active power reference P_{ref} may be the output of a higher level controller, including inputs from a battery energy management system, a system dispatcher, an active power modulation scheme (e.g. power system stabilizer), and/or a power regulator. Similarly, the frequency reference may be modified, although in most instances it would be set to

the nominal frequency. The active power flow control shown within the dotted line represents a generic control, as the one used for moderating power swings from a disturbed load. The remaining two-state model closely resembles that of the mechanical model of a synchronous machine. The difference is that the limit to the angle of the internal voltage angle δ is set by the current capability of the PCS.

$$\delta_{\max} = \sin^{-1} \left(\frac{X_T I_{T \max}(t)}{|V_T|} \right)$$

X_T is the converter transformer reactance, $I_{T \max}$ the maximum terminal current, V_T the terminal voltage. δ_{\min} would normally be the negative of δ_{\max} .

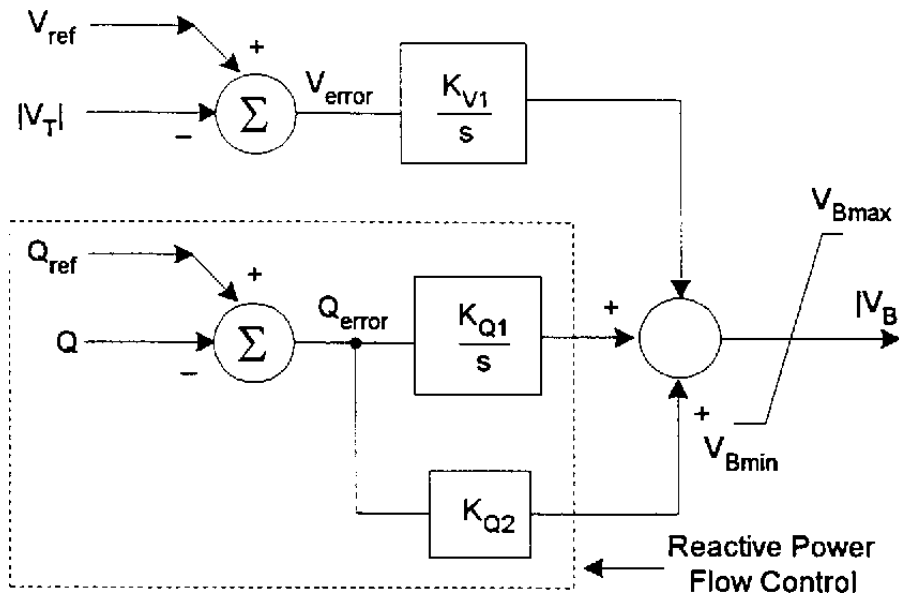


Figure 4.50 Reactive Power Control

The reactive power control of Figure 4.50 represents one type of implementation. In practice, the PCS is capable of essentially instantaneously imposing any V_B within the equipment capability. V_B must be limited however, so as to prevent excessive current in the PCS.

$$|V_T| - X_T I_{T \max}(t) \leq |V_B| \leq |V_T| + X_T I_{T \max}(t)$$

Some installations may also limit V_B to avoid overvoltages.

The PCS function must accomplish two objectives:

1. Combine angle δ and voltage V_B , so that the device current rating is not violated.
2. Deliver an equivalent internal voltage V_B' to the network equations, subject to a small delay for the device firing logic.

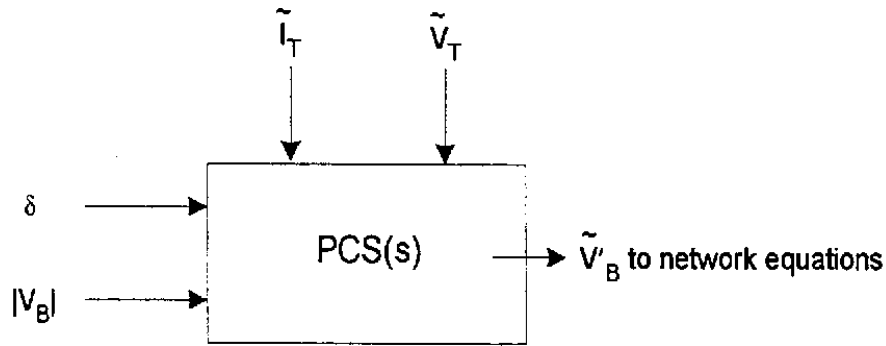


Figure 4.51 BESS PCS Function

The PCS block represents the delay of the power electronics control circuit. The delay can be modeled simply as a delay or as a lag circuit.

It should be noted that the limits set to the angle and voltage magnitude outputs to avoid overload do not address the possibility that the required combination of P and Q exceeds the PCS capability. Given the requested internal voltage phasor V_B , if I_T exceeds the current rating, then several means can be employed to limit the current, depending on the performance objectives of the BESS, i.e. active or reactive power priority [40].

4.7 Flywheels

This section presents the modeling of a flywheel energy storage system based on a vector-controlled induction machine drive with bi-directional power control. The examined VSI drives the flywheel IM under vector control operation and in both constant flux and field weakening modes. [44-46]. The system that will be described is shown in Figure 4.52.

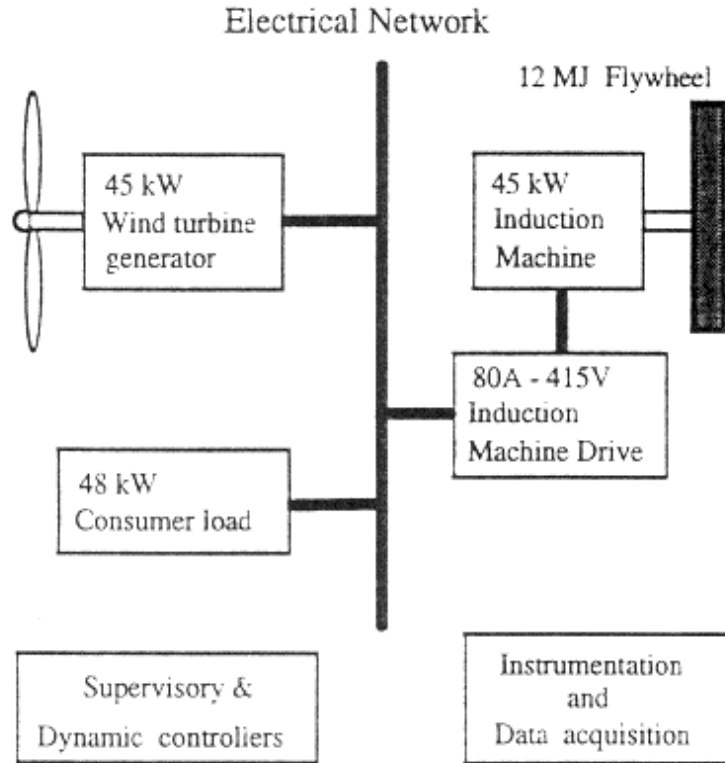


Figure 4.52: The structure of the examined power system

The Induction Machine Drive

The Flywheel Induction Machine Model is provided in Section 3.5.2. The WTG provides power to an autonomous power system, backed up by a diesel generator and an energy storage facility, which filters power fluctuations and can also reduce the on/off cycling of the diesel. The structure of the induction machine drive is shown in Figure 4.53.

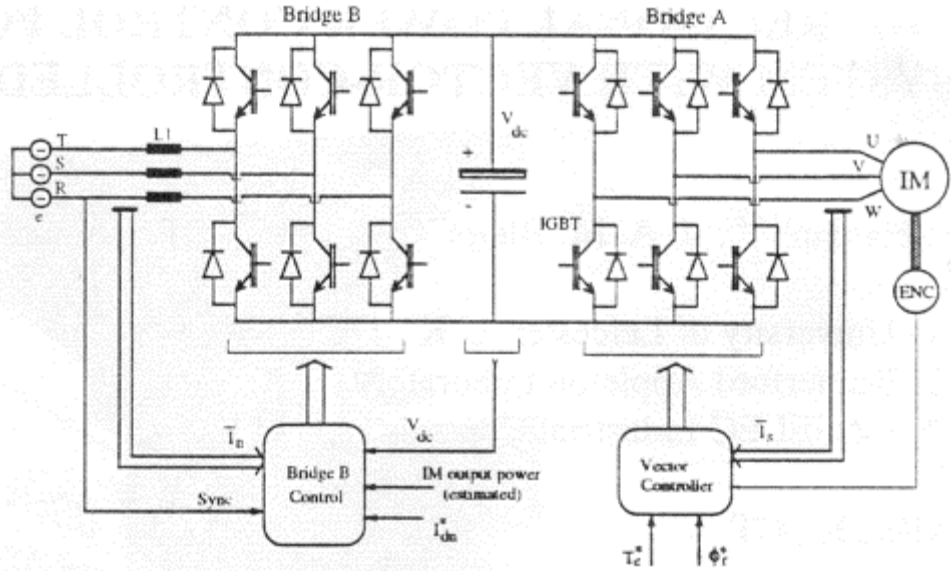


Fig. 4.53 The diagram of the controllers and the power electronic system.

The main function of the network bridge control is to stabilize the power transfer from the grid to the IM and vice versa. This is achieved by controlling the drive's active current to maintain the DC link voltage at a pre-set level. On the other hand, the reactive current component of the drive is usually controlled to zero for unity power factor. However, this can be dynamically regulated according to reactive power requirements in the power system. Therefore, the network powers are entirely controlled via the drive's current controllers with de-coupled current control in the steady state operation. This reflects on the drive's active and reactive powers which are only coupled during the transient operation of the current controllers which may not exceed 4 msec.

Vector control offers the highest performance amongst other existing techniques for induction machine control. In principle this is realized when de-coupling between flux and torque-producing components is obtained. As a result the IM torque can be defined as

$$T_e = \frac{P}{2} \frac{L_m}{L_r} \Psi_r I_{qs}$$

Where P , L_m , L_r are number of poles, mutual inductance and rotor self inductance of the IM respectively, ϕ_r is the rotor flux-linkage and I_{qs} is the Q axis stator current. The rotor flux-linkage, as a function of d-axis stator current, can also be defined

$$\Psi_r = \frac{L_m I_{ds}}{(1 + p\tau_r)}$$

Where I_{ds} is the d-axis stator current, p is the differential operator and τ_r is the IM rotor constant.

The block diagram, given in Fig. 4.54 illustrates the de-coupling structure implied in the IM under vector control operation, where τ_m , B are the mechanical time constant and damping factor respectively.

In order to ensure satisfactory operation of the vector controller so as an indirect active power flow, the IM rotor time constant has to be tuned properly or set to an optimum value in the range of the operating speed.

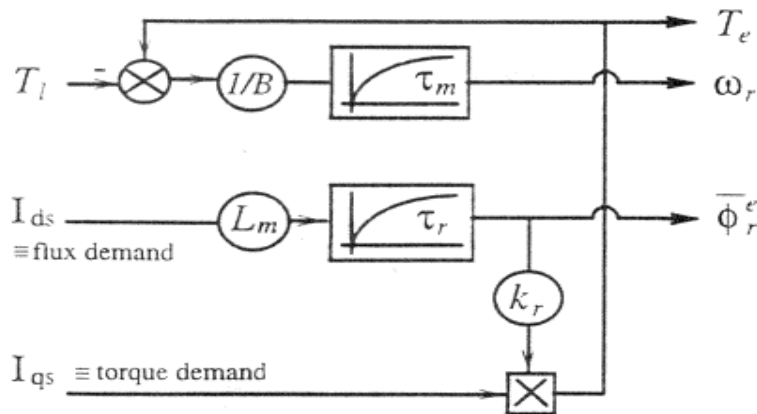


Figure 4.54: The de-coupling structure of the IM under vector control operation.

Although drive's active and reactive powers can be controlled directly via the current controllers of the drive's network bridge, however, the active current component cannot be available for direct access without considerable modification of the standard firmware/software. To avoid doing so the active power of the drive has been indirectly controlled through the torque demand of the flywheel IM, providing that the power feed-forward link between the Im and the network bridges compensates for the delay expected in the active power response.

In a three phase power system, the instantaneous power can be expressed as follows

$$P = V^T I$$

Where

$$V^T = [V_a, V_b, V_c], I = [i_a, i_b, i_c]^T$$

Are the instantaneous three-phase voltage and current vectors respectively, T denotes vector transpose.

Under balanced condition, the values of the instantaneous currents and voltages can be replaced by the equivalent vectors I_{dq} and V_{dq} in the dq plane. Therefore, the instantaneous active and reactive powers can be expressed invariantly in the dq frame as

$$P = \text{Re}(V_{dq}^T I_{dq}^*), Q = \text{Im}(V_{dq}^T I_{dq}^*)$$

Where * denotes conjugate vector.

Active power control

The structure of one possible controller for the active power is shown in Fig. 4.55, where ω_r is the flywheel speed and k_{fd} is a feed-forward gain. Feedback power P_n is calculated via the real part of the following equation:

$$P_n = V_{qn} I_{qn} + V_{dn} I_{dn}$$

where V_{dn} , V_{qn} , and I_{dn} , I_{qn} are d- and q-axis components of the drive voltage and current vectors respectively. Whilst the torque feed-forward path creates an instantaneous torque command which should correspond to the power demand, the PI action nulls any mismatch between the actual network power and its demand due to power losses and the effect of the vector-controller de-tuning.

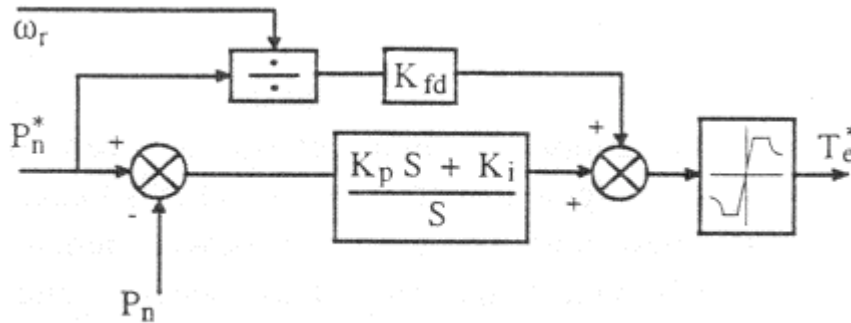


Fig. 4.55: The Active Power Controller

Reactive Power Control

Adding the feed-forward term, in a similar way to that of the active power controller, enhances the control performance and make both controller structures similar. The block diagram of this controller is shown in Fig. 4.56, where v_{ii} is the grid line voltage. Feedback of reactive power, Q_n , can be obtained from the equation 4 which yields

$$Q_n = V_{qn} I_{qn} - V_{dn} I_{qn}$$

In this case, whilst the feed-forward element provides the expected d-axis current demand, the PI action nulls the difference between the reactive power and its demand when orientation errors occur in the voltage and current vectors.

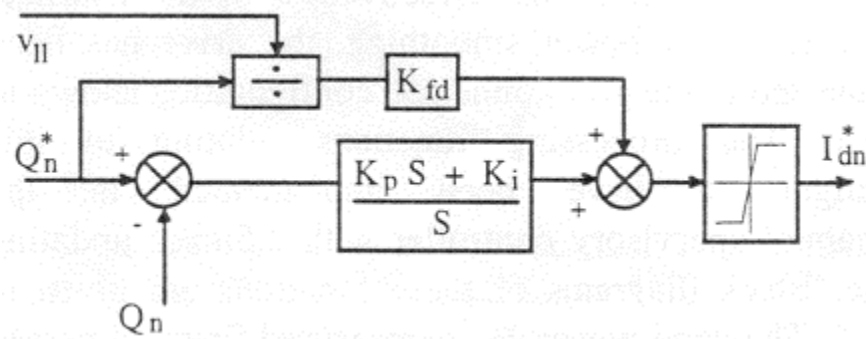


Figure 4.56: The Reactive Power Controller

Wind Power Smoothing - Var Compensation

In order to provide wind power smoothing, the VSI should be configured according to the processing functions given in the block diagram of Fig. 4.57. The wind power is measured first and passed through 2nd order high pass filter (HPF). The output of the filter, which represents the components of the wind power above the specified frequency is then demanded from the drive along with an amount of power P_{loss} to compensate for the drive’s power losses.

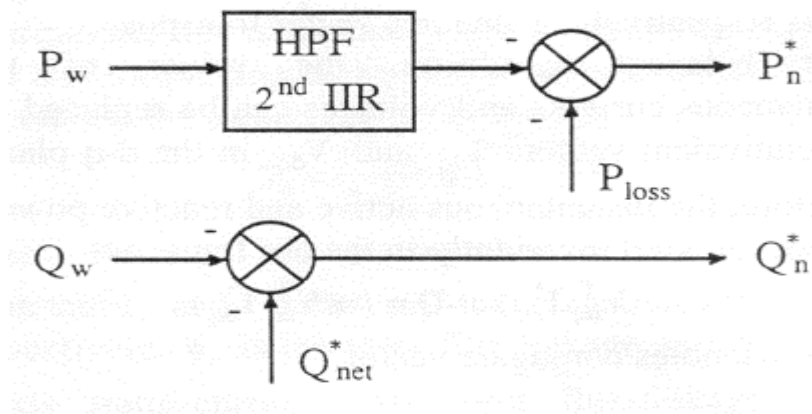


Figure 4.57: The processing functions for the wind power smoothing.

Whilst active power demand is extracted via high pass filter, the command for the drive's reactive power is directly worked out to compensate for the reactive power of the WTG Q_w and maintain the reactive power of the grid at a preset level.

Chapter 5

Software Tools

5.1 Introduction

The integration of new forms of generation is done, most of the time, at the distribution level in a dispersed way, requiring some impact studies in order to evaluate the consequences for the operation of the grids.

The impact studies to be performed can involve:

- Steady state analysis to evaluate changes in losses, voltage profiles and load flow congestion in branches;
- Dynamic state analysis to evaluate the behavior of some system variables, following disturbances in the system or disturbances resulting from the presence of these sources (for instance wind power changes);
- Harmonic penetration, when electronic converters are among the technologies used to connect these sources to the grid;
- Flicker level evaluation.

Most of the conventional commercial simulation tools are able to provide the results needed, although sometimes it is necessary to assure the availability of adequate models to tackle the special characteristics of some of these sources, like for instance asynchronous generators or inverters.

The following aspects need to be addressed by means of simulation software that can take the electro-mechanical transients into account.

- Precise evaluation of the short-circuit currents at various points of the system. Detailed modeling of spinning power (induction motors or generators) makes it possible to determine the short-circuit values for adequate sizing of the breaking devices and correct adjustment of the protections.
- Transient stability analysis of the units, by defining the critical clearing times of electrical faults. This enables to verify the adequacy of the site's protection plan and ensure unit tripping in case of loss of synchronism.
- Selection of the criteria and tuning for the decoupling protection, which has to rapidly disconnect the unit when the unit finds itself in a subsystem that is no longer connected to the supply grid. The protection must act quickly so that the subsystem may be re-supplied in case of auto-reclosing of the faulted components. Adjusting this protection on the basis of local values (voltage phase and module, frequency) is not easy. Indeed, various parameters affect the evolution of these values : the behaviour of the unit controls; the behaviour of the load, and particularly that of the induction motors;

- In certain particular situations the dispersed generation means must be able to supply part of the distribution network although they are disconnected from the supply network. This implies that various elements must be examined such as the protection plan behaviour, the capabilities of the units to face load fluctuations, the possible activation of a load-shedding plan, ... This particular point, which rather concerns industrial networks, is not discussed next.

Facilities provided by modern software tools for modeling new forms of generation and storage are indicatively shown next.

5.2 Interactive Power System Analysis Package

Traditionally, power system CAD work is approached from two different angles:-

1. Using software developed for large system design work, with well established models for each type of plant, for steady state and transient conditions. Efficient handling techniques are used to produce analysis results quickly and to allow effective man-machine interaction.
2. Modelling of new equipment designs using generic User Defined Modelling techniques which can model equipment to any required degree of detail. Using this approach to simulate the performance of such equipment within a power system, usually involves an approximate, equivalent circuit representation of the main power system, which must also be user defined. Engineers using this technique must therefore be very competent system modellers as well as experienced power system designers. Also, the effort required to set up and execute such studies is quite significant.

The requirement to examine the feasibility of new equipment designs and to establish their likely steady state and transient performance is a challenge that has to be addressed by modern software tools. The approach followed by the Interactive Power System Analysis (IPSA) package, developed at UMIST, is presented next.

IPSA provides a procedure by which the built-in models of the package can be replaced by appropriate User Defined Models [47, 48], when required. The procedure enables users to start by generating special functional block diagram models for any piece of equipment: AVRs, speed governors, special automatic voltage and frequency regulators, static converters and generalised non-linear radial elements [49]. Next, the validity and performance of each of these models is assessed by a built-in transient response simulation. When users are satisfied that the model performs in the required way, the model's functional configuration and parameters are stored with a unique type number and can be subsequently used to embed these models into the large scale IPSA simulation package, wherever required.

This procedure avoids the need to simplify the network which, in many cases, would involve some risky assumptions. The full network configuration and the conventional built-in models are used to do this. The integration of user defined models into the established simulation procedures also opens the way to using the steady state system performance information to automatically initialise the operating conditions of the special models. This automatic initialisation offers a sure footed way of defining the initial conditions prior to transients and also relieves the user from the requirement to stipulate these conditions when the simulation is done in isolation.

There is a simple procedure for associating a «type number» of each special model generated with the data set of any appropriate selected system component. When user defined models are used, the transient simulation results give details of the operating conditions of the entire system and in addition an element-by-element listing of output signals within each of the special models. This is used to highlight the interplay between the various model parameters and overall system performance and help tune the design.

Figure 5.1. shows the network diagram of a power system comprising a very basic representation of a supply network (the GRID), a windfarm based on induction generators with a bank of power factor correction capacitors, a typical model for a synchronous generator/PWM converter set, the alternative induction generator arrangement and the model of a generalised DC network made up of a generator, battery and a resistive load. Each rotating machine and static converter in the system can have appropriate built-in controllers. These are not shown on the diagrams but are modelled to various degrees of detail, depending on the data supplied.

Libraries of special models for all these controllers can be built up using the User Defined Modelling facility. Figure 5.2. shows a User Defined Model (UDM) of a combined wind turbine and governor. The upper two rows of block functions (blocks 1-4 and 6-10) are used to model wind velocity variations, whilst the lower part (blocks 11-27) generate the turbine and governor model.

After construction of the functional block diagram, the correct operation of the model can be demonstrated by plotting the input/output characteristics for each element of the model. The graphical displays are user controlled and can be adjusted to give specific bundles of information as in Figure 5.3. Here graph 1 shows the generation of a linearly increasing wind velocity ramp; graph 2 shows the generation of a sinusoidal wind gusting effect and the sequencing of the two effects through the adder. Graphs 3 and 4 show the output signals of some significant elements of the turbine and governor locks and the generated turbine torque characteristic. It will be noted that this mirrors the wind velocity pattern with some "ringing" introduced by the values of the turbine and governor model gains and time constants.

There is an automatic initialisation procedure for the signals of each model for both the individual model simulation performance and also the operation within the system. For the latter, conditions are derived from the basic user specified state constraints and the resulting detailed loadflow solution Figure 5.4. Note that the standard built-in static

converter models can model power factor control (unity power factor at busbars AC3-1 and AC4-1) as one of various modes of control.

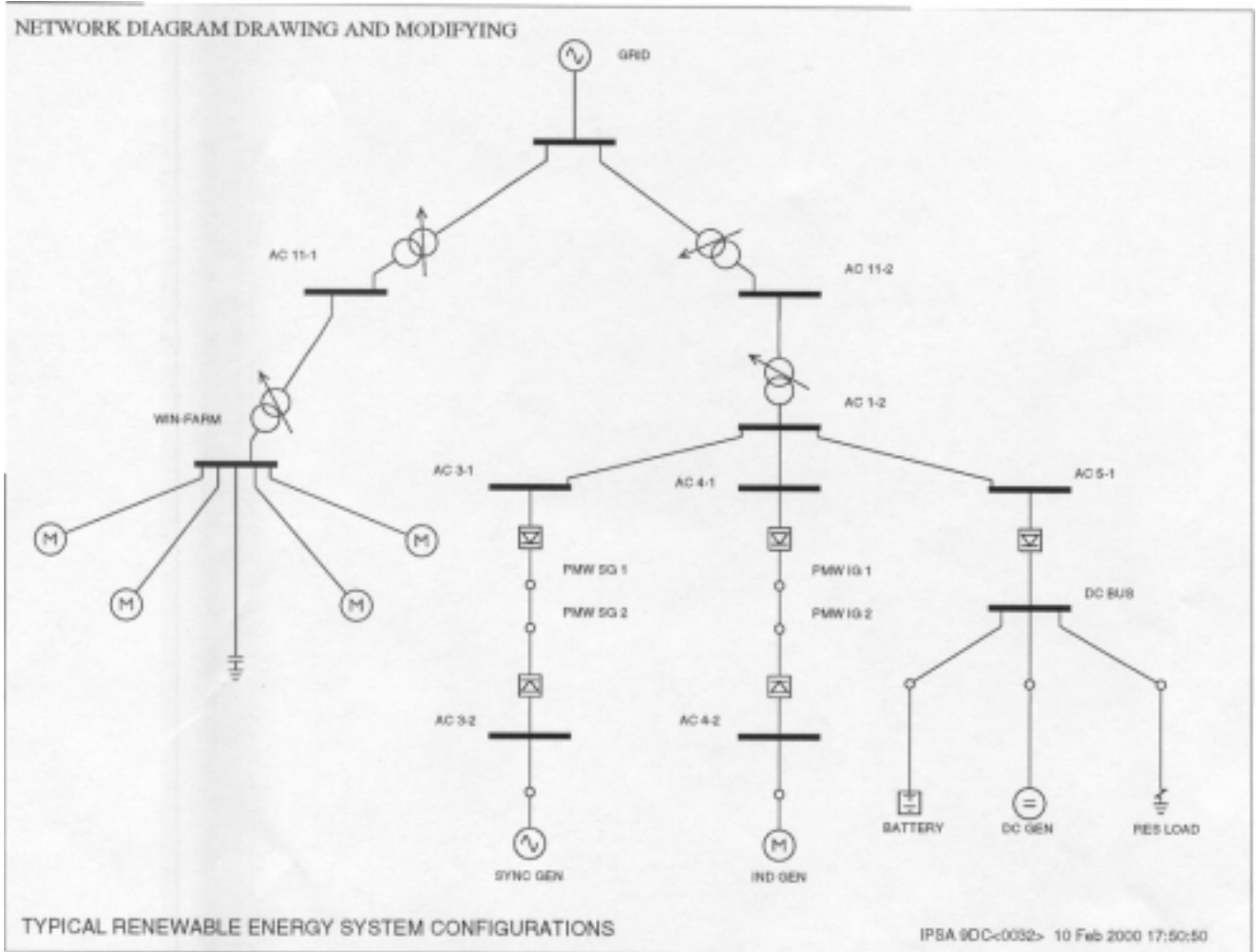


Figure 5.1

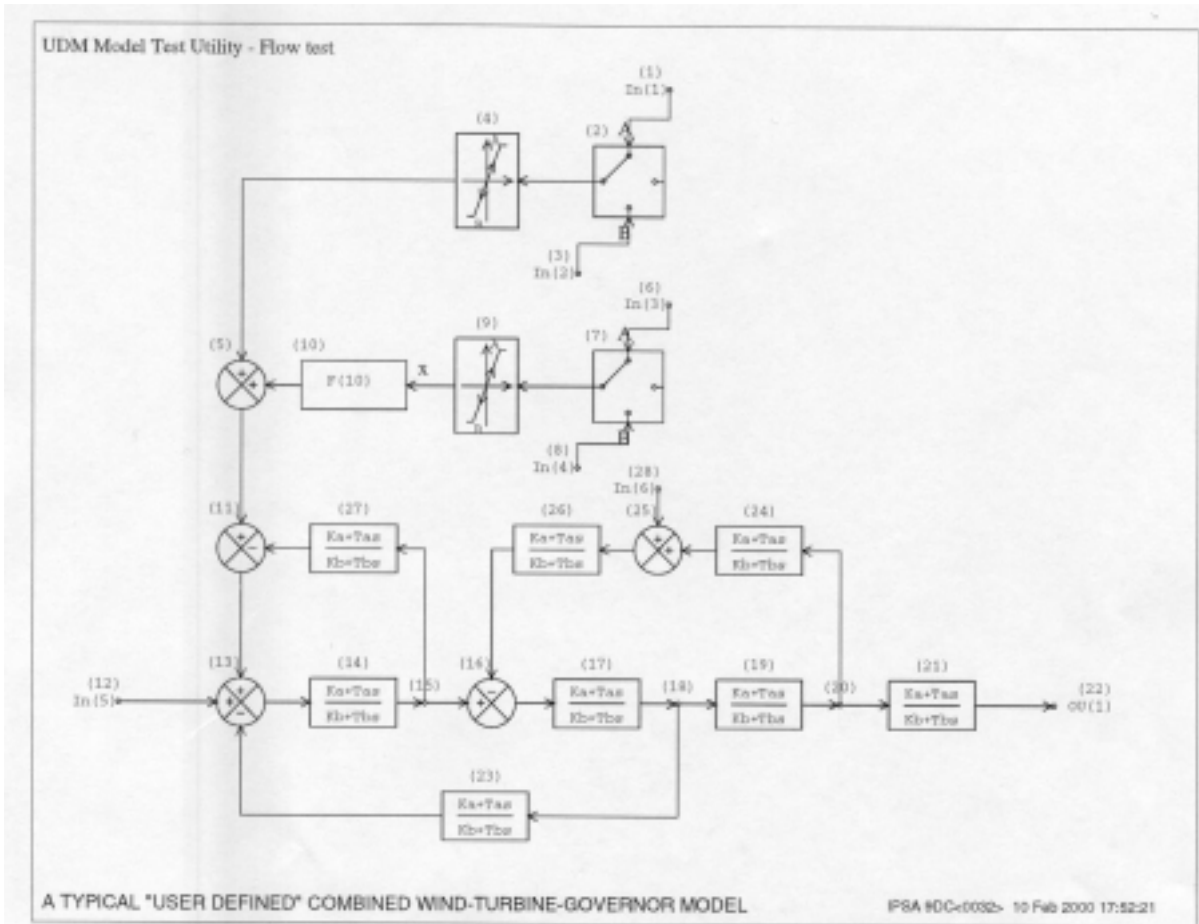


Figure 5.2

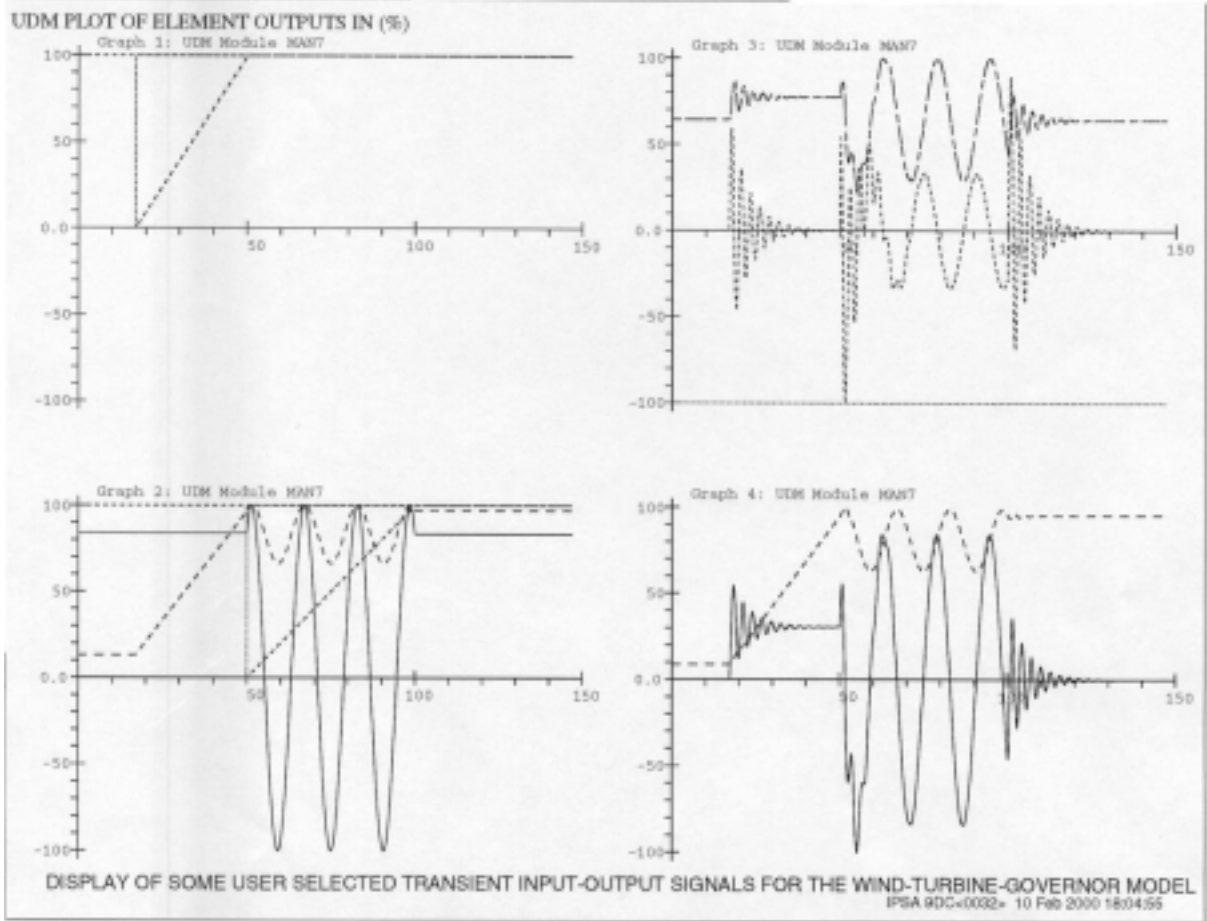


Figure 5.3

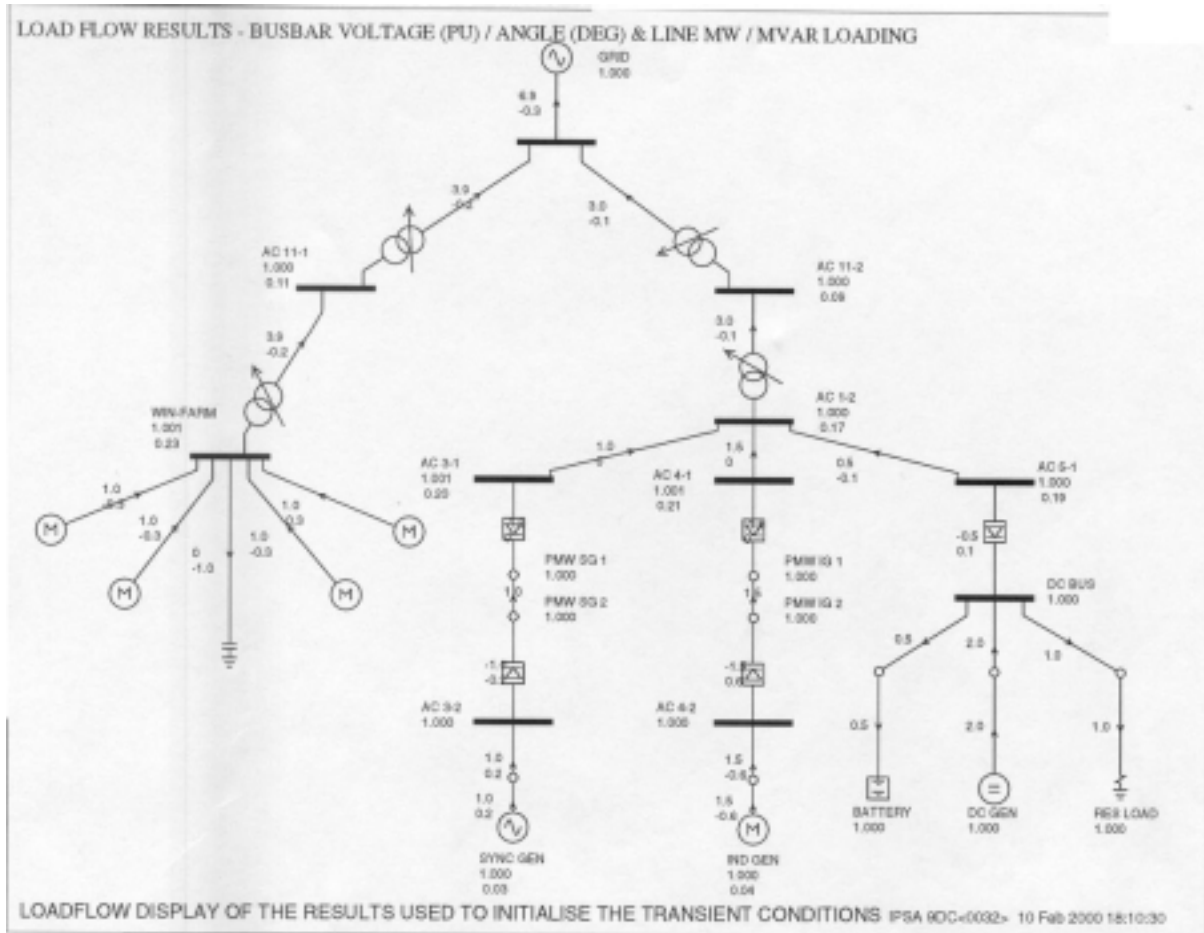


Figure 5.4

5.3 EUROSTAG program

General description

EUROSTAG is a time simulation program developed by Tractebel and Electricité de France to study the transient, mid- and long term dynamics of large power systems [50, 51]. It uses the same type of component modelling whatever the type of disturbance, network behaviour or duration of the simulation, reproducing continuously both rapid and slow phenomena.

The differential and algebraic equations are solved simultaneously using a variable integration step. The size of the step changes automatically according to the actual behaviour of the system (generally from 1 ms to 100 s) in order to guarantee constant

accuracy of the integration process. The truncation error is in fact calculated at each step to determine the exact step length required.

The program is able to reach any stabilised network state and can be used to analyse quasi-steady states. An interactive calculation of own values makes it possible to study the static stability of all steady states obtained during the simulations.

The Fortescue transformation allows any kind of computations related to unbalanced conditions (short-circuit, phase opening).

Modelling functions

EUROSTAG has extensive modelling capabilities in addition to the detailed models representing basic elements (alternators, induction motors). A graphic data entry program enables the user to code directly the network single line diagram and the block-diagram of the new model he wishes to define.

The graphic macro languages is used to code models of voltage regulators, speed governors, turbines and systems such as asynchronous generator, power electronic devices, static or dynamic loads, etc. A library of standard models is also available to the user.

EUROSTAG is also able to simulate automatic control systems. The moment at which these systems must act upon the network is determined by means of equations describing their operation. They are used, for example, to represent protective relays, the automatic tap changers of transformers or the automatic load shedding systems.

DECOUPLING PROTECTION FOR DISPERSED GENERATION

The principle behind decoupling protection [52-57] is generally to prevent the generator from continuing to supply the network when islanded or under abnormal voltage conditions. If that section of the network to which dispersed generating facilities are connected is no longer supplied or the voltage is no longer normal, it must be possible to immediately and automatically decouple the independent generating facilities from the network. The following criteria are generally used to activate the decoupling protection and trip the dispersed generation:

- the min. and max. frequency thresholds without time delay (typically 49.5 Hz and 50.5 Hz in 50 Hz systems);
- the upper minimum voltage with a time delay (typically : 0.2 s);
- the lower minimum voltage with a time delay (typically : 1.5 s);
- the presence of a zero sequence voltage with a time delay (typically : 1.5 s);
- maximum current with a time delayed (typically 3 s);
- optionally, the undelayed detection of a vector shift (typically 7° on the 3 phases) locked with a minimum voltage (typically 80 %);
- maximum voltage with a time delay

- frequency derivative df/dt (ROCOF) locked by a frequency deviation (typically ± 0.2 Hz) delayed in time (typically 0.1s),

CONTINGENCY SELECTION FOR PROTECTION PERFORMANCE EVALUATION

A generic decoupling protection has been introduced in EUROSTAG allowing all the above criteria to be concentrated in only one automatic control system.

Various network events, incidents or network operations have to be simulated. The generally considered events are given in table I. For each of these events, the reaction time of all decoupling protection criteria are examined for each dispersed generating unit.

TABLE I

<i>INCIDENTS</i>	
Fault HV	long three-phase fault, 300 ms, on the HV network
Fault HV	short three-phase fault, 80 ms, on the HV network
Fault MV	three-phase fault on the 3 wires of a MV feeder causing the feeder to trip after 100 ms
Fault MV	single-phase fault on a feeder, opening the feeder after 1 s.
Fault MV	distant three-phase fault on the MV network during 300 ms, on a feeder
Fault MV	transient single-phase fault on the MV network on a feeder

NETWORK OPERATIONS	
Opening HV	opening the HV/MV transformer supply which islands out the whole MV network
Opening MV	tripping the feeder of a transformer causing a vector shift in the MV network
Opening MV	tripping a MV feeder causing the islanding of dispersed generators
Closing MV	closing the circuit causes the parallel operation on the MV network
Opening MV	tripping a MV feeder islands out dispersed generators for various active and reactive power deficits and generator inertia.
Closing MV	Starting a high-powered engine on the MV network

ANALYSIS OF RESULTS

Thanks the dynamic simulation, the following results could be highlighted. The best criteria are the frequency and the derivative frequency ones.

Uo criterion can be useful for revealing islanding resulting from a long single-phase short-circuit. The Umin criteria provides backup and guarantees the voltage quality. They

are also useful when a voltage dip provokes the deactivation of the frequency or vector shift criteria. The I_{max} criterion also plays a backup role.

Vector surge does not always live up to expectations. It leads to unwanted tripping, while locking by a voltage criteria considerably reduces unwanted actions but at the same time is detrimental for the criterion's behaviour when the system is islanded out.

The frequency criterion guarantees generally a good selectivity. The performed simulations also have shown that the df/dt criterion improves the speed reaction without decreasing the selectivity.

Besides, these criterion characteristics do not request an accurate adjustment of the thresholds.

CONCLUSIONS

Connection of dispersed generating units to distribution networks results in new operational constraints in the MV networks.

EUROSTAG software enables to address these constraints at both the design and operation stages of these networks in order to achieve optimal reliability and security. It further enables to check on real case, the selected choices for the decoupling protection, which adjustment is reputedly delicate. The analysis of the various criteria to be used for evaluating this protection on a typical Belgian MV-system demonstrated that frequency and derivative frequency criteria leads to better results than a vector shift criterion with or without interlocking.

5.4 PSAPAC Simulation Capabilities

PSAPAC, developed by Powertech Labs Inc. for the Electrical Power Research Institute (EPRI) consists of a comprehensive suite of advanced computer programs that work together to provide a complete package for power system stability analysis.

1. Interactive Power Flow Program – IPFLOW

- user-defined configurations with any number of terminals (no coding required)
- line-commutated converter model with any feasible combination of two of the following control modes : firing angle, extinction angle, dc voltage, dc current, real power, reactive power, and transformer tap.
- self-commutated voltage-sourced converter model with any feasible combination of three of the following control modes: power angle, modulation ratio, dc voltage, dc current, real power, reactive power, and transformer tap.
- dc circuit breaker/disconnect model consisting of RLC combinations
- automatic converter disconnection from the ac system

2. Voltage Stability Program - VSTAB

- same as those of IPLOW

3. Extended Transient and Midterm stability Program - ETMSP

- user-defined controls with any combinations of blocks and loops (no coding required)
- line-commutated converter interface with any of the following modes : firing angle control, extinction angle control , dc voltage control, dc current control, bypass block, and commutation failure
- self-commutated voltage-sourced converter interface with any two of the following modes: power angle control, modulation ratio control, dc voltage control, dc current control, bypass, and block
- converter transformer tap interface with stepwise control
- dc circuit breaker/disconnect interface with the following modes: opening, open and closed
- dc network component interfaces to modify RLC combinations
- control input signal interfaces to both dc and ac systems.
- automatic initialization by sub-systems and/or by pre-calculations
- stand-alone feature with automatic Thevenin equivalent replacement of the ac system
- block-loading feature with automatic replacement of each dc link / FACTS device
- different integration time steps for ac system, dc network, and dc controls

4. Small Signal Stability Programs - SSSP

- same as those of EMTSP, but with automatic linearization around the initial conditions

Chapter 6

Conclusions and Further Work

1. The level of new forms of generation and storage is increasing worldwide. Most of these generating devices are connected at the distribution level, changing drastically its passive behavior. There is an increasing need to consider the contribution of these devices to dynamic stability studies.
2. The derivation of a general “generic” model appropriate for the different stability studies is not possible, however specific cases and general guidelines have been provided in this report.
3. Due to the large variety of the different devices, control schemes etc. there is a strong requirement for flexibility. Modern Software packages should provide the facility to conveniently build up user-defined models and interface them to the standard device models.
4. In modeling new forms generation and storage it is important to consider their protections. Additional work is needed in this area.
5. For stability studies at the transmission level it is important to develop appropriate equivalencing (aggregation) techniques. This is a very interesting area that needs more work.

REFERENCES

[1] “Impact of Increasing Contribution of Dispersed Generation on the Power System”, CIGRE WG 37-23, September 1998.

[2] “Dispersed Generation”, CIRED WG04, June 1999.

[3] “Dispersed System Impacts: Survey and Requirements Study”, EPRI TR-103337, Project 3357-01, July 1994.

[4] European Commission “Energy for the Future: Renewable Sources of Energy”, White paper for a Community Strategy and Action Plan, COM (97) 599 final, Brussels, 26.11.1997.

[5] R.H. Lasseter, “Control of Distributed Resources”, presented at Bulk Power System dynamics and Control IV – Restructuring, August 24-28, Santorini, Greece

[6] L. Monition, M. Le Nir, J. Roux, “Micro Hydroelectric Power Stations”, John Wiley and Sons, 1984.

[7] Wind and Solar Power Systems, M.R. Patel, CRC Press, 1999.

[8] Solar Electricity, T. Markvart (editor), John Wiley & Sons, 1996.

[9] Renewable Energy-Power for a Sustainable Future, G. Boyle (editor), Oxford University Press/The Open University, 1998.

[10] “The Future of Energy Storage in a Deregulated Environment”, Panel session at IEEE, PES Summer Meeting, 16-20 July 2000, Seattle, Washington.

[11] P. Kundur, G.K. Morison, “A Review of Definitions and Classification of Stability Problems in Today’s Power Systems”, presented at the panel session on Stability Terms and Definitions, IEEE PES Meeting, Feb. 2-6, 1997, New York.

[12] “Electricity Tariffs for Embedded Renewable Generation”, European Commission DGXII, JOULE III Project JOR3-CT98-201, Task 1 Progress Report, December 1998.

[13] “Dynamic Behaviour of Power Systems in Large Islands with High Wind Power Penetration”, N.D. Hatzigrygiou, E.S. Karapidakis, D. Hatzifotis, Bulk Power Systems Dynamics and Control Symposium – IV Restructuring, Santorini, Greece, 23-28 August 1998.

- [14] "Effect of high wind power penetration on the reliability and security of isolated power systems", E.N. Dialynas, N.D. Hatziargyriou, N. Koskolos, E. Karapidakis, paper 38-302, 37th Session, CIGRE, Paris, 30th August-5th September 1998.
- [15] S. Heier "Grid Integration of Wind Energy Conversion Systems", John Wiley & Sons, 1998 (1996)
- [16] N. Vilsbøll, A.L. Pinegin, T. Fischer, J. Bugge "Analysis of Advantages on the Double Supply Machine with Variable Rotation Speed Application in Wind Energy Converters." *DEWI Magazin* No. 11 August 1997.
- [17] P. Kundur *Power System Stability and Control*. EPRI, 1994.
- [18] P. Ledesma, J. Usaola, J.L. Rodríguez "Models of WECS for Power System Dynamic Studies." *Proceedings of the UPEC'98*. September 1998.
- [19] J.L. Rodríguez, M. Chinchilla, S. Arnalte, J.C. Burgos "Comparison of Two Variable Speed Wind Energy Generators and their Control: Direct Driven PM Synchronous Generator and Doubly Fed Induction Generator." *Proceedings of the UPEC'98*. September 1998.
- [20] S.M. Chan, R.L. Cresap, D.H. Curtice, "Wind Turbine Cluster Model", IEEE Trans. on Power Apparatus and Systems, Vol. PAS-103, N°7, Jul. 1984.
- [21] R. Chedid, N. LaWhite, M. Ilic, "Simulating Dynamic Interactions of Grid-Linked Wind Turbines", IEEE Computer Applications in Power, Oct. 1994.
- [22] R. Castro, J.M.F. de Jesus, "A Wind Park Reduced-Order Model Using Singular Perturbations Theory", IEEE Transactions on Energy Conversion, Dec. 1996.
- [23] R. Castro, J.M.F. de Jesus, "A Wind Park Linearized Model", Proc. 1993 British Wind Energy Association Conference (BWEA), York, Oct. 1993.
- [24] J.M. Undrill, A.E. Turner, "Construction of Power System Electromechanical Equivalents by Modal Analysis", IEEE Trans. on Power Apparatus and Systems, Vol. PAS-90, Sep./Oct. 1971.
- [25] B.C. Moore, "Principal Component Analysis in Linear Systems: Controllability, Observability, and Model Reduction", IEEE Trans. on Automatic Control, Vol. AC-26, N°1, Feb. 1981.
- [26] P. Bongers, "Modelling and Identification of Flexible Wind Turbines and a Factorizational Approach to Robust Control", PhD Thesis, Delft University of Technology, Delft, Jun. 1994.

- [27] P. Kokotovic, "A Control Engineer's Introduction to Singular Perturbations", 1972 Joint Automatic Control Conference on Singular Perturbations: Order Reduction in Control System Design, ASME, New York, 1972.
- [28] P.V. Kokotovic, J.J. Allemong, J.R. Winkelman, J.H. Chow, "Singular Perturbation and Iterative Separation of Time Scales", *Automatica*, Vol.16, Pergamon Press Ltd., 1980.
- [29] A. Estanqueiro, R. Aguiar, J. Saraiva, R. Castro, J.M.F. de Jesus, "The Development and Application of a Model for Power Output Fluctuations in a Wind Park", Proc. 1993 European Community ind Energy Conference and Exhibition, Lubbeck, Mar. 1993.
- [30] S. Ahmed-Zaid, P.W. Sauer, M.A. Pai, M.K. Sarioglu, "Reduced Order Modelling of Synchronous Machines Using Singular Perturbation", *IEEE Trans. on Circuits and Systems*, Vol. CAS-29, N°11, Nov. 1982.
- [31] P.W. Sauer, S. Ahmed-Zaid, M.A. Pai, "Systematic Inclusion of Stator Transients in Reduced Order Synchronous Machine Models", *IEEE Trans. Power Apparatus and Systems*, Vol. PAS-103, N°6, Jun. 1984.
- [32] A.J. Germond, R. Podmore, "Dynamic Aggregation of Generating Unit Models", *IEEE Trans. on Power Apparatus and Systems*, Vol. PAS-97, N°4, Jul/Aug. 1978.
- [33] P.W. Sauer, D.J. LaGesse, S. Ahmed-Zaid, M.A. Pai, "Reduced Order Modelling of Interconnected Multimachine Power Systems Using Time-Scale Decomposition", *IEEE Trans. on Power Systems*, Vol. PWRS-2, N°2, May 1987.
- [34] U.M. Al-Saggaf, "Reduced-Order Models for Dynamic Control of a Power Plant with an Improved Transient and Steady-State Behaviour", *Electrical Power Systems Research*, 26, 1993.
- [35] "Automatic Control of Small Hydroelectric Plants", P. A. Frick *IEEE Transactions on Power Apparatus and Systems*, Vol. PAS-100, No. 5, May 1981
- [36] S. Rahman and K. S. Tam, "A Feasibility Study of Photovoltaic-Fuel Cell Hybrid Energy System", *IEEE Transactions on Energy Conversion*, vol. 3, No. 1, pp. 50-55, March 1988.
- [37] O. Wasynczuk, N.A. Anwah, «Modeling and Dynamic Performance of a Self-Commutated Photovoltaic Inverter System», *IEEE Trans. on Energy Conversion*, Vol.4, No.3, Sept. 1989.
- [38] O. Wasynczuk, «Modeling and Dynamic Performance of a Line-Commutated Photovoltaic Inverter System», *IEEE Trans. on Energy Conversion*, Vol.4, No.3, Sept. 1989.

[39] C.M. Ong, «Operational Behavior of Line-Commutated Photovoltaic Systems on a Distribution Feeder», IEEE Trans. on Power Apparatus and Systems, Vol.103, No.8, Aug. 1984.

[40] CIGRE TF 38-01-08, “Modelling of Power Electronics Equipment (FACTS) in Load Flow and Stability Programs: a Representation Guide for Power System Planning and Analysis”, Final Report 1999.

[41] J.G. DeSteele and J.E. Dagle, “Electric Utility System Application of Fast-Acting Energy Storage as Illustrated by SMES”, International Journal of Global Energy Issues, May 1997.

[42] Saeed Arabi, “A SMES Model for Comprehensive Power System Stability Studies”, EPRI Conference – The Future of Power Delivery in the 21st Century, San Diego, November 18-20, 1997, TR-109806, Final Report, May 1998, pp. 4-95 to 4-109.

[43] C.-F. Lu, C.-C. Liu, and C.-J. Wu, “Effect of Battery Energy Storage System on Load Frequency Control Considering Governor Deadband and Generation Rate Constraint”, IEEE Transactions on Energy Conversion, Vol. 10, No.3, September 1995.

[44] F. Hardan, J.A.M. Bleijs, R. Jones, P. Bromley “Bi-directional power control for flywheel energy storage system with vector-controlled induction machine drive” PEVD’98 Conference, Sept. 98, London, U.K.

[45] Ruddel A. J., Sconnenbeck G. Jones R and Bleijs J A M. “Flywheel energy systems”, EuroSun ’96, Freiburg, Germany, Sep. ’96.

[46] Ruddel A J, Bleijs J A M, Freris L L, Infield D G and Smith G A, “ A wind /Diesel System for Variable Speed Flywheel Storage”, Wind Engineering , Vol. 17 No 3, 1993 .

[47] A.J.B. Heath “Simulation of Generalized Power System Controllers”, PhD thesis, University of Manchester, 1985.

[48] S. Montasser Koussari, “Interactive User Defined Equipment Modelling in Power System Analysis”, PhD thesis, University of Manchester, 1987.

[49] A.E. Efthymiadis, N. Jenkins, N.D. Hatziargyriou “Transient Simulation of Wind Farms Connected to Utility Networks”, Proceedings of EWEC’94, Thessaloniki, 10-14 October 1994.

[50] “STAG - A new Unified Software Program for the study of the Dynamic Behaviour of Electrical Power Systems”. IEEE Transactions on Power Systems - February 1989, Vol. 4, nr 1 - pp 129-138 - New York - M. Stubbe, A. Bihain, J. Deuse and J.C. Baader.

[51] “High Fidelity Simulation of Power System Dynamics” IEEE CAP- January 1995 - p37-41 - J.F. Vernotte, P. Pantiatoci, B. Meyer, J.P. Antoine, J. Deuse and M. Stubbe.

[52] F.P.E, “Prescriptions techniques de branchement d’installations de production décentralisées fonctionnant en parallèle sur le réseau de distribution” December 1997

[53] F. Wellens “ La protection des unités de production décentralisées” LABORELEC, Oct 1996

[54] G.W. Mc Dowell, “ Survey of rate of change of frequency and voltage phase shift relays for loss main protection” ERA Technology, July 1995

[55] M. Dussart “Problems encountered with connecting decentralized generating plants to the distribution networks” report 5.26 CIRED 1997

[56] L. Simoens, W. Herman, F. Wellens "Protection related connection conditions for independent power producers in Belgium" report 34-202 CIGRE 1998

[57] J. Dubois, M. Stubbe, F. Wellens, M. Dussart “Dynamic behavior of dispersed generation on the public MV network”. Paper presented at CIRED, Nice, June 1999